Historic, archived document
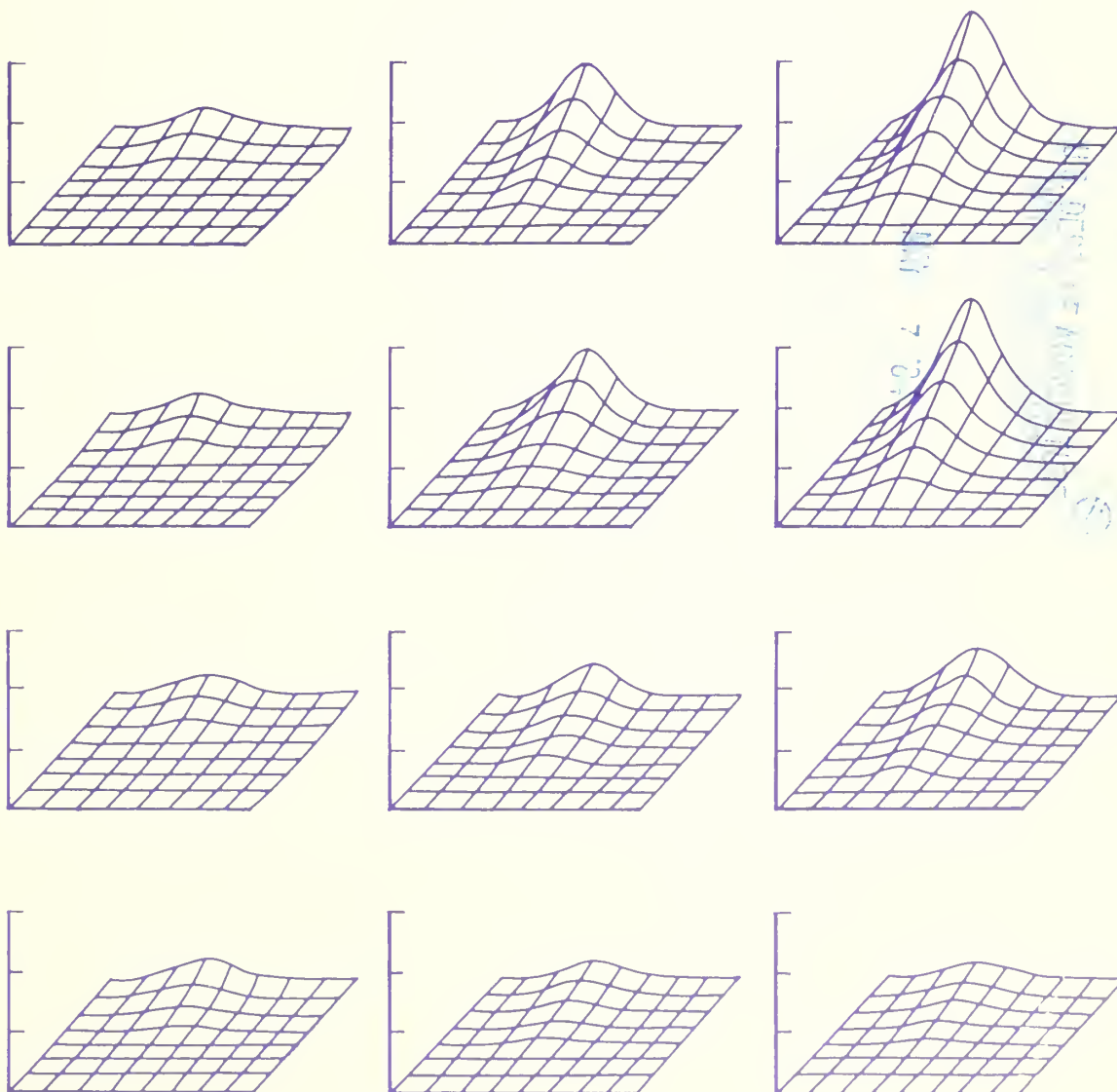
Do not assume content reflects current
scientific knowledge, policies, or practices.

Development of Structured Regression Hypotheses / Interactive Descriptive Geometry Through Five Dimensions

Chester E. Jensen

THE AUTHOR

CHESTER E. JENSEN, retired, served as principal statistician for the Intermountain Forest and Range Experiment Station from 1967–80. He held the same position at the Northeastern and Central States Forest Experiment Stations prior to coming to the Intermountain Station. Mr. Jensen can be reached by mail through the Intermountain Station or by telephone at 801–621–0791.

ACKNOWLEDGMENTS

TABLE OF CONTENTS

RESEARCH SUMMARY

Regression hypotheses admitted to statistical evaluation should, of course, be germane to relations between the variables considered. This constraint is easily violated with the screening of arbitrarily adopted sets of hypotheses. Sequential polynomials in additive models, for example, may include components that are not commensurate with expectation (prior knowledge) and may not include those that are (e.g., unique interaction terms) and, since the analytical results from the screening of meaningless hypotheses may themselves be meaningless, there is substantial incentive for serious preanalysis consideration of the hypotheses to be evaluated.

Where prior knowledge is reasonably strong, the relation under consideration is highly interactive and/or has unique curve form or intercept constraints, the development of a fairly specific (structured) hypothesis is probably advisable. This can be evaluated on pertinent data sets not involved in the hypothesis development.

Prior knowledge information sources can include theory resulting from past investigation as well as information derived from data sets or parts of such data sets devoted to hypothesis development. Methods for developing multidimensional graphic models from two-dimensional effects found in partitioned data and for incorporating even complex constraints are shown in both contrived- and live-application examples.

Mathematical descriptors for the resulting graphic models are assembled using two families of curves: X^n, $n \geq 1$; and e^{-K}, a highly manipulable function for bell-shaped curves or portions thereof. In either case, the X-axis for each two-dimensional effect is altered as needed to orient the curve in the upper-right quadrant. The analyst then simply compares a normalized-scale version of the resulting curve with graphed standard curves, Standards, and locates the two adjacent ones most nearly like his own in shape. Interpolation between the curves and their associated parameters, results in identification of the function for the best matching curve offered by the system.

The alternative of using a completely automated X-transform selection system from the Standards was considered at length. But, inability to define criteria (including the fitting process) that always result in the best choice of descriptor, regardless of data distribution or analytical objectives, resulted in retention of the less sophisticated, but still completely flexible graphic comparison technique shown herein. Methods of use are fairly well documented for each of the graphed-relation examples, which vary from two to five dimensions.

The mathematical descriptors can be regarded as pertinent hypotheses to be evaluated on data sets not used in their development. The evaluation on a single data set can involve a simple scale adjustment in $Y = b$ (hypotheses), as shown herein, or a variety of more complex testing formats (not shown) depending on complexity of the hypothesis itself, capacity of the analyst to linearize it, and/or on the nature of the fitting system adopted (linear, nonlinear). Also evaluation can be based on performance statistics compiled from real-world applications of the hypothesized descriptors.

Experience gained from the presentation of a dozen short courses covering methodology through the fourth dimension, suggests that this material can be assimilated by researchers with only college algebra-level mathematical background and brief training in the operation of programable electronic calculators. Also note that the graphic presentation scheme for the four- and five-dimensional relations used in this paper can, with nominal explanation, be readily interpreted by land managers having little or no interest in the complex mathematical descriptors that may be involved.

Development of Structured Regression Hypotheses/ Interactive Descriptive Geometry Through Five Dimensions

Chester E. Jensen

INTRODUCTION

Applications of statistics reported in biological literature were found by Mead and Pike (1975) to contain some prevalent and potentially damaging oversights. Among other things, they noted that, when transformations were used, simple polynomials predominated and seem to be used as the simplest readily available smoothing curve, without any appeal to their theoretical properties as approximations to the true response function. From this, it appears that analysts are inclined to adopt polynomials as a convenient curve-form panacea for all regression hypotheses rather than undertake purposeful preanalysis development of hypotheses specific to the relation under study.

In the presumed presence of incentive for analysts to follow technical direction, these findings suggest that this is the current (1975, at least) state of regression art insofar as applied statistics is concerned. One need only consult related text material to verify the notion. **Hypothesis development** is simply not a topic covered. Rather, integral polynomials are usually presented as a package of ready-made hypotheses that can be explored sequentially and mechanically using least squares fitting procedure. Discussion covering the inclusion of known constraints in these hypotheses is generally limited to that of the simple intercept. It is seldom, if ever, mentioned that the polynomials, or log-transforms, etc. cannot be presumed to provide adequate curve-form representation for all hypotheses. And, it is pertinent to note that failure to discuss hypothesis development and its potentially complex outcomes in text material constitutes *de facto* disapproval of any but simpler hypotheses, such as those by polynomials.

All told, there is ample cause for the hypothesis-related problems identified by Mead and Pike (1975) and attributed to authors of biological research papers. It would seem, however, that the source of the problem might more nearly be associated with limitations in text material and statistical curricula than with oversights by users of currently proffered statistical methodology.

An effort is made in this paper to initiate solutions to the hypothesis development problem through discussion and by showing analysts how to develop preanalysis hypotheses graphically, regardless of complexity, from accumulated knowledge and existing data. For biological subject matter, these hypotheses will be curvilinear and highly interactive as often as not.

Mathematical formulation of graphed hypotheses is accomplished through use of two families of curves: X^n, $n \geq 1$ (revamped herein from Jensen and Homeyer 1970); and e^{-K} (Jensen 1979), a highly manipulable function for bell-shaped curves or parts thereof. Descriptor development can be accomplished by analysts with a knowledge of basic algebra and access to a programable calculator.

HYPOTHESIS DEVELOPMENT, GENERAL

A condition for valid statistical evaluation of hypotheses is that they be developed independently of data used for evaluation. So, the analyst's first undertaking in a regression analysis should be to establish the strongest possible concept of the underlying form of the relation from accumulated knowledge on the relations being investigated. It can be anticipated for a broad array of problems that these concepts will vary from extremely weak, with little or no basis for form definition, to very firm expectations for even specific algebraic forms.

In the weak-concept case, there is little reason to allow for any but simple curve-form hypotheses. Low-order polynomials in a linear model will probably suffice. Where well-established algebraic forms already exist for the form of the relation, the exact hypothesis is already available and evaluation can be initiated. The more common and perhaps more challenging circumstance, however, involves some intermediate level of prior knowledge where the analyst is sure of some elements in the relation being considered and less sure of others. His or her deliberations on the nature of the relation may result directly in a mathematical hypothesis or, more commonly, they may result in a graphed form wherein the analyst imposes reasonable intercept-, form-, and scale-constraints. These elements of the resulting graph, then, must be represented with suitable mathematical accuracy to establish the final intermediate-strength hypothesis.

If the graphed hypothesis involves unique curve forms, substantial effort might be required to search through **existing functions** like those in the list provided by Mead and Pike (1975), for those with the capacity to mimic unique forms of the hypothesis. (Note that mathematical descriptors should meet the acceptance criteria of the analysts involved [Bartlett 1947; Draper and Hunter 1969]).

A generally more efficient alternative may be that of **analyst-developed** functions to describe graphed hypotheses. Relatively simple methods for describing even complex multidimensional curvilinear interactions are included in this paper. Curves of only two classes are utilized: X^n, $n \geq 1$; and the very versatile three-parameter bell-shaped function e^{-K}. Methods and related examples shown include a variety of research applications to lend realism to the instruction. Additional research applications not cited in the text are given under Additional References to provide the reader with the opportunity for expanded self-study of descriptor development.

Given a mathematical hypothesis, it can be evaluated using data sets not used in its development. The evaluation can vary from a test of general performance in $y = b$ (hypotheses), as shown herein, to more complex formats designated to test performance of individual components of the hypothesis. The testing format adopted is likely to depend on the complexity of the hypothesis itself, the capacity of the analysts to linearize it, and/or on the nature of the fitting system to be used (linear, nonlinear). Also evaluation can be based on performance statistics compiled over repeated real-world applications of the hypothesized descriptor. See Mosteller and Tukey (1977) and Box, Hunter, and Hunter (1978) for discussion of empirical and structural (mechanical) models, and fitting systems, etc.

GRAPHIC HYPOTHESIS DEVELOPMENT – TWO DIMENSIONS

Accumulated knowledge on the general nature of the regression relation under consideration may be used to enhance the derivation of finite graphed hypotheses from data. A common analytical ploy is to dedicate part (perhaps half) of a current data set to the development of a hypothesis, reserving the rest for hypothesis evaluation.

To illustrate, accumulated knowledge regarding the relation between Y and X is such that the curve is expected to pass through the origin, to have a positive slope over X, and to be linear- to concave-upward in form. Within these constraints, a specific estimate of the true shape of the relation is developed from half of a current data set (fig 1).

Here, the analyst visually estimates the curve form expressed in the data and simultaneously draws and hand-fits the form to the data by approximate least deviations (Karst 1958). All of this is accomplished within the constraints of expectation.

In another case, prior knowledge leads to a strong expectation for a positive intercept and, above this, a sigmoid upward to the right with Y asymptoting at a value of 100 percent over large values of X. Within these constraints, a specific estimate is again developed from half of a current data set (fig. 2).
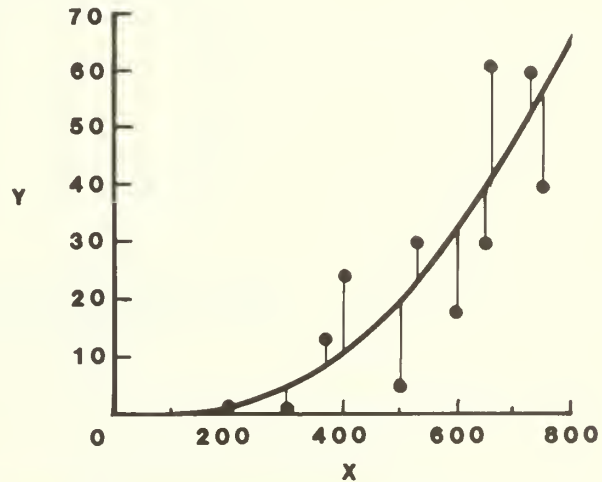
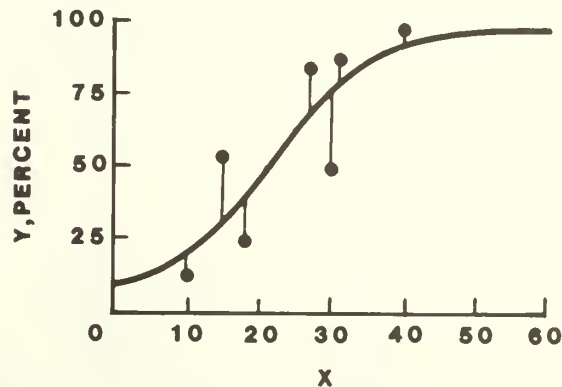Figure 1.—A graphed estimate of the true form of the relation between X and Y.

Figure 2.—A graphed estimate of the true form of the relation between X and Y.

The foregoing procedures apply to any curve shape in any quadrant or combinations of quadrants. They also apply to two-dimensional segments within three-dimensional relations.

GRAPHIC HYPOTHESIS DEVELOPMENT – THREE DIMENSIONS

Extension of two-dimensional procedures to a three-dimensional case is shown in figure 3.

Note that $X1$ and $X2$ are invariably correlated to a greater or lesser extent so that estimates of the $X1$ effect will generally improve with a reduction in breadth of the $X2$ segments. While only three $X2$ segments are shown in figure 3 for the sake of simplicity, five or more segments would have been more desirable if more data points had been available. The same procedure applies to additional independent variables, such as $X3$ in figure 4 (following).
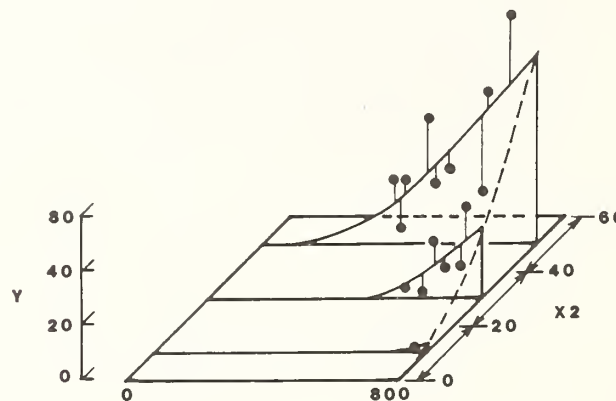

Figure 3.—A graphed estimate of the true form of the relation developed over $X1$ within each of three segments of the range in $X2$.

GRAPHIC HYPOTHESIS DEVELOPMENT – FOUR OR MORE DIMENSIONS

Extension of three-dimensional procedures to a four-dimensional case is shown in figure 4. The same procedures can be extended to five or more dimensions.
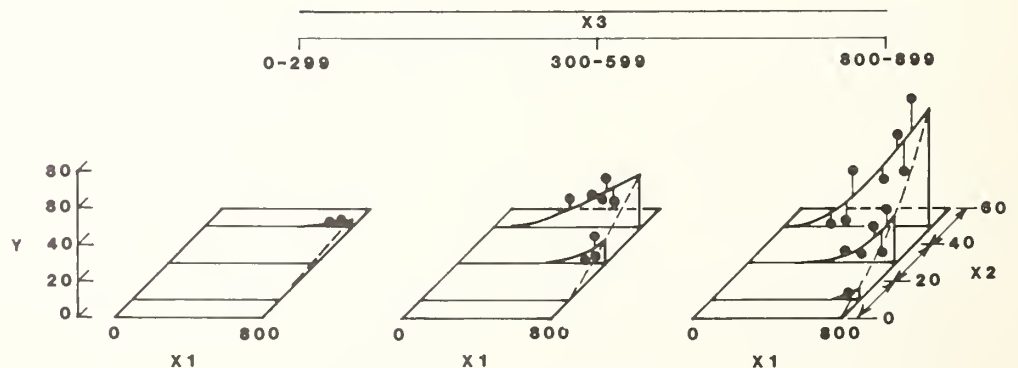

Figure 4.—A graphed estimate of the true form of the relation developed over $X1$ for three segments of the range in $X2$ within each of three segments in the range of $X3$.
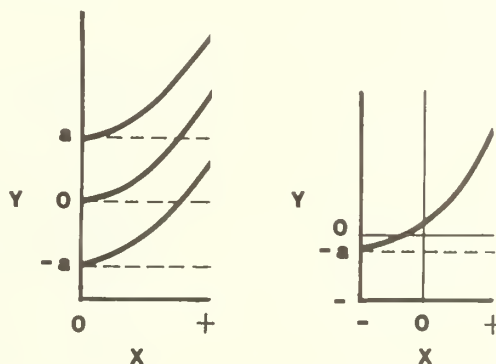
MATHEMATICAL DESCRIPTIONS OF GRAPHED HYPOTHESES – TWO DIMENSIONS

Regardless of the number of dimensions and complexity of the relation to be described, it is ultimately sorted into two-dimensional effects that are described individually. These are finally reassembled, additively or multiplicatively as appropriate, to arrive at the whole descriptor.
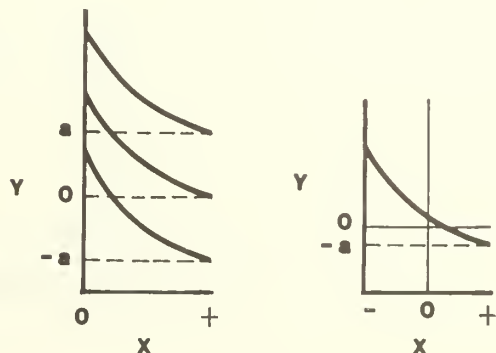
Each two-dimensional element is described with either one or both of two families of curves, X^n, $n \geq 1$, or e^{-K}, a three-parameter sigmoidal function designed for easy use by the modeler.
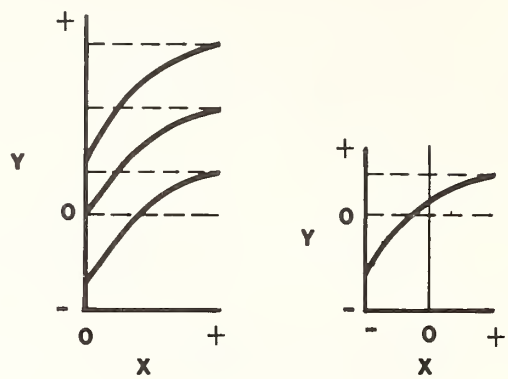
Outline for "TWO DIMENSIONS"

**Class–X^n, $n \geq 1$,
(Exponential Curves)**

Reference is made to Matchacurve-2 (Jensen and Homeyer 1971) in which use of X^n covers not only $n \geq 1$, but $0 < n \leq 1$ and $n < 0$ as well. Our experience since that work was published has indicated that almost all descriptor needs involving X^n are reasonably well met with the ($n \geq 1$) option; so methods and Standards in this summary publication include the ($n \geq 1$) option only, a great simplification over the Matchacurve-2 presentation (Jensen and Homeyer, 1971).

Descriptor development for graphed hypotheses accommodates all possible orientations in the upper-right quadrant of two-dimensional space (fig. 5), and those involving any combination of these up to four quadrants.
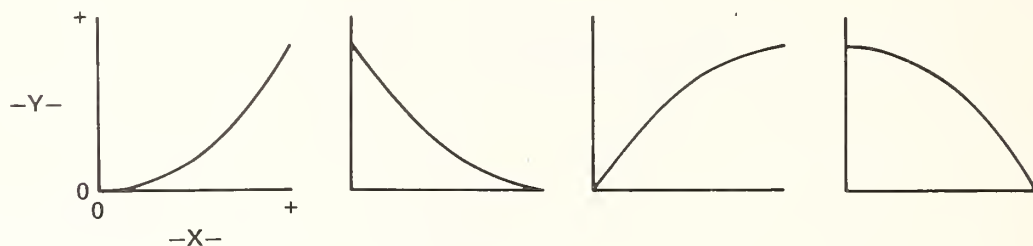
Figure 5.—Alternative orientations of X^n-curves in the upper-right quadrant.

Regardless of the form alternative or quadrant(s) involved, the X-axis can be altered as needed to orient the curve in the upper-right quadrant and through the origin. The analyst simply compares a normalized-scale version of this reoriented hypothesis with graphed standard curves, or Standards (appendix, marked for cut-out), and selects the two adjacent ones most nearly like his own in shape. Interpolation between the curves and their associated powers (n) results in identification of the best alternative offered by the system.

Note that if duplicates are made of the standards, the copies should be **exactly** the same scale as the Standards.

Example 1

Here (fig. 6), the hypothesis is a flat-to concave-upward, positive slope, and occupying any vertical position in the right half of two-dimensional space. Mathematical formulation for the middle alternative (zero Y-intercept) is detailed in figure 7 and in table 1, but the methods will accommodate any Y-intercept.
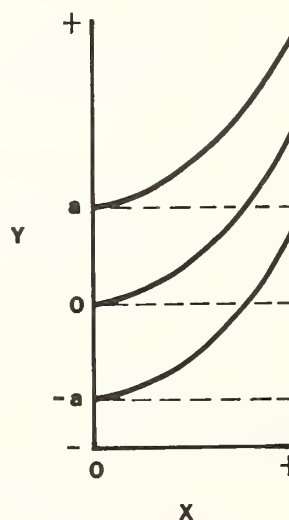
Figure 6.— $Y = a + bX^n$,
$0 \leq X \leq XP, n \geq 1$.

In figure 7, the analyst visually estimates the curve form expressed in the data and simultaneously draws and hand-fits the form to the data by approximate least deviations. All of this is accomplished within the constraints of expectation. Mathematical formulation procedures follow in table 1.
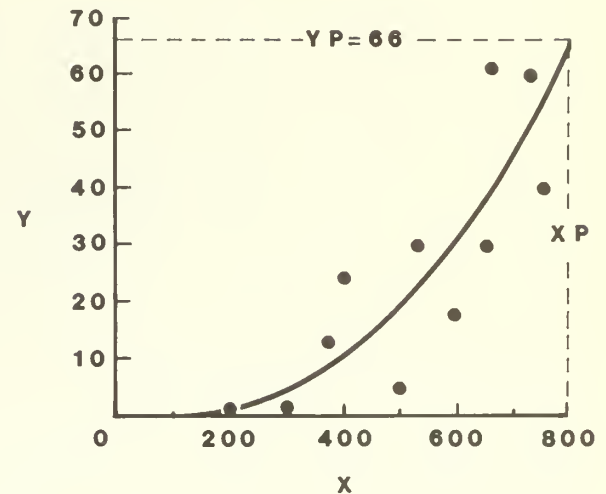
Figure 7.— $Y = 0 + bX^n$.
$0 \leq X \leq XP, n \geq 1.$

Table 1.—Mathematical hypothesis development

Control points		X =	$(Y - a)$ =	Overlay control points		$b(X1)^{2.70}$ =	Performance of $\hat{Y}1$	$b(X1)^{2.64}$ =	Performance of $Y2$	$a + \hat{Y}2$ =
X	Y	$X1$	$Y1$	$XP1$	$Y1/YP1$	$\hat{Y}1$	$(\hat{Y}1 - Y1)$	$\hat{Y}2$	$(\hat{Y}2 - Y1)$	$\hat{Y}$
(1)	(2)	(3)	(4)	(5)	(6)	(7)	(8)	(9)	(10)	(11)
0	0.0	0	0.0	0.00	0.00	0.0	0.0	0.0	0.0	0.0
200	1.3	200	1.3	.25	.02	1.6	+ .3	1.7	+ .4	1.7
400	10.6	400	10.6	.50	.16	10.2	− .4	10.6	.0	10.6
600	31.4	600	31.4	.75	.48	30.4	− 1.0	30.9	− .5	30.9
800	66.0	800	66.0	1.00	1.00	66.0	.0	66.0	.0	66.0

• Columns 1 and 2: Select representative control points (point coordinates) from the graphed hypothesis, including XP, the largest value of X to be represented by the hypothesis (800, in this case), and YP, the corresponding smoothed value of Y (66 here). Five control points have been selected and are listed in these columns, along with computations necessary to the search for a suitably similar mathematical curve-form. Use fewer control points where the desired sensitivity is less; use more for greater sensitivity.

• Column 3: The X-scale remains unchanged, but is relabeled as $X1$ for consistency with procedures for subsequent, more complex examples. XP is called $XP1$ in the $X1$-scale.

• Column 4: Subtract the intercept, a, from all control point Y-values to produce $Y1$. Whether a is zero (as here) or any positive or negative value, $Y1$-values will have zero intercept and will be in the upper-right quadrant of two-dimensional space. Such orientation of the curve is necessary to use of the Standards. YP is called $YP1$ in the $Y1$-scale.

• Columns 5 and 6: Compute ratios of $X1$ and $Y1$ to $XP1$ and $YP1$, respectively. These arrays of ratios are the normalized (proportional) scales for the $X1$ and $Y1$ control points. The resulting overlay points can now be plotted on a sheet of conventional graph paper (10×10 to ½ inch is best), at the exact scale specified in figure 8. Although not necessary, it may help to draw a smooth curve through the points. Call this the overlay curve. It is the normalized version of the original hypothesis plotted at the same scale used for the Standards (fig. 8).
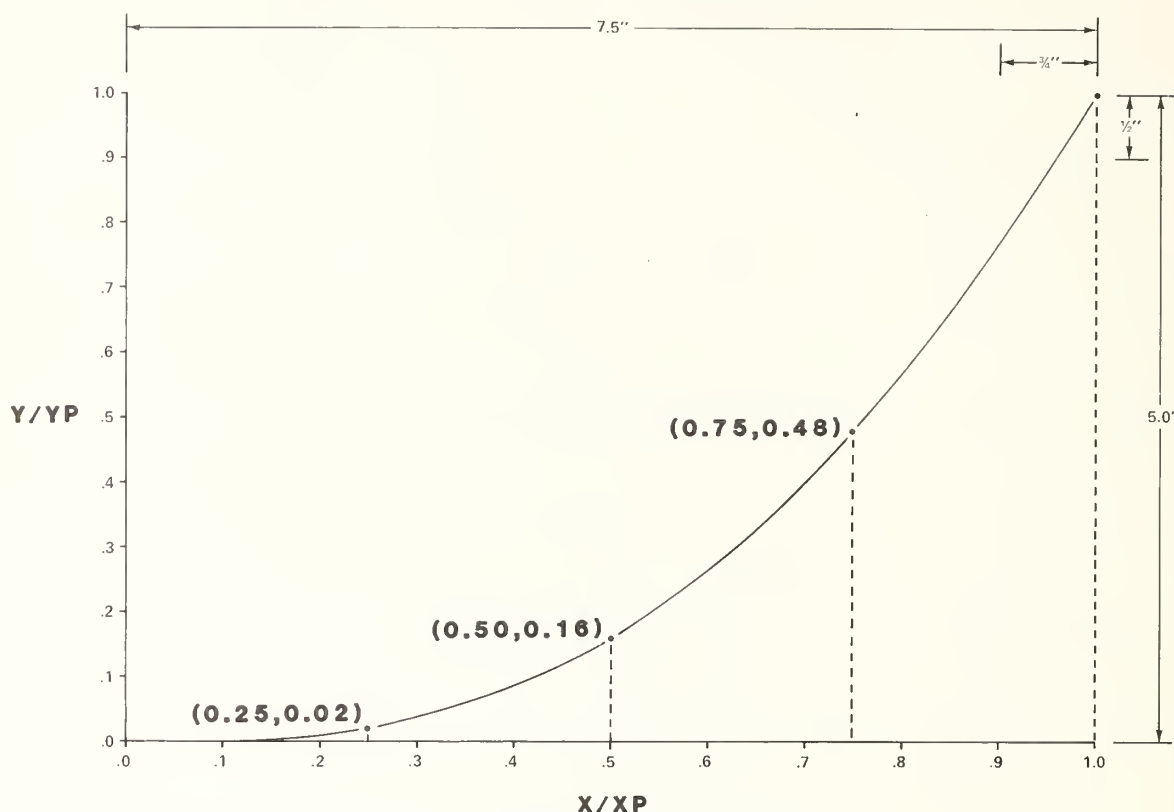
Figure 8.—Here the graphed curve has been normalized and plotted at the same scale as the Standards.

• Place the overlay graph over the Standards, being certain that the X- and Y-axes are matched exactly. Find the Standards that most nearly bracket the overlay curve (fig. 9). In this case, $n = 2.5$ and 3.0 bracket the overlay curve nicely. Note that a light source behind the graphs that are being compared will assist in the matching process. Where the hypothesized curve is not suitably matched by the Standards, a segmented or multicomponent X^n-function, or some portion of a sigmoid may suffice (see Contents).

Use proportional departure of the overlay curve from the left bracketing Standard to approximate an interpolated value between $n = 2.5$ and 3.0. This is best done at a point where curve-form accuracy is most crucial—the point of sharpest bend was adopted in this case. From figure 9, the interpolated n is 2.7.

• Column 7: After the analyst has made the first approximation of the mathematical form of the hypothesis, $Y1 = b(X1)^{2.70}$, where $b = YP1/(XP1)^{2.70} = 66/(800)^{2.70} = 9.576 \times 10^{-7}$, he can make associated estimates, $\hat{Y}1$, at each control point $X1$ value as shown.

• Column 8: Differences between estimated and original $Y1$ values indicate that $b(X1)^{2.70}$ has a preponderance of negative departures (that is, too much curvature). Try flatter curves (less power) iteratively.
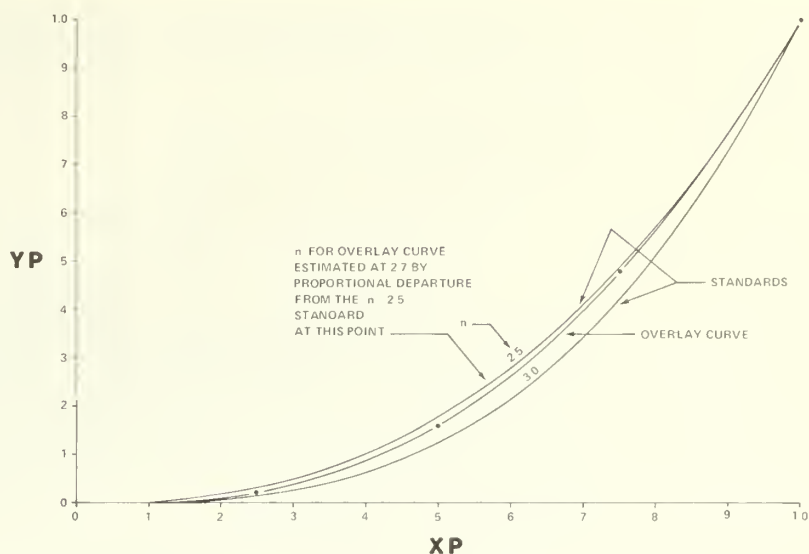
Figure 9.—The Standards best matched to the
original curve bracket the overlay curve.

• Column 9: A second estimator, $\hat{Y}2 = b(X1)^{2.64}$, where $b = YP1(XP1)^{2.64} = 1.430 \times 10^{-6}$, produces $\hat{Y}2$ values as shown.

• Column 10: Differences between estimated $\hat{Y}2$ and original $Y1$ values are small and well balanced (+ and −); so $b(X1)^{2.64}$ is adopted.

• Column 11: The final hypothesis is then, $\hat{Y} = a + bX^n = 0 + 1.430 \times 10^{-6} (X1)^{2.64}$, or, since $X = X1$, $\hat{Y} = 1.430 \times 10^{-6} (X)^{2.64}$.
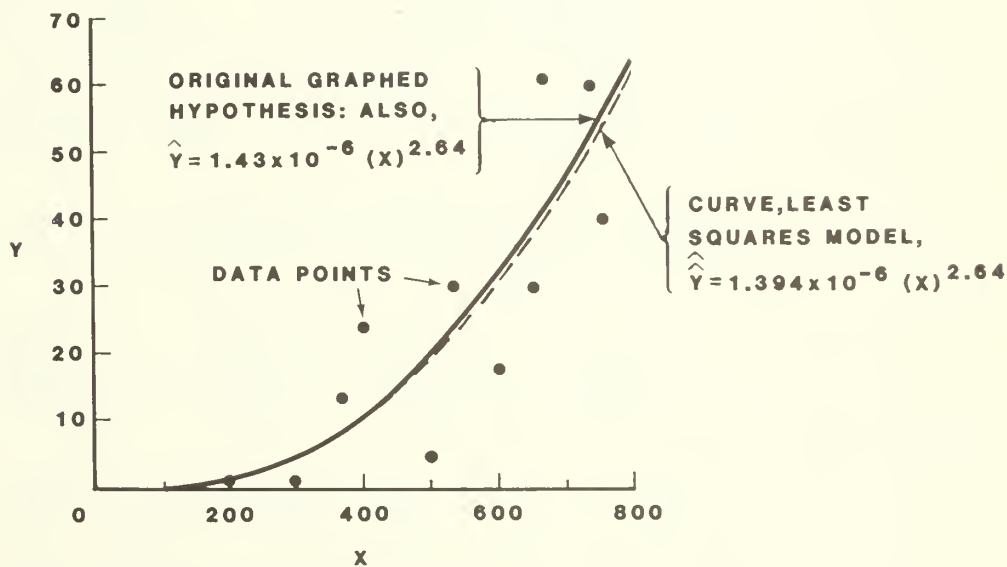
Figure 10.—The fitted model has been plotted
over the original graphed form.

Note that at the scale shown in figure 10, differences between the graphed hypothesis and $\hat{Y} = 1.430 \times 10^{-6} (X)^{2.64}$ are barely discernible. This example produced a closer mathematical match for the objective curve than one might expect on the average, but serves to demonstrate the procedures very well.

13

- As a matter of fitting-methods interest, the hypothesis was then fitted by least squares (forced through the origin) back to the data from which it was partially derived

and: $\hat{Y} = c(XT)$, where $XT = b(X1)^n$

$c = \Sigma(XT*Y)/\Sigma(XT)^2 = 0.9748$

or: $\hat{Y} = 1.394 \times 10^{-6}(X)^{2.64}$ and is plotted in figure 10 as a dashed line.

The least squares model is quite close to the graphed hypothesis as might be expected, but the mathematical hypothesis should not be evaluated statistically on this used half of the data set. Rather, the same fitting procedures can be applied to the unused half of the data set and, for this, conventional statistical evaluations are appropriate.

- Given the same general hypothesis, $Y = a + 1.430 \times 10^{-6}(X)^{2.64}$, but with a being a **fixed constraint** other than zero, the fitting process is identical to that just specified. Assuming for example that a is fixed at -20, the final form would be $\hat{Y} = -20 + 1.394 \times 10^{-6}(X)^{2.64}$, $0 \le X \le 800$.
- Where a is *variable* (not fixed), linear curve-fitting techniques can be used to estimate both a and b in $Y = a + b(X1)^n$. Then, letting $X = (X1)^n$, $b = \Sigma xy/\Sigma x^2$ and $a = \bar{Y} - b\bar{X}$, as in conventional notation.

Example 2

Assume a graphed hypothesis like that in figure 11 (flat- to concave-upward, positive slope, with negative Y-intercept, a, and crossing into the left half of two-dimensional space). Mathematical formulation procedures follow closely those of example 1 and are summarized in table 2.

Figure 11.— $Y = a + b(X - k)^n$,
$k \le X \le XP, n \ge 1$.

Table 2.—Mathematical hypothesis development

Control points		$(X - k)$ =	$(Y - a)$ =	Overlay control points		$b(X1)^{2.70}$ =	Perform- ance of $\hat{Y}1$	$b(X1)^{2.64}$ =	Perform- ance of $\hat{Y}2$	$a + \hat{Y}2$ =
X	Y	X1	Y1	X1/XP1	Y1/YP1	Y1	$(\hat{Y}1 - Y1)$	$\hat{Y}2$	$(\hat{Y}2 - Y1)$	$\hat{Y}$
(1)	(2)	(3)	(4)	(5)	(6)	(7)	(8)	(9)	(10)	(11)
− 400	− 10.0	0	0.0	0.00	0.00	0.0	0.0	0.0	0.0	− 10.0
− 200	− 8.7	200	1.3	.25	.02	1.6	+ .3	1.7	+ .4	− 8.3
0	.6	400	10.6	.50	.16	10.2	− .4	10.6	.0	.6
200	21.4	600	31.4	.75	.48	30.4	− 1.0	30.9	− .5	20.9
400	56.0	800	66.0	1.00	1.00	66.0	.0	66.0	.0	56.0

- Columns 1 and 2: List control points representative of the curve.
- Shift the curve to the upper-right quadrant to match the position of the Standards:
  Column 3: Let $X1 = (X - k)$, where k = the smallest value of X to be represented by the equation (-400 here). Then, $X1 = (X - [-400]) = (X + 400)$, and $XP1 = 800$.
  Column 4: $Y1 = (Y - a) = (Y - [-10]) = (Y + 10)$, and $YP1 = 66.0$.
- Columns 5–10: Identical to example 1, table 2, columns 5–10.
- Column 11: The final hypothesis is then, $\hat{Y} = a + bX^n = -10 + 1.430 \times 10^{-6}(X + 400)^{2.64}$, $-400 \le X \le 400$.
- Least squares fit.
  With a fixed; $\hat{Y} = c(XT)$, where $XT = b(X1)^n$, $c = \Sigma(XT*Y1)/(\Sigma XT)^2$, and $\hat{Y} = a + c(b(X1)^n)$. In this case, $\hat{Y} = -10 + c(b[X1]^n)$.
  With a variable, $\hat{Y} = a + b(X1)^n$. Letting $X = (X1)^n$ and, under conventional notation, $b = \Sigma xy/\Sigma x^2$ and $a = \bar{Y} - b\bar{X}$.

Example 3

Assume a hypothesis like that in figure 12 (flat- to concave-upward, negative slope, and occupying any vertical position in the right half of two-dimensional space). Mathematical formulation for the middle alternative (a = zero) is detailed in table 3, but the methods will accommodate any a value. Procedures follow closely those of example 1.

Figure 12.— $Y = a + b(XP - X)^n$.
$0 \le X \le XP, n \ge 1$.

Table 3.—Mathematical hypothesis development

Control points		$(XP - X)$ =	$(Y - a)$ =	Overlay control points		$b(X1)^{2.70}$ =	Performance of $\hat{Y}1$	$b(X1)^{2.64}$ =	Performance of $\hat{Y}2$	$a + \hat{Y}2$ =
X	Y	$X1$	$Y1$	$X1/XP1$	$Y1/YP1$	$\hat{Y}1$	$(\hat{Y}1 - Y1)$	$\hat{Y}2$	$(\hat{Y}2 - Y1)$	$\hat{Y}$
(1)	(2)	(3)	(4)	(5)	(6)	(7)	(8)	(9)	(10)	(11)
0	66.0	800	66.0	1.00	1.00	66.0	0.0	66.0	0.0	66.0
200	31.4	600	31.4	.75	.48	30.4	− 1.0	30.9	− .5	30.9
400	10.6	400	10.6	.50	.16	10.2	− .4	10.6	.0	10.6
600	1.3	200	1.3	.25	.02	1.6	+ .3	1.7	+ .4	1.7
800	.0	0	.0	.00	.00	.0	.0	.0	.0	.0

- Columns 1 and 2: List control points representative of the curve.
- Shift the curve to the upper-right quadrant to match the position of the Standards:
  Column 3: Let $X1 = (XP - X) = (800 - X)$, and $XP1 = 800$.
  Column 4: Since a = zero here, $Y1 = (Y - a) = (Y - 0) = Y$, and $UP1 = 66.0$.
- Columns 5–10: Identical to example 1, table 2, columns 5–10.
- Column 11: The final hypothesis is then,
  $$\hat{Y} = a + b(XP - X)^n = 0 + 0.1430 \times 10^{-6}(800 - X)^{2.64}, \ 0 \le X \le 800.$$
- Least squares fit.
  With a fixed at any value; $\hat{Y} = c(XT)$, where $XT = b(X1)^n$, $c = \Sigma)XT * Y1)/(\Sigma XT)^2$,
  and $\hat{Y} = a + c(b(X1)^n)$.
  With a variable; $\hat{Y} = a + b(X1)^n$. Letting $X = (X1)^n$ and, under conventional notation,
  $b = \Sigma xy / \Sigma x^2$ and $a = \bar{Y} - b\bar{X}$.

Example 4

Assume a hypothesis like that in figure 13 (flat- to concave-upward, negative slope, with negative Y-intercept, a, and crossing into the left half of two-dimensional space). Mathematical formulation procedures follow closely, those of example 1 and are summarized in table 4.
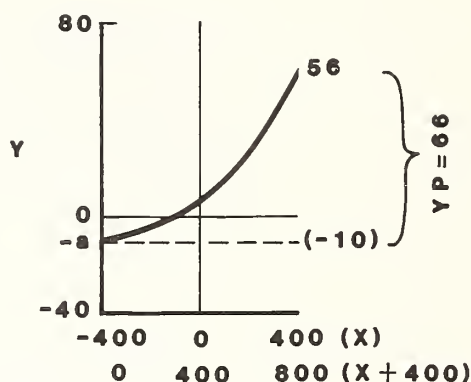

Figure 13.— $Y = a + (XP - X)^n$,
$k \le X \le XP, n \ge 1.$

Table 4.—Mathematical hypothesis development

Control points		$(XP - X)$ =	$(Y - a)$ =	Overlay control points		$b(X1)^{2.70}$ =	Perform- ance of $\hat{Y}1$	$b(X1)^{2.64}$ =	Perform- ance of $\hat{Y}2$	$a + \hat{Y}2$ =
X (1)	Y (2)	X1 (3)	Y1 (4)	X1/XP1 (5)	Y1/YP1 (6)	$\hat{Y}1$ (7)	$(\hat{Y}1 - Y1)$ (8)	$\hat{Y}2$ (9)	$(\hat{Y}2 - Y1)$ (10)	$\hat{Y}$ (11)
− 400	56.0	800	66.0	1.00	1.00	66.0	0.0	66.0	0.0	56.0
− 200	21.4	600	31.4	.75	.48	30.4	− 1.0	30.9	− .5	20.9
0	.6	400	10.6	.50	.16	10.2	− .4	10.6	.0	.6
200	− 8.7	200	1.3	.25	.02	1.6	+ .3	1.7	+ .4	− 8.3
400	− 10.0	0	.0	.00	.00	.0	.0	.0	.0	− 10.0

- Columns 1 and 2: List control points representative of the curve.
- Shift the curve to the upper-right quadrant to match the position of the Standards:
  Column 3: Let $X1 = (XP - X) = (400 - X)$, and $XP1 = 800$.
  Column 4: Let $Y1 = (Y - a) = (Y - (-10)) = (Y + 10)$, and $YP1 = 66.0$.
- Columns 5–10: Identical to example 1, table 2, columns 5–10.
- Column 11: The final hypothesis is then,
  $\hat{Y} = a + b(XP - X)^n = -10 + 1.430 \times 10^{-6}(400 - X)^{2.64}$, $k \le X \le 400$, and $k =$ the lower applicable limit (-400 here) of the X-range.
- Least squares fit.
  With a fixed at any value; $\hat{\hat{Y}} = c(XT)$,
  where $XT = b(X1)^n$, $c = \Sigma(XT * Y1)/(\Sigma XT)^2$, and $Y = a + c(b(X1)^n)$.
  With a variable, $\hat{\hat{Y}} = a + b(X1)^n$. Letting $X = (X1)^n$ and, under conventional notation, $b = \Sigma xy/\Sigma x^2$ and $a = \bar{Y} - b\bar{X}$.

Example 5

Assume a hypothesis like that in figure 14 (flat- to convex-upward, positive slope, and occupying any vertical position in the right half of two-dimensional space). Mathematical formulation for the middle alternative is detailed in table 5. Procedures follow closely those of example 1.
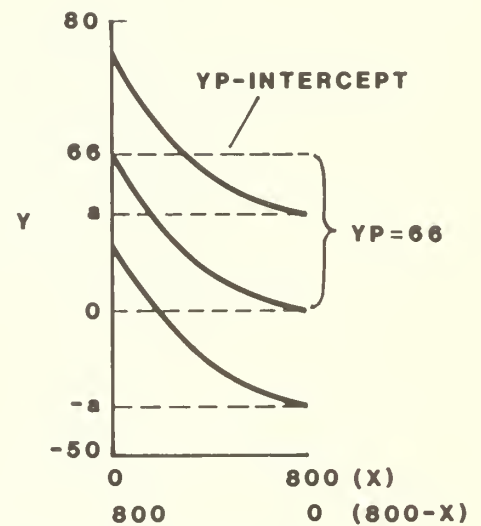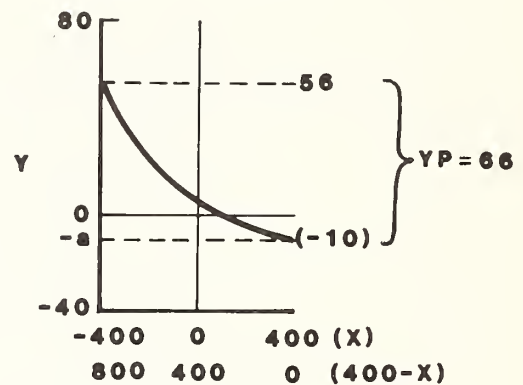

Figure 14.— $Y = YP - b(XP - X)^n$,
$0 \le X \le XP, n \ge 1$.

Table 5.—Mathematical hypothesis development

Control points		$(XP - X)$ =	$(YP - Y)$ =	Overlay control points		$b(X1)^{2.70}$ =	Performance of $\hat{Y}1$	$b(X1)^{2.64}$ =	Performance of $\hat{Y}2$	$a + \hat{Y}2$ =
X	Y	X1	Y1	X1/XP1	Y1/YP1	$\hat{Y}1$	$(\hat{Y}1 - Y1)$	$\hat{Y}2$	$(\hat{Y}2 - Y1)$	$\hat{Y}$
(1)	(2)	(3)	(4)	(5)	(6)	(7)	(8)	(9)	(10)	(11)
0	0.0	800	66.0	1.00	1.00	66.0	0.0	66.0	0.0	0.0
200	34.6	600	31.4	.75	.48	30.4	− 1.0	30.9	− .5	35.1
400	55.4	400	10.6	.50	.16	10.2	− .4	10.6	.0	55.4
600	64.7	200	1.3	.25	.02	1.6	+ .3	1.7	+ .4	64.3
800	66.0	0	.0	.00	.00	.0	.0	.0	.0	66.0

- Columns 1 and 2: List control points representative of the curve.
- Shift the curve to the upper-right quadrant to match the position of the Standards:
  Column 3: Let $X1 = (XP - X) = (800 - X)$, and $XP1 = 800$.
  Column 4: Let $Y1 = (YP - Y) = (66.0 - Y)$, and $YP1 = 66.0$.
- Columns 5–10: Identical to example 1, table 2, columns 5–10.
- Column 11: The final hypothesis is then,
  $\hat{Y} = YP - b(XP - X)^n = 66.0 - 1.430 \times 10^{-6}(800 - X)^{2.64}$, $0 \le X \le 800$.
- Least squares fit.
  With YP fixed at any value; $\hat{Y} = c(XT)$, where $XT = b(X1)^n$, $c = (XT*Y1)/(XT)^2$, and $\hat{Y} = YP - c(b(X1)^n)$.
  With YP variable, $\hat{Y} = a + b(X1)^n$. Letting $X = (X1)^n$ and, under conventional notation, $b = \Sigma xy / \Sigma x^2$ and $a = \bar{Y} - b\bar{X}$.

Example 6

Assume a hypothesis like that in figure 15 (flat- to convex-upward, positive slope with negative Y-intercept, and crossing into the left half of two-dimensional space). Mathematical formulation for this curve is detailed in table 6. Procedures closely follow those of example 1.
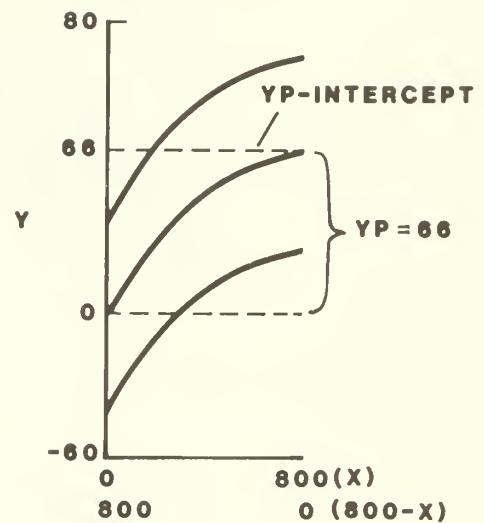

Figure 15.— $Y = YP - (XP)^n$,
$k \le X \le XP, n \ge 1$.

Table 6.—Mathematical hypothesis development

Control points		$(XP-X)$ =	$(YP-Y)$ =	Overlay control points		$b(X1)^{2.70}$ =	Performance of $\hat{Y}1$	$b(X1)^{2.64}$ =	Performance of $\hat{Y}2$	$a + \hat{Y}2$ =
X	Y	X1	Y1	X1/XP1	Y1/YP1	$\hat{Y}1$	$(\hat{Y}1 - Y1)$	$\hat{Y}2$	$(\hat{Y}2 - Y1)$	$\hat{Y}$
(1)	(2)	(3)	(4)	(5)	(6)	(7)	(8)	(9)	(10)	(11)
−400	−40.0	800	66.0	1.00	1.00	66.0	0.0	66.0	0.0	−40.0
−200	−5.4	600	31.4	.75	.48	30.4	−1.0	30.9	−.5	−4.9
0	15.4	400	10.6	.50	.16	10.2	−.4	10.6	.0	15.4
200	24.7	200	1.3	.25	.02	1.6	+.3	1.7	+.4	24.3
400	26.0	0	.0	.00	.00	.0	.0	.0	.0	26.0

- Columns 1 and 2: List control points representative of the curve.
- Shift the curve to the upper-right quadrant to match the position of the Standards:
  Column 3: Let $X1 = (XP - X) = (400 - X)$ and $XP1 = 800$.
  Column 4: Let $Y1 = (YP - Y) = (66.0 - Y)$ and $YP1 = 66.0$.
- Columns 5–10: Identical to example 1, table 2, columns 5–10.
- Column 11: The final hypothesis is then,
  $\hat{Y} = YP - b(XP - X)^n = 66.0 - 1.430 \times 10^{-6}(400 - X)^{2.64}, \ -400 \le X \le 400$.
- Least squares fit.
  With YP fixed at any value; $\hat{\hat{Y}} = c(XT)$, where $XT = b(X1)^n$, $c = \Sigma(XT * Y1)/\Sigma(XT)^2$,
  and $\hat{\hat{Y}} = YP - c(b(X1)^n)$.
  With YP variable, $\hat{\hat{Y}} = a + b(X1)^n$. Letting $X = (X1)^n$ and, under conventional notation,
  $b = \Sigma xy/\Sigma x^2$, and $a = \bar{Y} - b\bar{X}$.

Example 7

Assume a hypothesis like that in figure 16 (flat- to convex-upward, negative slope and occupying any vertical position in the right half of two-dimensional space). Mathematical formulation for the middle alternative is detailed in table 7. Procedures closely follow those of example 1.
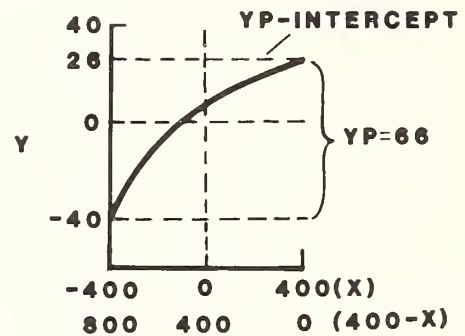

Figure 16.— $Y = YP - b(X)^n$,
$0 \le X \le XP, n \ge 1$.

Table 7.—Mathematical hypothesis development

Control points		X =	$(YP - Y)$ =	Overlay control points		$b(X1)^{2.70}$ =	Perform-ance of $\hat{Y}1$	$b(X1)^{2.64}$ =	Perform-ance of $\hat{Y}2$	$a + \hat{Y}2$ =
X (1)	Y (2)	X1 (3)	Y1 (4)	X1/XP1 (5)	Y1/YP1 (6)	$\hat{Y}1$ (7)	$(\hat{Y}1 - Y1)$ (8)	$\hat{Y}2$ (9)	$(\hat{Y}2 - Y1)$ (10)	$\hat{Y}$ (11)
0	66.0	0	0.0	0.00	0.00	0.0	0.0	0.0	0.0	66.0
200	64.7	200	1.3	.25	.02	1.6	+ .3	1.7	+ .4	64.3
400	55.4	400	10.6	.50	.16	10.2	− .4	10.6	.0	55.4
600	34.6	600	31.4	.75	.48	30.4	− 1.0	30.9	− .5	35.1
800	.0	800	66.0	1.00	1.00	66.0	.0	66.0	.0	.0

- Columns 1 and 2: List control points representative of the curve.
- Shift the curve to the upper-right quadrant to match the position of the Standards:
  Column 3: Let $X1 = X$, and $XP1 = 800$.
  Column 4: Let $Y1 = (YP - Y) = (66.0 - Y)$, and $YP1 = 66.0$.
- Columns 5–10: Identical to example 1, table 2, columns 5–10.
- Column 11: The final hypothesis is then,
  $\hat{Y} = YP - b(X)^n = 66.0 - 1.430 \times 10^{-6}(X)^{2.64}, 0 \le X \le 800$.
  - Least squares fit.
  With YP fixed at any value; $\hat{\hat{Y}} = c(XT)$, where $XT = b(X1)^n$, $c = \Sigma(XT*Y1)/\Sigma(XT)^2$,
  and $\hat{\hat{Y}} = YP - c(b(X1)^n)$.
  With YP variable, $\hat{\hat{Y}} = a + b(X1)^n$. Letting $X = (X1)^n$ and, under conventional notation,
  $b = \Sigma xy/\Sigma x^2$, and $a = \bar{Y} - b\bar{X}$.

Example 8

Assume a hypothesis like that in figure 17 (flat- to convex-upward, negative slope with negative Y-intercept and crossing into the left half of two-dimensional space). Mathematical formulation for this curve is detailed in table 8. Procedures closely follow, those of example 1.
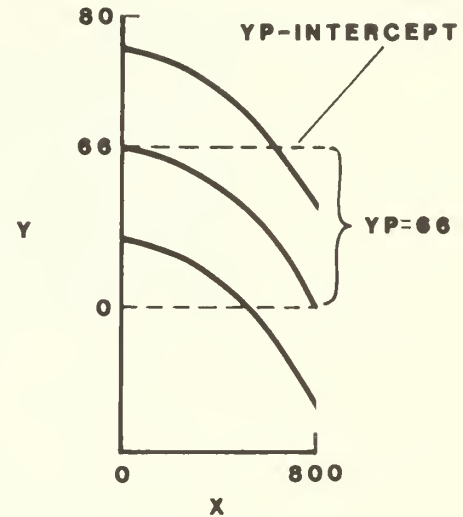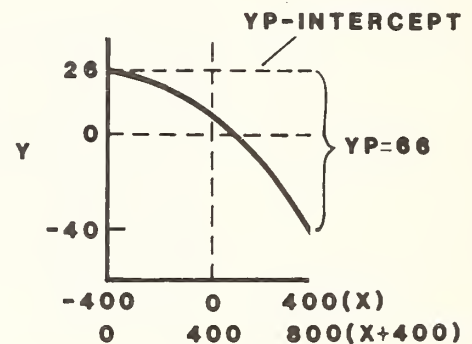

Figure 17.— $Y = YP - (X - k)^n$,
$k \le X \le XP, n \ge 1$.

Table 8.—Mathematical hypothesis development

Control points		$(X - K)$ =	$(YP - Y)$ =	Overlay control points		$b(X1)^{2.70}$ =	Perform-ance of $\hat{Y}1$	$b(X1)^{2.64}$ =	Perform-ance of $\hat{Y}2$	$a + \hat{Y}2$ =
X (1)	Y (2)	X1 (3)	Y1 (4)	X1/XP1 (5)	Y1/YP1 (6)	$\hat{Y}1$ (7)	$(\hat{Y}1 - Y1)$ (8)	$\hat{Y}2$ (9)	$(\hat{Y}2 - Y1)$ (10)	$\hat{Y}$ (11)
− 400	26.0	0	0.0	0.00	0.00	0.0	0.0	0.0	0.0	26.0
− 200	24.7	200	1.3	.25	.02	1.6	+ .3	1.7	+ .4	24.3
0	15.4	400	10.6	.50	.16	10.2	− .4	10.6	.0	15.4
200	− 5.4	600	31.4	.75	.48	30.4	− 1.0	30.9	− .5	− 4.9
400	− 40.0	800	66.0	1.00	1.00	66.0	.0	66.0	.0	.0

- Columns 1 and 2: List control points representative of the curve.
- Shift the curve to the upper-right quadrant to match the position of the Standards:

Column 3: Let $X1 = (X - k)$, where $k =$ the smallest value of X to be represented by the equation, -400 here. Then, $X1 = (X + 400)$, and $XP1 = 800$.

Column 4: Let $X1 = (YP - Y) = (26.0 - Y)$, and $YP1 = 66.0$.

- Columns 5–10: Identical to example 1, table 2, columns 5–10.
- Column 11: The final hypothesis is then,

$\hat{Y} = YP - b(X)^n = 26.0 - 1.430 \times 10^{-6}(X)^{2.64}$, $-400 \le X \le 400$.

- Least squares fit.

With YP fixed at any value; $\hat{\hat{Y}} = c(XT)$, where $XT = b(X1)^n$, $c = \Sigma(XT * Y1)/\Sigma(XT)^2$, and $\hat{Y} = YP - c(b(X1))^n$.

With YP variable, $\hat{\hat{Y}} = a + b(X1)^n$. Letting $X = (X1)^n$ and, under conventional notation, $b = \Sigma xy/\Sigma x^2$, and $a = \bar{Y} - b\bar{X}$.

Class e^{-K}, (Bell-Shaped or Sigmoidal Curves)

By reason of e^{-K} symmetry, shape parameters for this bell-shaped function are identical for either sigmoidal half (see e^{-K} ITS DERIVATION, CAPABILITIES, AND LIMITATIONS, appendix A). So, the e^{-K}-Standards are limited to sigmoids and these have normalized (proportional) X- and Y-scales, are in the upper right quadrant of two-dimensional space, and have zero intercept and slope upward to the right.

Representative control points (point-coordinates) are selected from a graphed sigmoidal hypothesis and these points are shifted to the position of the Standards through manipulation of the X- and Y-scales as needed. These revised scales are normalized (converted to proportions) and the normalized control points are plotted on graph paper at the exact scale of the Standards. This point-representation of the hypothesis (with or without the corresponding curve sketched in) can be laid over and compared with alternative sigmoids on any page of the Standards. When Standards are found that bracket the overlay curve and are suitably similar to it, the analyst can interpolate between parameters of these Standards to arrive at the best sigmoid provided by the system.

The result is a mathematical hypothesis that can be fitted to new data and evaluated statistically. For example, assume the graphed hypothesis shown in figure 18.
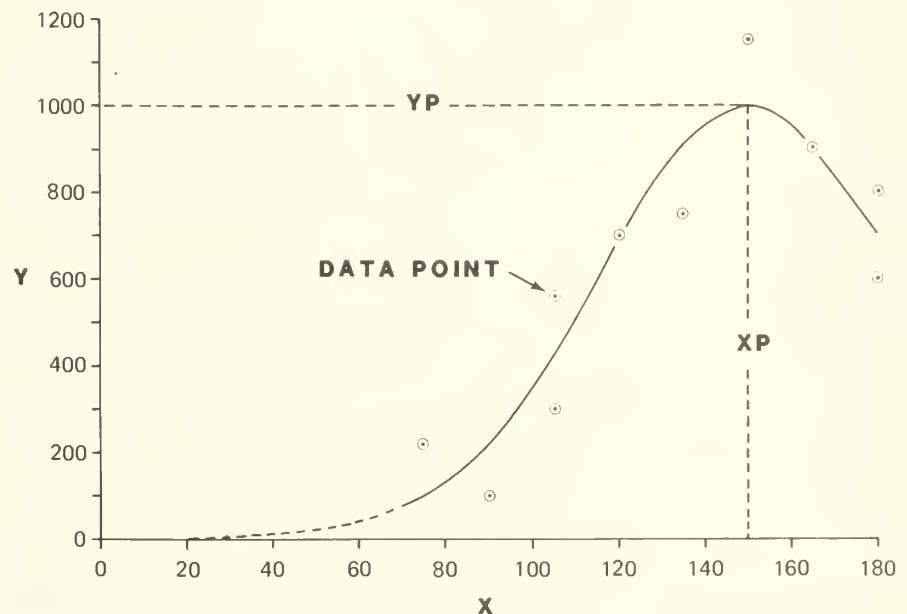

Figure 18.—Here, the expected curve form has been hand-fitted through plotted data points by approximate least deviations, (Karst 1958).

Recognizing that the shape of the curve on each side of the peak is about the same, it seems likely that a symmetrical curve fitting the left, most completely specified side of the relation, will also fit the top segment of the implied sigmoid to the right of the peak. So, we only need identify the mathematical form of the sigmoid to the left of the peak ($0 \le X \le 150$) to describe the entire graphed hypothesis. Mathematical formulation of this curve is detailed in table 9.

Table 9.—Mathematical hypothesis development

Control points		X =	(Y − a) =	Overlay control points		$n=2, l=.67$ $XP1=150,$ $YP1=1000$ $a=0, Y1=$	Perform-ance of Ŷ1	$n=2, l=.6701$ $XP1=150,$ $YP1=1000$ $a=0, Y2=$	Perform-ance of Y2
X (1)	Y (2)	X1 (3)	Y1 (4)	X1/XP1 (5)	Y1/YP1 (6)	$a+YP1^*e^{-K}$ (7)	$(Ŷ1-Y)$ (8)	$a+YP1^*e^{-K}$ (9)	$(Ŷ2-Y)$ (10)
0	0	0	0	0.00	0.00	0.0	0.0	0.0	0.0
75	100	75	100	.50	.10	100.6	+ .6	100.5	+ .5
105	430	105	430	.70	.43	437.5	+7.5	437.3	+7.3
120	700	120	700	.80	.70	692.6	−7.4	692.4	−7.6
150	1000	150	1000	1.00	1.00	1000.0	.0	1000.0	.0

Procedures generally follow those of example 1 for curves of the X^n-class.

• Columns 1 and 2: Five control points representative of the curve (including XP, the point in X at which Y peaks, and YP, the peak value of Y) have been selected from the sigmoid and are listed here. Use fewer control points where the desired sensitivity is less, more for greater sensitivity.

• Columns 3 and 4: The Standards for e^{-K} are oriented at zero in the upper-right quadrant (as for the X^n-Standards) and, since this curve already conforms, there are no transformations of the X- and Y-axes. So, $X1 = X$ and $Y1 = Y$, respectively. The $X1$- and $Y1$-variables will be shown and used here to be consistent with procedures for more complex examples that follow. Note that $XP1$ is the maximum value of $X1$ and that $YP1$ is the maximum value of $Y1$.

• Columns 5 and 6: Compute ratios of $X1$ and $Y1$ to $XP1$ and $YP1$, respectively. These arrays of ratios are the normalized (proportional) scales for the $X1$- and $Y1$-control points. The resulting overlay points can now be plotted on a sheet of conventional graph paper (10×10 to ½ inch is best), at the exact scale specified in figure 19 (5 inches for the YP range and ½ inch per 1/10 unit of $Y1$, 7½ inches for the XP range and 3/4 inch per 1/10 unit of $X1$). Although not necessary, it may help to sketch a smooth curve through these plotted points as shown in figure 19.

• Use this curve as an overlay for any page of the Standards, being careful to match exactly, the X- and Y-axes of the overlay with those of each page examined. Find adjoining sigmoids that are most nearly shaped like the overlay curve and bracket it (fig. 20).

Note in the Standards that I is the proportional distance of the inflection point from zero to 1.0 and n is the power of the negative exponents for e in e^{-K} (appendix). Curvature of the sigmoids becomes more pronounced with increased n, and n changes between
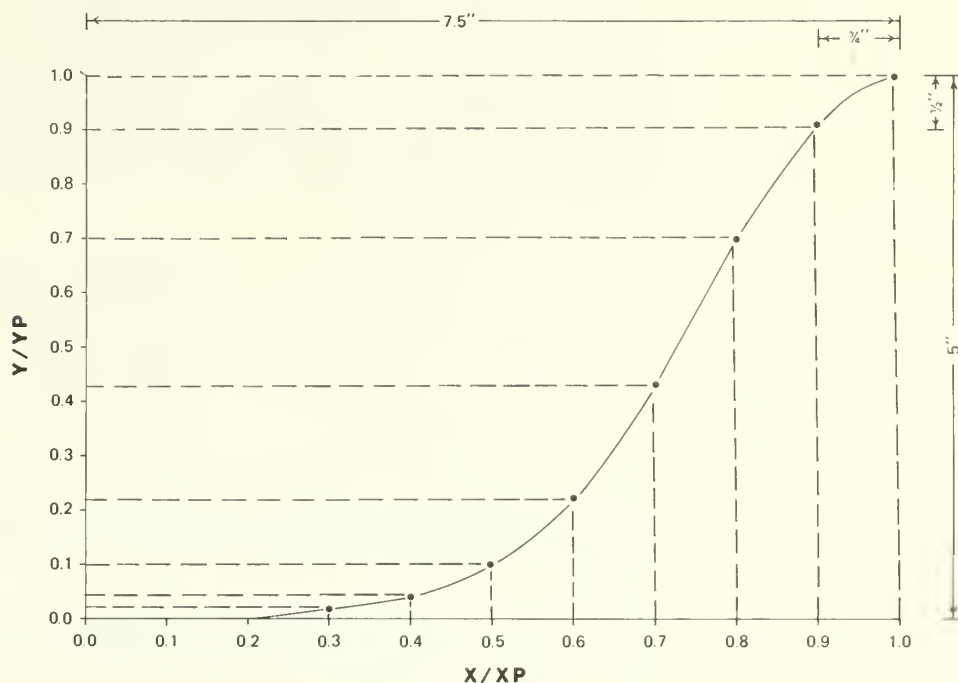
Figure 19.—The plotted overlay points.
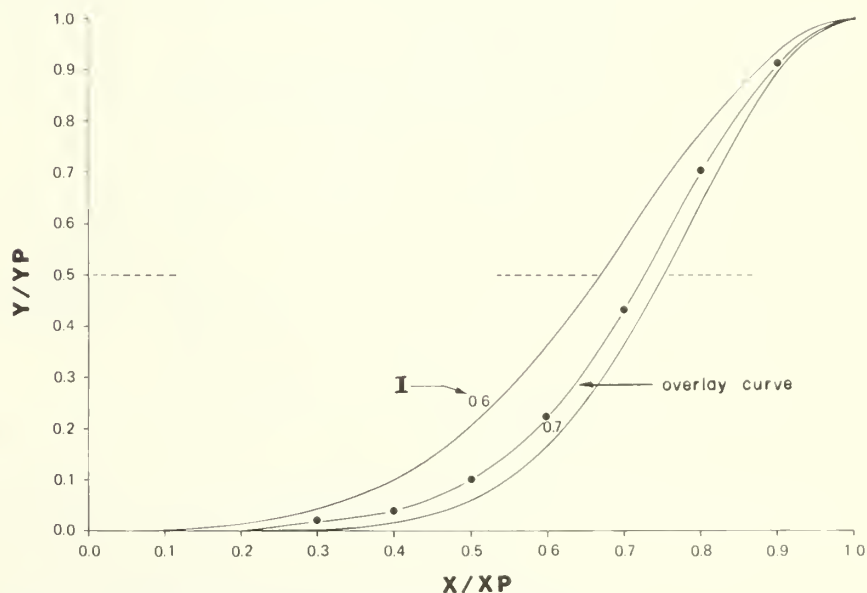
Figure 20.—The Standards of set ($n = 2$) are best matched to
the original curve. Several adjoining curves of this set
bracket the overlay curve.

pages of the Standards. There are nine sigmoids on each of the 10 graphs. In this case,
the sigmoids $I = 0.6$ and 0.7 (fig. 20) bracket the overlay curve nicely.

Having found an acceptable pair of adjoining sigmoids that bracket the overlay curve,
the analyst can interpolate between the proportional inflection points they represent and

thus select a sigmoid more nearly matching the hypothesis. Proportional horizontal departure of the overlay curve from the left bracketing sigmoid at $Y/YP1 = 0.5$ can be used as the basis for interpolation. In figure 20, the overlay curve lies at about the 70 percent point between inflection points 0.6 and 0.7; so the interpolated $I = 0.67$. (This same interpolating principle can also be used between Standards of different sets for refined "n" estimates as the need arises.) Then substituting in the parent e^{-K}-equation, we have:

$$e^{-K} = \left\{ \frac{e^{-\left|\frac{\frac{X}{XP}-1}{1-I}\right|^n} - e^{-\left\{\frac{1}{1-I}\right\}^n}}{1 - e^{-\left\{\frac{1}{1-I}\right\}^n}} \right\} = \left\{ \frac{e^{-\left|\frac{\frac{X}{150}-1}{.33}\right|^2} - e^{-\left\{\frac{1}{.33}\right\}^2}}{1 - e^{-\left\{\frac{1}{.33}\right\}^2}} \right\}$$

This is easily programed on a small desk-top computer (with the number of steps required generally being less than 100) and solved for $\hat{Y}1$-values at control-point $X1$-values.

• Column 7: e^{-K} (ranging only from 0 to 1) is scaled to the graphed hypothesis by simply multiplying e^{-K} by $YP1$ ($= YP$ here), the height of the sigmoid at its peak. Adding the intercept a, produces $\hat{Y}1$.

• Column 8: The selected sigmoid is reasonably close to that of the hypothesis with a slight surplus of positive values ($+0.6$), as shown. In the light of the Y-values involved (100, 430, 700), the departures $+0.6$, $+7.5$, and -7.4, respectively, are small and this sigmoid would most likely be adopted. But, as might be more appropriate in other cases, computer iteration can be used to select an even closer e^{-K}-approximation of the hypothesized sigmoid.

• Columns 9 and 10: $\hat{Y}2$ and its performance are slightly better at $I = 0.6701$. Assuming this to be the final form adopted, we have:

$$\hat{Y}2 = 0 + 1000 \left\{ \frac{e^{-\left|\frac{\frac{X}{150}-1}{0.3299}\right|^2} - 0.001}{1 - 0.001} \right\}$$

And, since the right numerator is very small and the denominator approaches 1.0,

$$\hat{Y}2 = 0 + 1000 * e^{-\left|\frac{\frac{X}{150}-1}{0.3299}\right|^2}, \text{ the final hypothesis.}$$

Note that at the scale shown in figure 21, differences between the graphed hypothesis and $\hat{Y}2$ are not discernible.

This example produced a closer mathematical match for the objective curve than one might expect on the average, but serves to demonstrate the procedures very well. As a
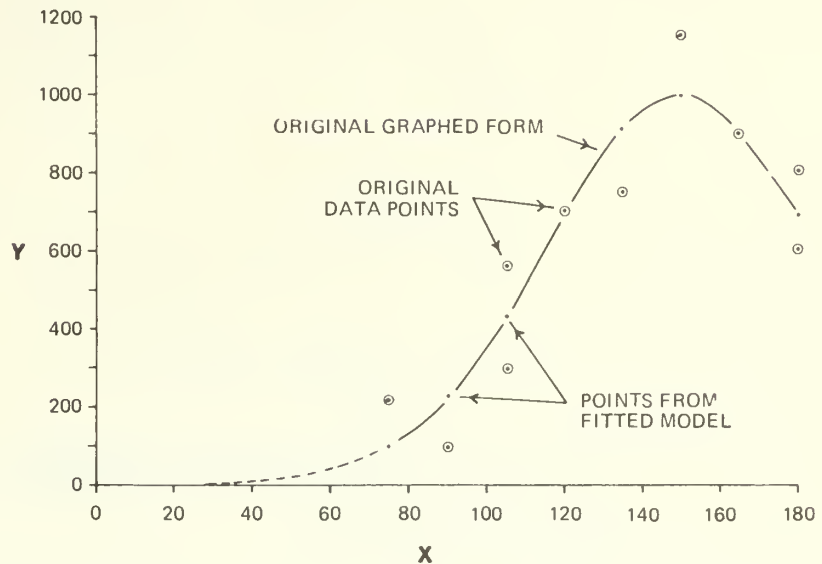
Figure 21.—Points from the fitted model have been plotted over the original graphed form.

matter of fitting methods interest, the hypothesis was then fitted by least squares (forced through the origin) back to the data from which it was partially derived.

And: $\hat{Y} = cXT,\ XT = 1000 * e^{-\left|\dfrac{\frac{X}{150} - 1}{0.3299}\right|^2}$,

$c = (\Sigma(XT)Y)/\Sigma(XT)^2 = \ \ 0.9960$ or ,

almost no change.

$$\hat{Y} = 0.9960 \left\{ 1000 * e^{-\left|\dfrac{\frac{X}{150} - 1}{0.3299}\right|^2} \right\},$$

which again, is not distinguishable from the hypothesis at the scale shown in figure 21.

While this result shows the development process has not deteriorated the fit of the hypothesis to the source data, statistical evaluation should be reserved for a new data set. The same fitting procedures are applicable.

Alternative Arrangements in Space

Unique spacial arrangement of the bell-shaped or sigmoidal form may necessitate adjustment of the Y-values for an intercept and/or manipulation of the X-scale to shift the objective figure to the upper right quadrant (like the Standards). Commonly encountered spacial alternatives and associated shifting techniques are shown in figures 22–26 which follow.
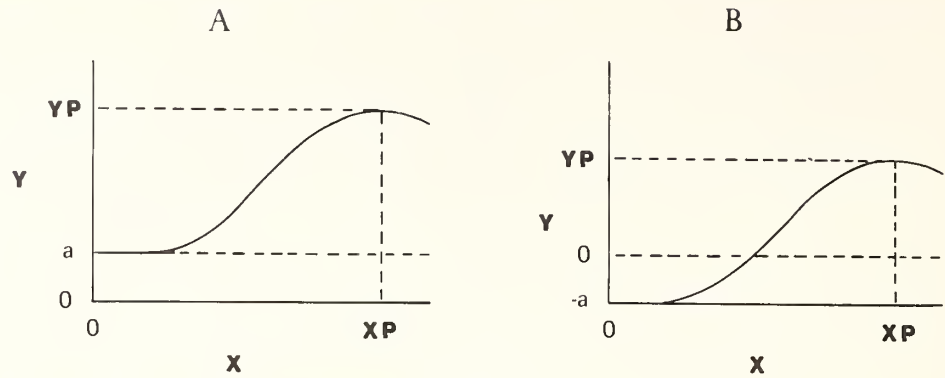
Figure 22.—Intercepts other than zero.

- Here, the sigmoid never drops below the intercept a, regardless of whether a is positive (fig. 22A) or negative (fig. 22B) and is suitably adjusted by (Y-a), as shown at the top of column 4, table 9.

Given the same hypothesis,

$$\hat{Y} = 0 + 1000 * e^{-\left|\dfrac{\dfrac{X}{150} - 1}{0.3299}\right|^{2}}$$

, but with a being a constraint other than zero, the fitting process is identical to the one just specified. If, for example, the fixed $a = -20$, the final form would be:

$$\hat{Y} = -20 + 0.9960(1000 * e^{-\left|\dfrac{\dfrac{X}{150} - 1}{0.3299}\right|^{2}}), \quad 0 \le X \le (2XP = 300).$$

Where a is *variable* (not fixed), use linear curve-fitting techniques to estimate both a and b in

$$\hat{Y} = a + b(1000 * e^{-\left|\dfrac{\dfrac{X}{150} - 1}{0.3299}\right|^{2}}).$$

Then, letting $X = 1000 * e^{-K}$, as above, $b = \Sigma xy/\Sigma x^2$ and $a = \bar{Y} - b\bar{X}$, as in conventional notation.
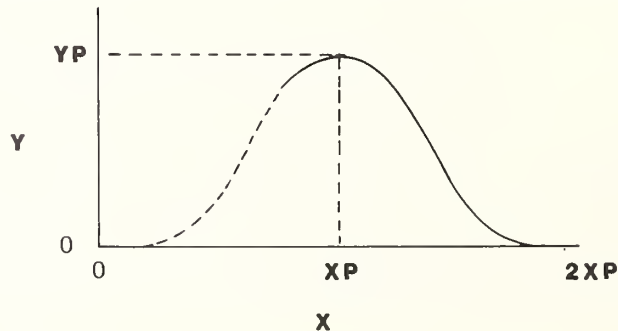

Figure 23.—Right half of implied bell-shaped curve specified.

• Plot the mirror image of the right side over the range $0 \leq X \leq XP$ and identify an appropriate sigmoid using X- and Y-values from that range, as in table 9. The sigmoid adopted will apply equally on either side of XP.
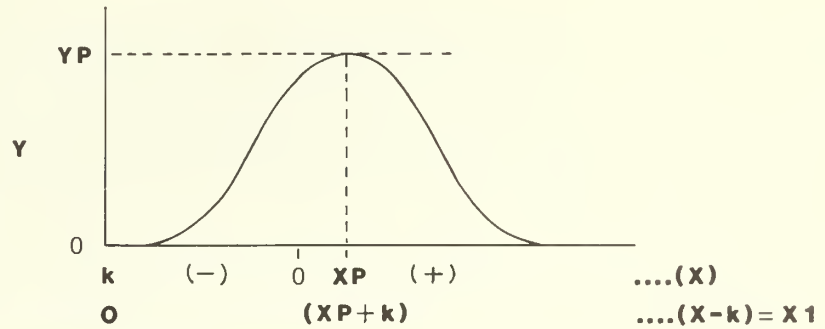
Figure 24.—$X = 0$ included in the range $XP \pm XP$.

• Substitute $X1 = (X - k)$ for X in the range $XP \leq X \leq (XP + k)$. Then follow table 9 procedures to identify an e^{-k}-sigmoid for the left side of the bell-shaped curve (= right side by virtue of symmetry here.)
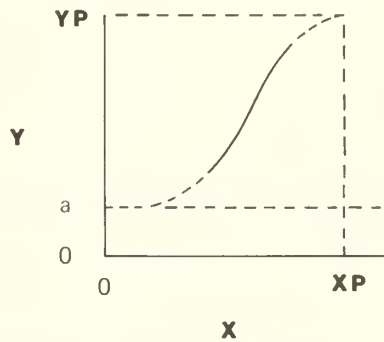
Figure 25.—Incomplete sigmoid specified.

• Complete the implied sigmoid in accord with expectation and identify e^{-k} as in table 9. The hypothesis would be presumed to apply in the range $0 \leq X \leq XP$.

Figure 26.—Inverted bell-shaped curve, or portion thereof.

27

- Plot the negative departures of the curve from the intercept as positive departures on the intercept, that is, rotate the curve upward about a. Identify the appropriate sigmoid as shown previously and finally, $\hat{Y} = a - YP * e^{-K}$

Using Applicable parts of e^{-K}-curves
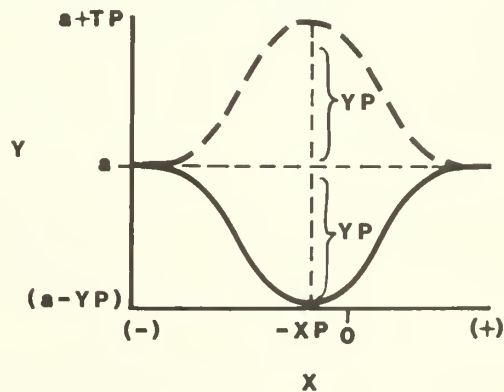
On occasion, the added effort required to compile a multi-component descriptor can be avoided by utilizing a portion of a single-component curve.

Assume the curve in figure 27A is to be described mathematically and that no satisfactory matching curve has been found using X^n. As an alternative, the analyst could undertake a multiple-component description, but another single-component possibility exists.

(A)

(B)

(R)

$Y =$
$(R + 500)$ (R)
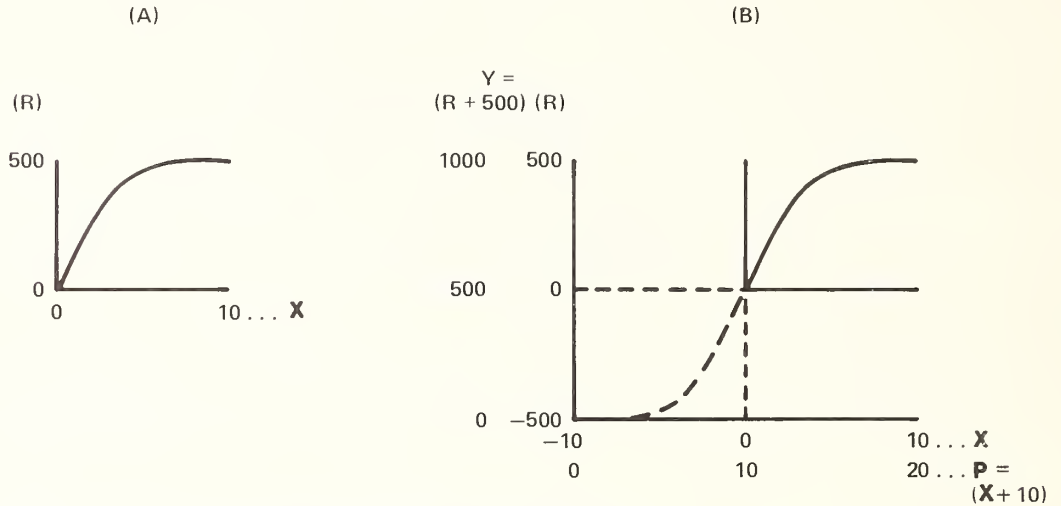
Figure 27.—Using the upper half of a sigmoid: (A) the problem, and (B) a solution.

- Extend the desired curve in figure 27A such that the resulting form approximates that of a sigmoid. Add a constant to the abscissa such that $XP \pm XP$ covers the pertinent range of X. $(X + 10)$ turns the trick here. Also, add a suitable constant, 500 in this case, to R to shift the entire sigmoid vertically to the upper-right quadrant. For representative points from the right half of this curve (for example, figure 27B), construct an overlay curve and find a matching Standard for the upper half of the overlay. The adopted single-component Standard fitted to the X- and Y-values then represents the original curve in the region $0 \leq X \leq 10$. The resulting descriptor is

$$Y = 1000 * e^{-K} - 500, \ 0 \leq X \leq 10,$$

or

$$Y = 1000 \left\{ \frac{e^{-\left| \frac{\frac{(X+10)}{20} - 1}{1 - I} \right|^n} - e^{-\left(\frac{1}{1-I} \right)^n}}{1 - e^{-\left(\frac{1}{1-I} \right)^n}} \right\}.$$

- Procedures for any fraction of any form are analogous.

Notes on e^{-K}

There may be cases where the e^{-K}-transform determined from the Standards is not sufficiently accurate for the purposes of the analyst. In such cases, curve-form description procedures beyond the scope of this paper must be used.

The portion of the curve to the right of XP is a mirror image of the left in e^{-K}. Once n and the proportional inflection point, I, have been selected and held constant, changes in Y values depend only on departure of X/XP from 1.0. Equal departures on opposite sides of 1.0 will result in equal Y-values. For the occasions when the analyst's curve is bell shaped and symmetrical, we really need only identify the e^{-K}-transform for one side (left), as for figure 18 and in table 9 procedures.

Every e^{-K}-transform is forced to zero at $X = 0$ and at $X = 2XP$ and should only be used within these limits (appendix, e^{-K} DERIVATION).

Multiple-Component Descriptors

When a suitable match for a graphed two-dimensional hypothesis of the X^n-class cannot be found in the X^n-Standards, more satisfactory descriptors can often be developed by matching unique portions of the curve sequentially and adding descriptors for the parts to arrive at the whole. Also, development of descriptors for contiguous segments of the X-axis constitutes another flexible alternative.

One example, a commonly encountered kind of curve form that departs from the single-component Standards of the X^n-class, is represented by the graphed hypothesis in figure 28.
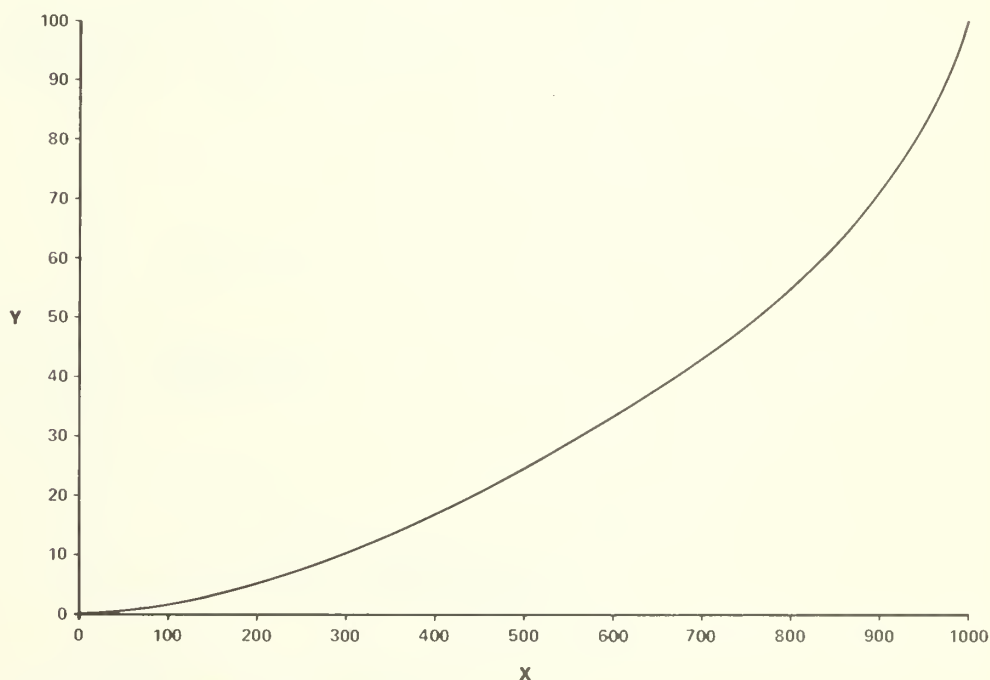

Figure 28.—A graphed hypothesis.

Assume this is the curve to be described. The discerning analyst will immediately reject it as a single-component X^n form because of the second pronounced bend in the range $700 \leq X \leq 1000$. But, let us run it through the X^n-single component procedures to provide a contrast for the two-component form to be developed subsequently.

Control points for the curve are normalized in table 10 and are replotted as a 5- by 7.5-inch overlay curve the same size as the Standards (fig. 29).

Table 10.—Normalized control points for figure 28

Control points		X =	(Y − a) =	Overlay control points	
X (1)	Y (2)	X1 (3)	Y1 (4)	X1/XP1 (5)	Y1/YP1 (6)
0	0	0	0.0	0.00	0.00
200	5.2	200	5.2	.20	.05
400	17.0	400	17.0	.40	.17
600	33.5	600	33.5	.60	.34
700	43.0	700	43.0	.70	.43
800	54.8	800	54.8	.80	.55
900	71.1	900	71.1	.90	.71
1000	100.0	1000	100.0	1.00	1.00
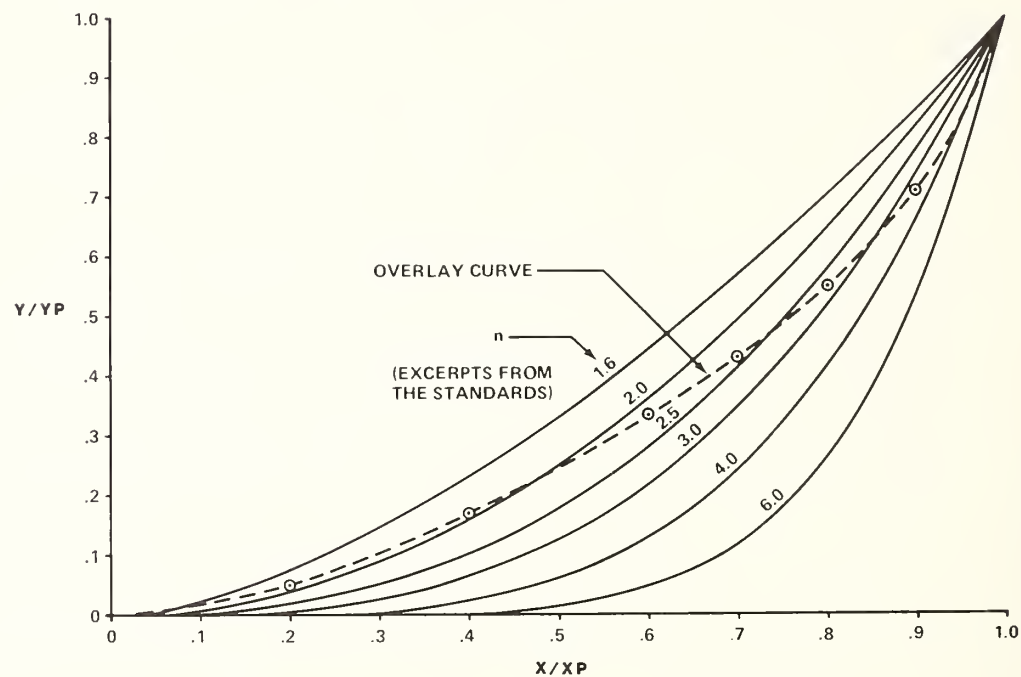
Figure 29.—Overlay curve for entire X-range compared to the X^n-Standards.

There is no suitable match for the overlay curve in the X^n-Standards; so we resort to description of the graphed curve with two components. The first component covers the range $0 \le X \le 700$ since that portion of the curve in figure 28 has only one point of bend and seems reasonably similar in conformation to the X^n-Standards. Next, X and Y are scaled to 1.0 at $X = 700$ (table 11, columns 1–4).

Table 11.—Mathematical hypothesis development

X =	(Y − a) =	Overlay control points 1st portion		† $bX^{1.65}$	Perform- ance of $\hat{Y}1$	Overlay control points 2nd portion		†† $cX^{12.5}$	Perform- ance of $\hat{Y}2$
X1 (1)	Y1 (2)	X1/700 (3)	Y1/43.0 (4)	$\hat{Y}1$ (5)	$(\hat{Y}1 − Y1)$ (6)	X1/1000 (7)	|Col.6|/22.5 (8)	$\hat{Y}2$ (9)	$(\hat{Y}2 − $\|Col.6\|$)$ (10)
0	0.0	0.00	0.00	0.0	0.0			0.0	0.0
200	5.2	.29	.12	5.4	+ .2			.0	− .2
400	17.0	.57	.40	17.1	+ .1			.0	− .1
600	33.5	.86	.78	33.3	− .2			.0	+ .2
700	43.0	1.00	1.00	43.0	.0			.3	+ .3
800	54.8			53.6	− 1.2	0.80	0.05	1.4	+ .2
900	71.1			65.1	− 6.0	.90	.27	6.0	.0
1000	100.0			77.5	− 22.5	1.00	1.00	22.5	.0

† $b = YP1/(XP)^{1.65} = 43.0/(700)^{1.65} = 8.69 \times 10^{-4}$
†† $c = YP1/(XP)^{12.5} = 22.5/(1000)^{12.5} = 7.115 \times 10^{-37}$

After plotting the first-portion overlay curve and comparing it to the X^n-Standards (fig. 30), we find that $X^{1.65}$ gives a good match for the curve in the $0 \le X \le 700$ range. Scaled to 43 at $X = 700$, $X^{1.65}$ gives a fairly close approximation of the $Y1$-values (table 11, column 6). As might be expected, this relatively flat curve is too flat when extended
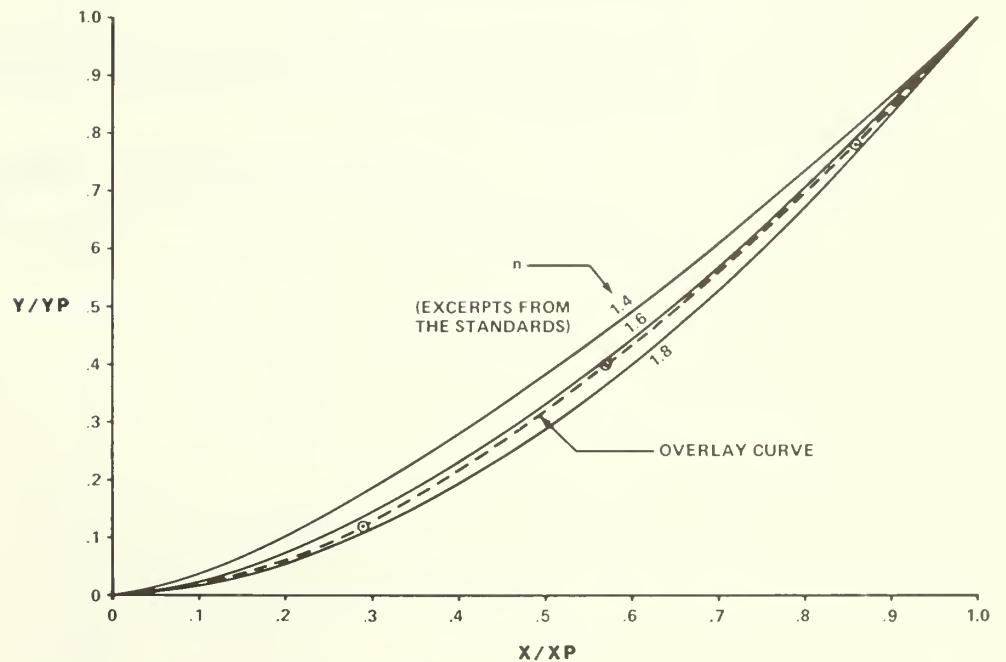

Figure 30.—First-portion overlay curve compared to the X^n-Standards.

to represent the desired curve in the $700 \leq X \leq 1000$ range (column 5). The differences, 1.2, 6.0, and 22.5, represent the curve of values that must still be added to match the right side of the desired curve. Needed in the descriptor is a second component that is essentially zero in the $0 \leq X \leq 700$ range and about equal to the curve of values still needed in the range $700 \leq X \leq 1000$.

Plotting the overlay curve for the second curve portion and comparing it to the X^n-Standards as in figure 31, we find that X^{13} might match the required curve fairly well
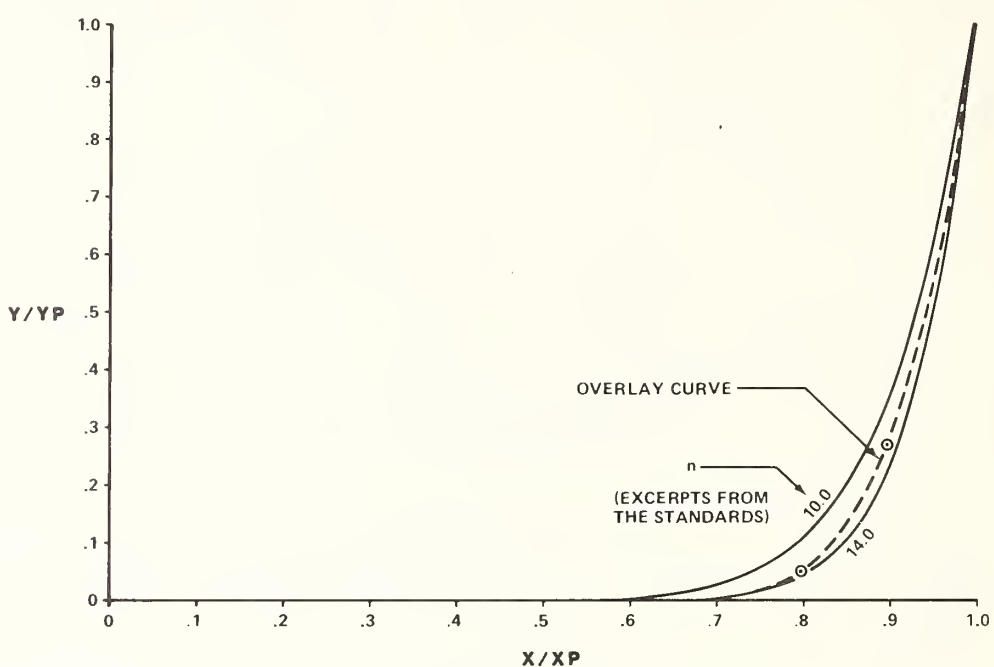
Figure 31.—Second-portion overlay curve compared to the X^n-Standards.

but, on trial, $X^{12.5}$ performs a little better. Scaling $X^{12.5}$ to 22.5 at $X = 1000$ gives values close to those desired in the $700 \leq X \leq 1000$ range (table 11, column 9). Then the complete descriptor is:

$$\hat{Y} = (8.691 \times 10^{-4}) X^{1.65} + (7.115 \times 10^{-37}) X^{12.5},$$

with final values listed in table 12. In this case, $\hat{Y}$ is regarded as being satisfactorily close to Y.

Table 12.—Model performance

X	Y	$\hat{Y}$
0	0.0	0.0
200	5.2	5.4
400	17.0	17.1
600	33.5	33.4
700	43.0	43.3
800	54.8	55.0
900	71.1	71.1
1000	100.0	100.0

The computational ideas just shown are applicable to other curve forms, but a larger array of ideas may be necessary to independent descriptor development efforts by the reader. The examples that follow are presented with decreasing explanatory detail as seems appropriate to the stage of discussion. We will start with an abbreviated version of descriptor procedures just presented in detail for the hypothesized curve in figure 28.

Two-Component X^n, No Inflection

• Read a set of representative XP points from the graphed hypothesis (fig. 32). Select one X-value in this set, point d, such that the curve over the range 0 to d appears to have about the same general conformation (one point of bend) as the X^n Standards.
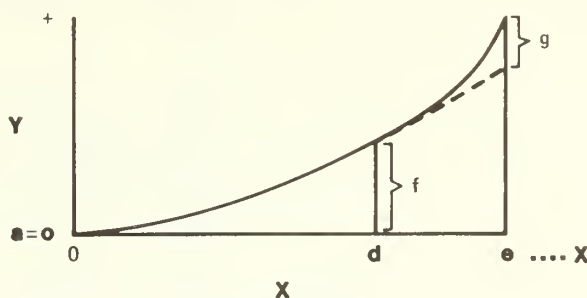

Figure 32.—The graphed hypothesis.

• Compare the corresponding overlay curve with the X^n-Standards and select an appropriate n in X^n.
• Scale X^n to f at d, $b = f/d^n$. Then, $\hat{Y}1 = 2 + bX^n$. Extend $\hat{Y}1$ over the range d to e (dashed line).
• Compare the overlay curve for the exponential curve of residuals over the range 0 to e with the X^n-Standards and select an appropriate m in X^m.
• Scale X^m to g at e, so that $c = g/e^m$. Then, $\hat{Y}2 = cX^m$.
• Add components $\hat{Y}1$ and $\hat{Y}2$. Then, $\hat{Y} = a + bX^n + cX^m$, and $a = 0$.

Alternative orientations of the above curve in space can be handled simply, as specified earlier in the section entitled "TWO DIMENSIONS".

Two-Component X^n, with Inflection

Figure 33 is a variant of the preceding sample. All steps of the descriptive process still apply, except that the second component is subtracted from the first. Then,
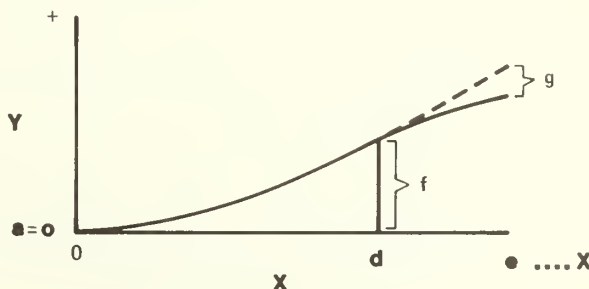
$$\hat{Y} = a + bX^n - cX^m.$$

Figure 33.—The graphed hypothesis.

Again, alternative orientations of this curve in space can be handled as specified in the X^n-text, along with appropriate changes in sign for the last component.

Three-Component, X^n, with Flat Central Segment

The descriptor for a curve that has an extended flat midsection (fig. 34) can be treated as follows:

• Determine the intercept, a, by graphic extension of the flat segment. Calculate the slope of the line. Then,
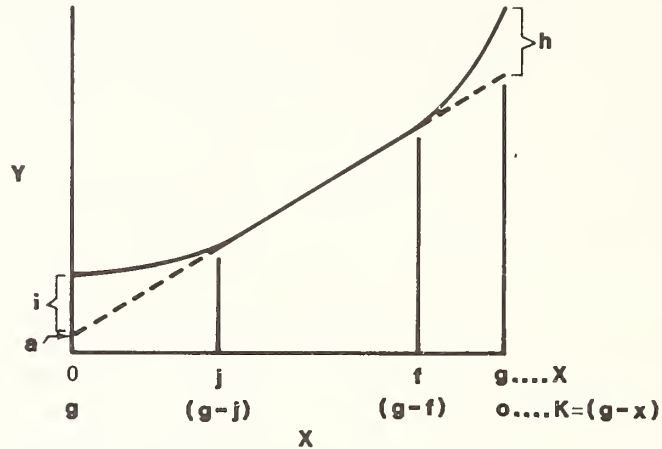$$\hat{Y}1 = a + bX.$$

Figure 34.—The graphed hypothesis.

• Determine the residuals of the curve from the straight line for representative points over X. Include three or four such points at each end of X, where the curve bends away from the straight line.

• For the right-end departures, plot an overlay curve and compare to the X^n -Standards. Find a suitable n in X^n and scale X^n to h at g, wherein $c = h/g^n$. Then,
$$\hat{Y}2 = cX^n.$$

• For the left-end departures, plot an overlay curve and compare to the X^n -Standards. Reverse the X-axis by substituting $K = (f - X)$. Plot the left-end overlay curve and compare with the X^n-Standards. Find a suitable m in K^m and scale K^m to i at j; such that, $d = i/j^m$.

• Then, the left-end descriptor is:
$$\hat{Y}3 = dK^m.$$

Then the entire descriptor is:
$$\hat{Y} = a + bX + cX^n + dK^m, \; 0 \le X \le g.$$

Variants from this curve include negative departures from either or both ends of the straight line. In such cases, the signs of the corresponding components simply become negative.

Alternative orientations of this figure in space can be handled as specified earlier in "TWO DIMENSIONS".

Segmentation with X^n

Where X^n does not provide a suitably accurate descriptor for Y over the entire range of X, describing $Y = f(X)$ for each of several contiguous segments of the X-range, will often remedy the problem. In figure 35:

$Y = 1.0 + 6.456 \times 10^{-11} (X)^{5.9}, \; 0 \le X \le 60$, results in departures from the objective curve of from $+0.03$ to -0.07.

$Y = 1.0, \; 0 \le X \le 30$, and

$Y = 1.0 + 5.708 \times 10^{-4} (X - 30)^{2.4}, \; 30 \le X \le 60$, results in departures of only ± 0.01.
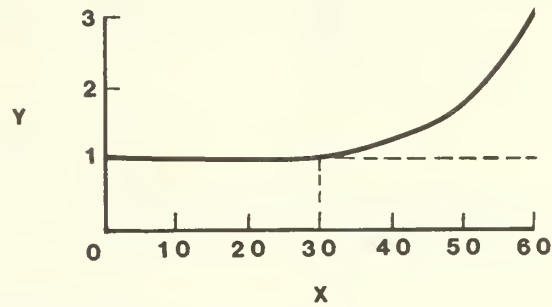
Figure 35.—The graphed hypothesis.

Straight-Line Slopes (X^n, $n = 1$) Plus or Minus Sigmoids

For any curve that has an inflection and a distinctive peak (positive or negative), e^{-k}-sigmoids may be appropriate. (Note that sigmoids may be created with two exponentials of opposite sign, as shown under multiple exponentials with inflection.) Sigmoids are shown here in combination with linear effects for added descriptive power.

In this case (fig. 36), we can use a straight line with slope $b = f/d$. The intercept plus the straight line is $Y1 = a + bX$. Then add to $\hat{Y}1$ a sigmoid matching the curve differences, Yd, from the linear function, scaled to g at the point in X (e here) where Yd peaks. (Follow the methods in table 9.) The sigmoid component is $\hat{Y}2 = ge^{-k}$.
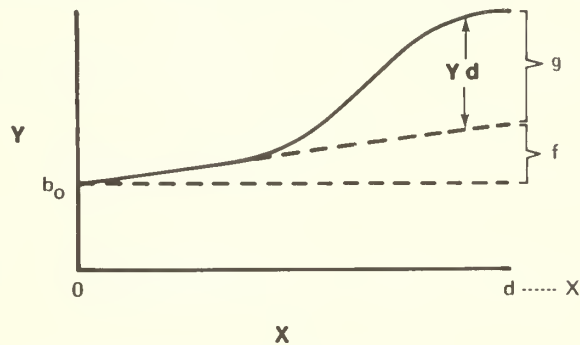

Figure 36.—The graphed hypothesis.

The final descriptor is then:

$$\hat{Y} = a + bX + ge^{-k}.$$

Alternative arrangements of the sigmoid about the straight line would require appropriate treatment (fig. 37a, b, and c).
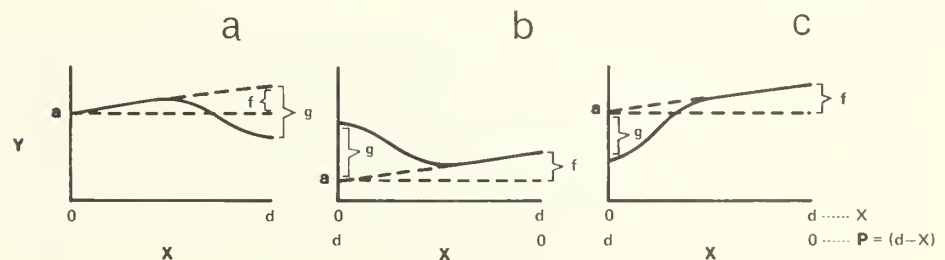

Figure 37.—The graphed hypotheses.

For figure 37a, $XP = d$ in the X-scale and the sign of the sigmoid component would become negative:

$$Y = a + bX - ge^{-K}.$$

For figure 37b, $P = (d - X)$ would be substituted for X in e^{-K}, $XP = d$ in the P-scale, and the sigmoids would be positive:

$$Y = a + bX + ge^{-K}, \, 0 \le X \le d.$$

For figure 37c, again, $P = (d - X)$ is substituted for X in e^{-K}, $XP = d$ in the P-scale, and the sigmoid is subtracted:

$$Y = a + bX - ge^{-K}, \, 0 \le X \le d.$$

The same sigmoid alternatives exist when the slope of the straight line is negative, the only change in the descriptors would be that the sign of the first component would be negative.

X^n, $n > 1$, Plus Sigmoids

Of course, exponentials and sigmoids can be used in combination (fig. 38). Where the left component is an X^n in P, subtracted from a, and the right component is a sigmoid in X added to a, then,

$$\hat{Y} = a - (f/d^n)P^n + ge^{-K}, \, 0 \le X \le d.$$
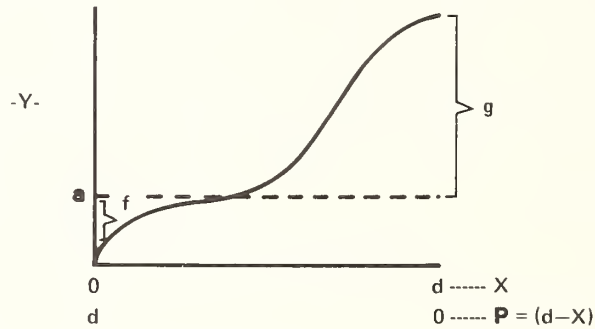
Figure 38.—The graphed hypothesis.

Multiple Sigmoids

Unsegmented

Sometimes the combination of several sigmoidal (upright or inverted) components can be used effectively to describe asymmetrical curves. Each sigmoid is matched and scaled independently and both are summed in the final descriptor.

For figure 39a, $P = (d - X)$ is substituted for X in e_L^{-K}, for the sigmoid to the left of c and e_R^{-K}, the sigmoid to the right of c, is described in the X-scale. $XP = d$ in X, for both X- and P-scales. Then,

$$\hat{Y} = a + fe_L^{-K} + ge_R^{-K}, \, 0 \le X \le d.$$

Figure 39.—The graphed hypothesis.

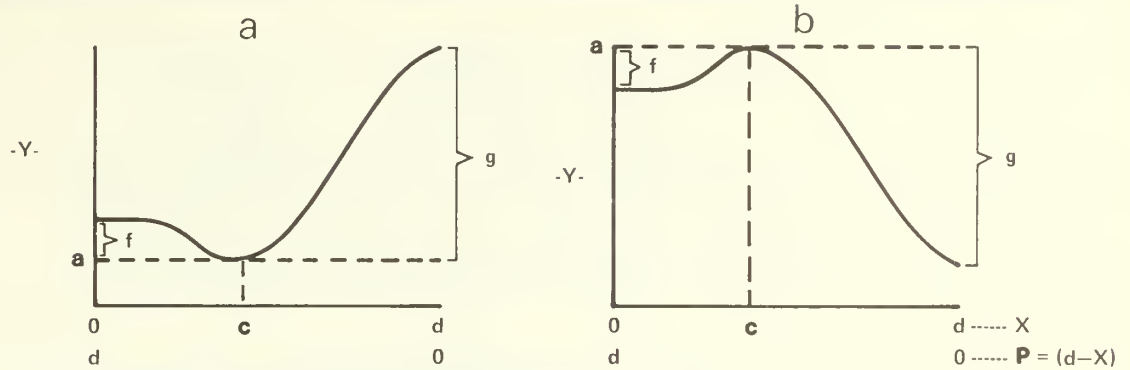For figure 39b, the descriptor is much the same as for figure 39a, but the *a*-value is higher and signs of the sigmoidal effects are reversed. Then,

$$\hat{Y} = a - fe_L^{-K} - ge_R^{-K},\ 0 \le X \le d.$$

Segmented

A simple way of handling asymmetry is to break the X range into two parts, $0 \le X \le XP$, and $XP \le X \le L$ (fig. 40). Identify a suitable sigmoid for each part of the skewed, bell-shaped curve and scale to YP using the X-scale for the left sigmoid and the $(L - X)$ scale for the one on the right. The result is a two-component descriptor

$$\hat{Y} = YPe_L^{-K},\ 0 \le X \le XP$$
$$\text{and}$$
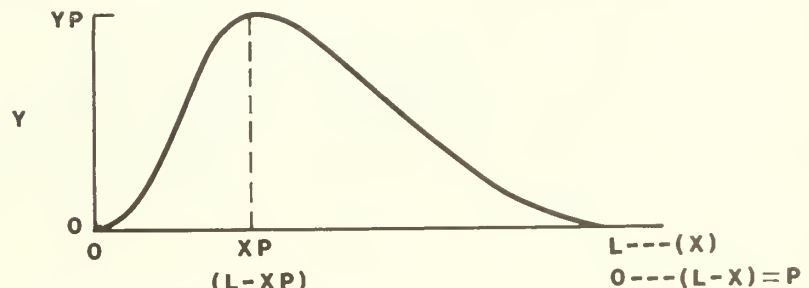$$\hat{Y} = YPe_R^{-K},\ XP \le X \le L.$$

Figure 40.—The graphed hypothesis.

Contiguous Bell-Shaped Curves

Bell-shaped curves, in whole or in part, can be summed in a descriptor. And, for this particular example (fig. 41), the peaks of the two leftmost bell-shaped curves occur at points other than the upper or lower extreme of the X-range, which is not true in previous examples involving sigmoids. A peculiarity of e^{-K} is that its controlled use is within $XP + XP$, where XP is the point in the X-range at which the Y-peak (either positive or negative) occurs, and $XP \pm XP$ are the points at which the tails of the bell-shaped curve drop to zero. Beyond these points, the sigmoid values become negative. Then, where an XP is located in such a way that $XP \pm XP$ does not cover the pertinent range of X, it becomes necessary to alter the X-scale so that it does. The discussion below for the foregoing graph (fig. 41) should clarify both the problem and its solution.
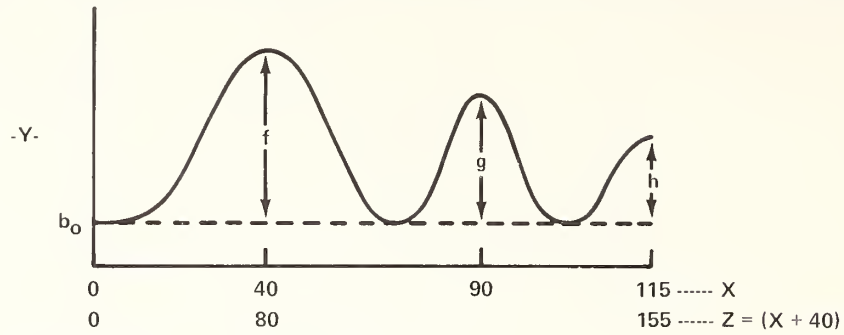
Figure 41.—The graphed hypothesis.

A symmetrical, bell-shaped curve with values ranging from 1.0 at XP to zero at $XP \pm XP$ is specified by e^{-K}. With $XP = 40$ for the first bell-shaped curve, the range of application for e^{-K} is 40 ± 40, or from zero to 80. Beyond $X = 80$, e^{-K} would actually dip below zero by some unspecified amount. The problem is simply remedied by adding a large enough constant to X such that $XP + XP$ in the new scale would cover the original maximum of 115. $P = (X + 40)$ accomplishes this nicely; so the descriptor would be:

For the first curve, $\hat{Y}1 = fe_1^{-K}$, where P replaces X in e^{-K} and $XP = 80$ in P;

For the second curve, $\hat{Y}2^5 = ge_2^{-K}$, where X is used without transformation in e^{-K}, since $XP = 90$ gives an applicable range for X of zero to 180, covering the X-extreme of 115 as required;

For the third curve, $\hat{Y}3 = he_3^{-K}$, where X is also used without transformation in e^{-K} since $XP \pm XP$ (115 ± 115) covers the pertinent range of X, $0 - 115$.

Then, the entire descriptor is:

$$\hat{Y} = a + fe_1^{-K} + ge_2^{-K} + he_3^{-K}, 0 \le X \le 115$$

where: e_1^{-K} involves P
e_2^{-K} involves X
e_3^{-K} involves X.

38

MATHEMATICAL DESCRIPTION OF GRAPHED HYPOTHESES – THREE DIMENSIONS

To reiterate what has been said prevously, the analyst's capability for developing sensitive multidimensional hypothesis models depends large on his or her 2-D talents. The examples shown here should provide enough procedural background to permit intuitive extension of the system to include more flexible curve-form alternatives. The **live** data examples included, serve to reinforce these ideas through application under real data circumstances.

Outline for "THREE DIMENSIONS"
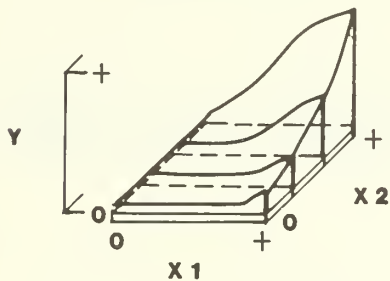
Asymmetrical Bell-Shaped Ridge Over $X1$, with Moving Peak in $X2$. This is Described in Two Segments and Interacts with a Sigmoidal $X2$-Effect.

Asymmetrical Bell-Shaped Ridge Over $X1$, with Moving Peak in $X2$. This is Described in Three Segments and Interacts with a Sigmoidal $X2$-Effect.
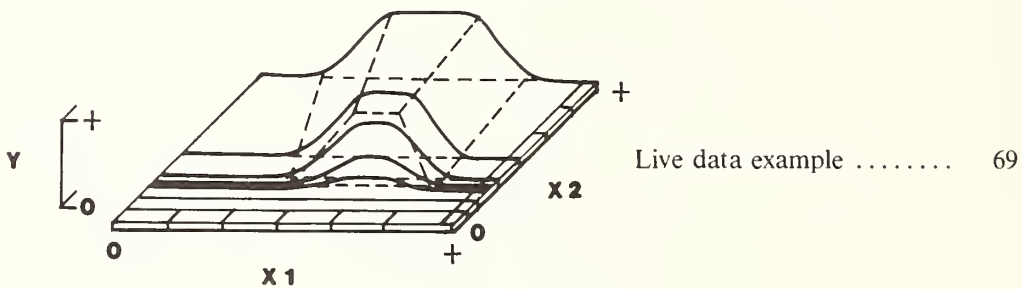
Symmetrical, Inverse Bell-Shaped Ridge Over $X1$, with Constant Point of Minimum in $X1$ and Interacting with a Concave-Upward $X2$-Effect.
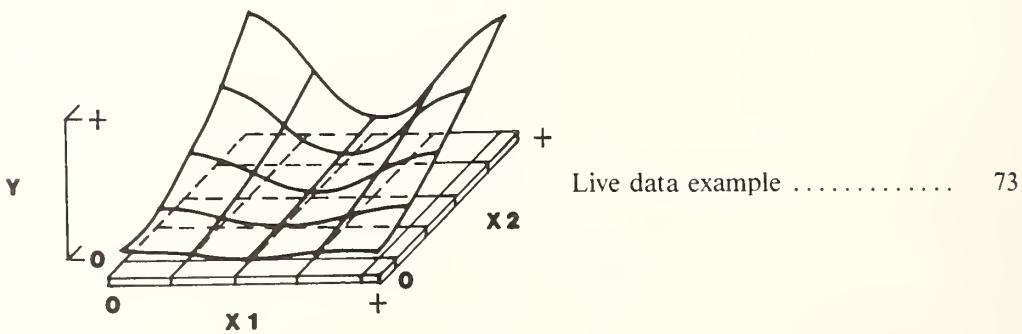
Concave-Upward Relation in Two Dimensions, with Constant Point of Peaking in $X1$ Over $X2$.
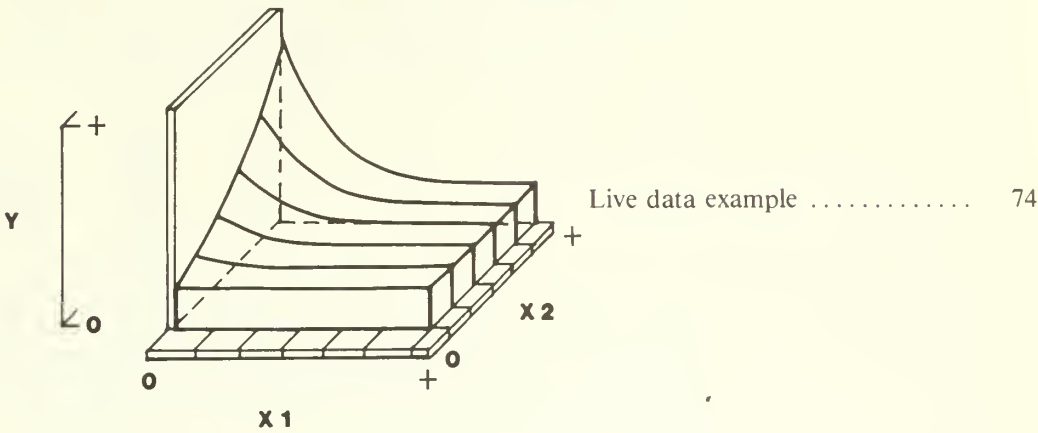
Sigmoidal $X1$-Effect, with Constant Point of Peaking in $X2$ and Interacting with a Concave-Upward $X2$-Effect
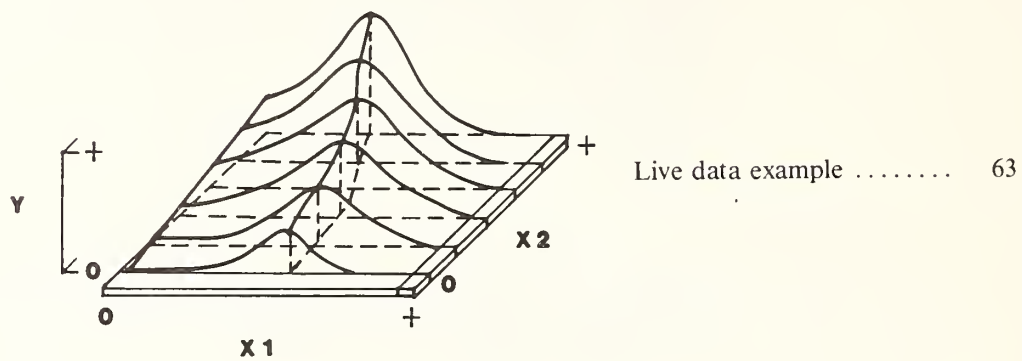
Contrived Example

Given graphed 2-D hypotheses over $X1$ for representative levels of $X2$ (fig. 42), and given the basic 2-D descriptor for the $X1$-effect ($\hat{Y}$ = intercept + scalar($X1$ sigmoid)) for each curve of the set, the analyst is in a position to formulate a descriptor for the implied surface. He simply expresses the changing intercepts, scalars, and parameter(s) of the $X1$-sigmoid in terms of $X2$ and then substitutes appropriately in the basic 2-D descriptor. Pertinent information for the four sigmoid curves above has been assembled in table 13, columns 1–6, by using information read directly from the graphs along with the X^n- and e^{-K}-Standards:
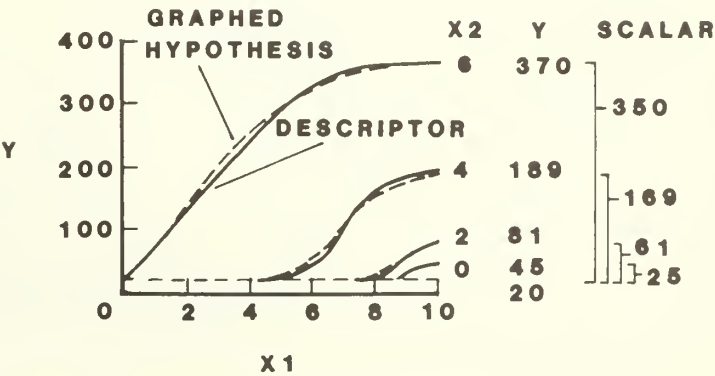
Figure 42.—The graphed hypothesis and descriptor performance.

Table 13.—Mathematical hypothesis development

	Sigmoid parameters						
$X2$ (1)	intercept (2)	XP (3)	n (4)	I (5)	scalar (6)	$\hat{I}$ (7)	scâlar (8)
0	20	10	3.0	0.90	25	0.900	25.0
2	20	10	3.0	.87	61	.870	61.1
4	20	10	3.0	.66	169	.663	169.4
6	20	10	3.0	.10	350	.100	350.0

Here, the intercept and sigmoid parameters, XP and n, are constant over $X2$, but the scalar increases and I decreases exponentially with increasing $X2$-values. Using the X^n-Standards, $\hat{I} = 0.9 - 0.003704(X2)^3$ and scâlar $= 25 + 9.028(X2)^2$. These estimators perform rather well as may be seen in columns 7 and 8. Then substituting in the basic equation for $\hat{Y}$,

$$\hat{Y} = \text{intercept} + \text{scalar}(X1 \text{ sigmoid}),$$
$$\hat{Y} = 20 + (25 + 9.028(X2)^2)(X1 \text{ sigmoid})$$

where:

$$\text{The } X1 \text{ sigmoid} = \left\{ \frac{e^{-\left|\frac{(X1/10)-1}{1-I}\right|^3} - e^{-\left\{\frac{1}{1-I}\right\}^3}}{1 - e^{-\left\{\frac{1}{1-I}\right\}^3}} \right\}$$

and $\hat{I}$, as specified previously, $= 0.9 - 0.003704(X2)^3$.

Application limits for this hypothesis are $0 \le X1 \le 10$, and $0 \le X2 \le 6$.

By plotting computer solutions for $\hat{Y}$ at pertinent combinations of $X1$ and $X2$, we can see that the descriptor lies quite close to the graphed curves (fig. 42). And, the entire predicted surface appears as follows (fig. 43):

Figure 43.—The mathematical hypothesis.

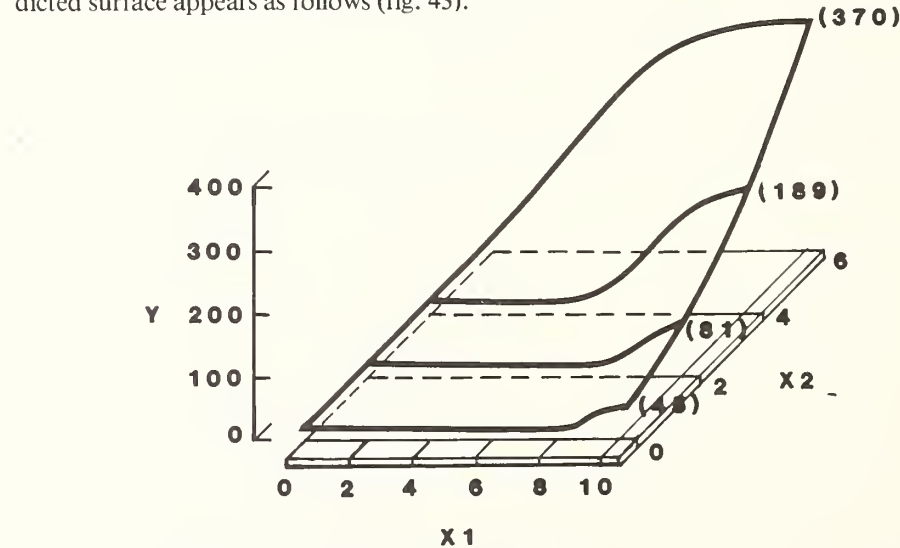Note that the original curves may be given over $X2$ instead of $X1$, in which case, the roles of $X1$ and $X2$ in descriptor development would be interchanged. Also, where multiple-component 2-D descriptors are involved, they are simply incorporated, like the single ones here, in the final descriptor.

This descriptor system is applicable to virtually any surface and is especially useful in emulating strong interactive relationships. An application to a live data set involving such interaction is documented in the next example as a means of demonstrating actual use of some of the 2-D alternatives available to the analyst.

Sigmoidal $X1$-Effect, with Constant Point of Peaking in $X2$ and Interacting with a Concave-Upward $X2$-Effect

Live Data Example

Wildlife managers have expressed interest in the thermal cover provided large game animals by the live crowns of lodgepole pine trees, as reported in Cole, D. M., and Jensen 1981. Related to such cover is the height to base of live crown (HBC) in lodgepole shown in figure 44 where HBC is expressed as a function of the average height of dominant trees (H) in the stand and stand density as reflected in Crown Competition Factor (CCF). This hypothesis reflects the expected effect for CCF, which is positive and sigmoidal, and that for H is positive with no strong expectation as to form.

These expected effects were found to exist in a data set dedicated to the formulation of a mathematical hypothesis for the relation. The 134 observations involved, were sorted into 10-foot height groups wherein HBC was plotted over CCF (fig. 45).

The expected sigmoidal CCF-effect was clearly visible in the data and appeared to break downward from the asymptotes at about the same point in CCF (180–200) for all height groups. The strongest expression of the sigmoidal form appeared to exist in the
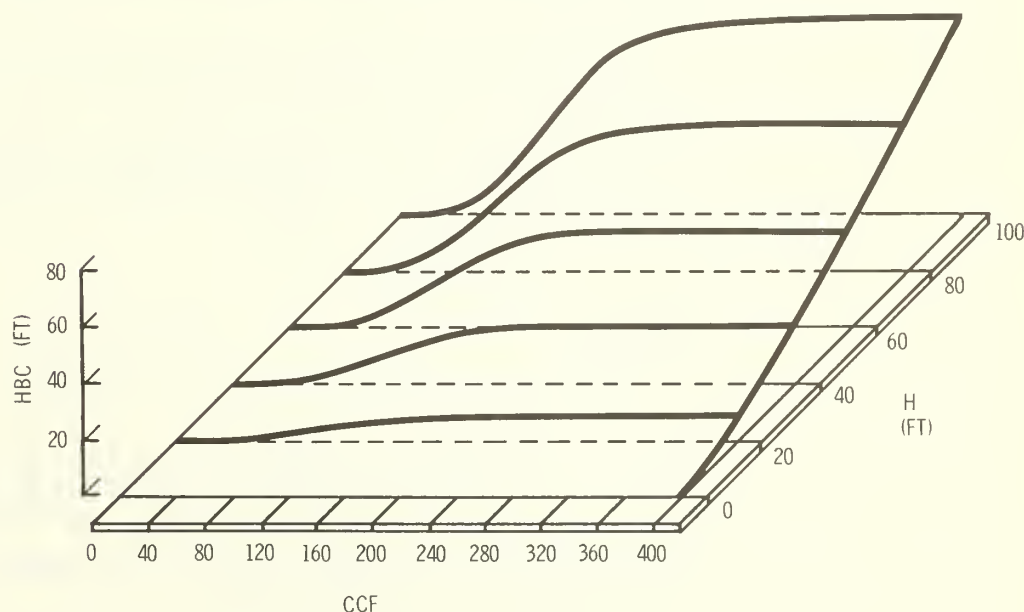
Figure 44.—The mathematical hypothesis.
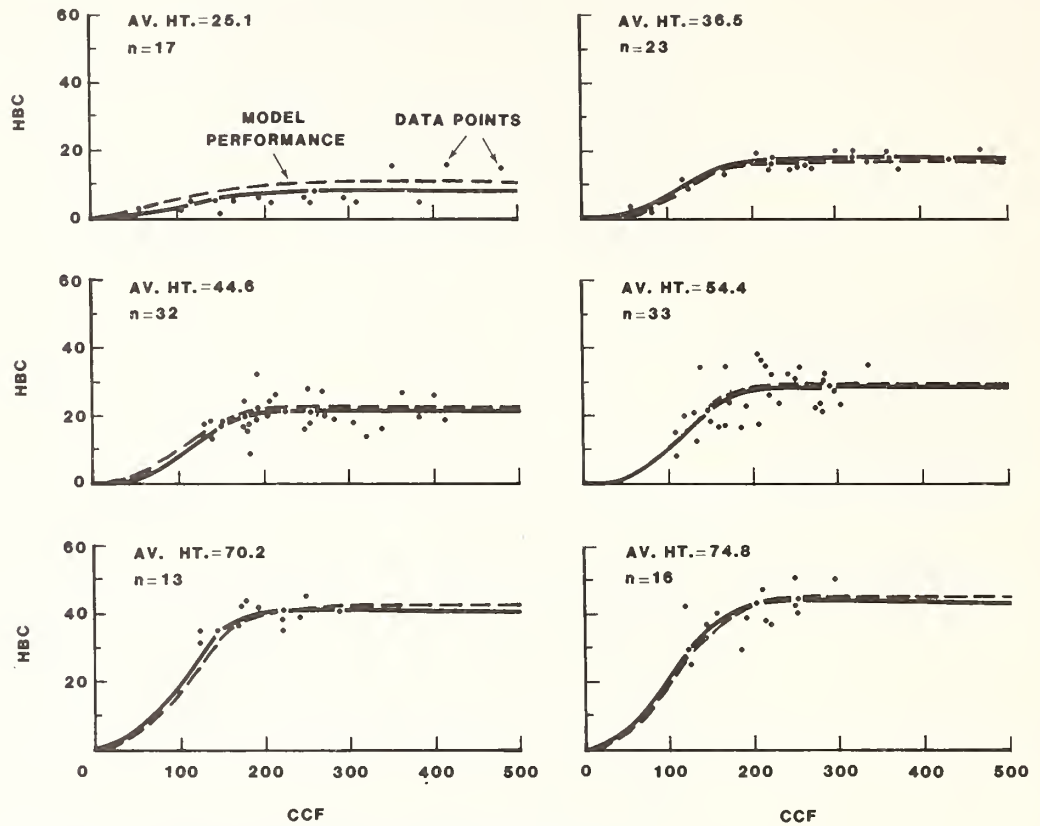
Figure 45.—Graphed hypotheses and model performance for partitioned data.

30- and 50-foot H-groups. Following procedures specified in the TWO DIMENSIONS text, control points were read from the approximate least deviations-fit, smoothed curves, and a specific sigmoidal form for each curve was determined (table 14) using the e^{-K}-Standards.

A single, unchanging sigmoidal form was suitably accurate in describing CCF effects at all heights. While the sigmoid, described by $n = 10$, $I = 0.183$, etc., provided the best match for the curve at $H = 36.5$ and that sigmoid with $n = 10$, $I = 0.190$, etc., was best for the curve at $H = 54.4$. An acceptable compromise was the sigmoid with I held constant at 0.186 (see the last column in table 14). Then, on simplifying,

$$H\hat{B}C = YP * e^{-\left| \dfrac{\frac{CCF}{500} - 1}{1 - 0.186} \right|^{10}},$$

where YP is the scalar for the sigmoids over H. Plotting and smoothing the heights of the graphed sigmoids (YP_i) at $CCF = 500$, a slightly concave-upward curve appears to exist (fig. 46).

Reading control points from the smoothed curve, a matching X^n-function was determined (table 15) from the X^n-Standards.

where, $b = 48.8/(80.0)^{1.37}$, and $\hat{YP} = 0.12056(H)^{1.37}$.

Table 14.—Mathematical hypothesis development

H	control points		Overlay control points		$n = 10, I = 0.183,$ $XP = 500,$ $YP = 18.0,$ $a = 0, HBC1 =$	Performance of HBC1	$n = 10, I = 0.186,$ $XP = 500,$ $YP = 18.0,$ $a = 0, HBC2 =$	Performance of HBC2
	CCF	HBC	CCF/500	HBC/18	$a + YP^*e^{-K}$	$(HBC1 - HBC)$	$a + YP^*e^{-K}$	$(HBC2 - HBC)$
36.5	80	5.0	0.16	0.28	4.8	-0.2	4.6	-0.4
	120	10.1	.24	.56	11.1	$+1.0$	10.9	$+0.8$
	160	16.1	.32	.89	15.3	-0.8	15.3	-0.8
	500	18.0	1.00	1.00	18.0	0.0	18.0	0.0

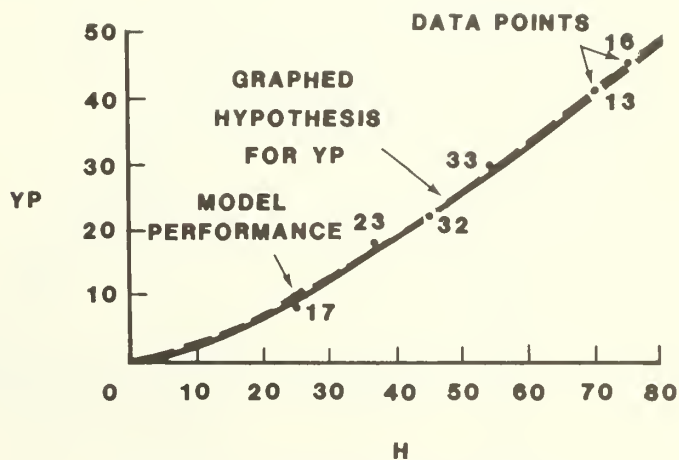| H	control points		Overlay control points		$n = 10, I = 0.190,$ $XP = 500,$ $YP = 29.5,$ $a = 0, HBC =$	Performance of HBC1	$n + 10, I = 0.186,$ $XP = 500,$ $YP = 29.5,$ $a = 0, HBC2 =$	Performance of HBC2
	CCF	HBC	CCF/500	HBC/29.5	$a + YP^*e^{-K}$	$(HBC1 - HBC)$	$a + YP^*e^{-K}$	$(HBC2 - HBC)$
54.4	80	7.7	0.16	0.26	7.0	-0.7	7.5	-0.2
	120	16.3	.24	.55	17.4	$+1.1$	17.8	$+1.5$
	160	25.4	.32	.86	24.8	-0.6	25.0	-0.4
	500	29.5	1.00	1.00	29.5	0.0	29.5	0.0

Figure 46.—Graphed hypothesis and model performance for YP.

Table 15.—Development of $\hat{Y}P$

Control points		Overlay control points		$b(H)^{1.37}$	Performance of $\hat{Y}P$
H	YP	H/80.0	YP/48.8	$\hat{Y}P$	$(\hat{Y}P - YP)$
25.1	9.3	0.31	0.19	10.0	+ 0.7
36.5	16.4	.46	.34	16.7	+ .3
44.6	21.0	.56	.43	21.9	+ .9
54.4	29.4	.68	.60	28.8	− .6
70.2	41.5	.88	.85	40.8	− .7
74.8	44.5	.94	.91	44.5	.0
80.0	48.8	1.00	1.00	48.8	.0

The complete hypothesis is then:

$$H\hat{B}C = (0.12056(H)^{1.37})*e^{-\left|\frac{\frac{CCF}{500}-1}{0.814}\right|^{10}}$$

with limits: $0 \le CCF \le 500$; $0 \le H \le 100$.

The performance of this model on the data from which it was partially derived ($R^2 = 0.87$) is shown as a dashed line within each H-group in figure 45. The final hypothesis presented in figure 44 is produced from model values in table 16.

Table 16.—$H\hat{B}C$ values from the model

AVH	CCF										
	40	60	80	100	120	140	160	180	200	300	500
10	—	—	1	1	2	2	3	3	3	3	3
20	—	1	2	3	5	6	6	7	7	8	8
30	—	2	3	6	8	10	11	12	13	13	13
40	1	2	5	9	12	15	17	18	19	20	20
50	1	3	7	12	16	20	23	25	26	27	27
60	1	4	9	15	21	26	29	32	33	35	35
70	1	5	11	18	26	32	36	39	41	43	43
80	2	6	13	22	31	38	43	47	49	51	51
90	2	7	15	26	36	45	51	55	57	60	60
100	2	8	18	30	42	52	59	64	66	69	70

← †
← †

† Limits within which data were included.

The mathematical hypothesis, then, can be adjusted to data sets from different populations of trees through simple rescaling with $b = \Sigma XY/\Sigma X^2$, as is indicated in the TWO DIMENSIONS text.

Symmetrical Bell-Shaped Ridge Over $X1$ with Moving Peak in $X2$ and Interacting with a Concave-Upward $X2$-Effect

Live Data Example

George and Blakely (1973) reported on the calibration of fire-retardant dispersal from delivery aircraft. On each of 16 passes over a level target area, 600 gal of fire retardant were dropped from an aircraft. Square-foot coverage and volume of material reaching the ground per 100 ft^2 were measured for each aerial drop along with drop height, windspeed, wind direction, aircraft speed, temperature, and humidity. Interest finally centered on the change in coverage of ≥ 2 gal/100 ft^2 over a controlled range of drop heights within a partially controlled range of windspeeds. (The effects of all other variables were either negligible or unidentifiable in this data set).

If the plane were rolling along the ground (drop height = 3 ft) at normal flying speed and in the absence of wind, it would be expected that a 600-gal drop would be distributed over a relatively narrow strip of ground and that the area covered by ≥ 2 gal/100 ft^2 would be held to some nominal value. Increased aircraft (and drop) height should result in greater dispersal; maximum coverage should be reached at some optimal height. As drop height is increased beyond the optimum, dispersal of the retardant from air friction and evaporation should become more complete; coverage should finally reach zero at some relatively great drop height.

So expectation at zero wind is for a bell-shaped curve truncated to the left of the peak. With increasing wind, optimal drop height and peak coverage should diminish, since dispersal of the retardant would be accentuated by the horizontal shearing force of the wind. Thus, the expected surface would be as shown in figure 47.
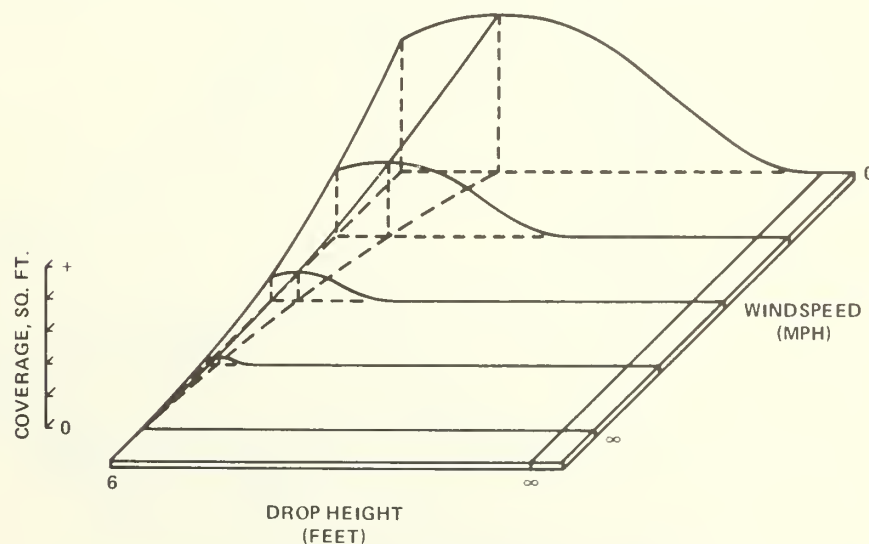

Figure 47.—The general expected relation.

Using these expectations as guides, coverage, C, was curved over height, H, fitting the curves to actual data points by approximate least deviations (Karst 1958) for each of three data groups in wind, W (fig. 48).
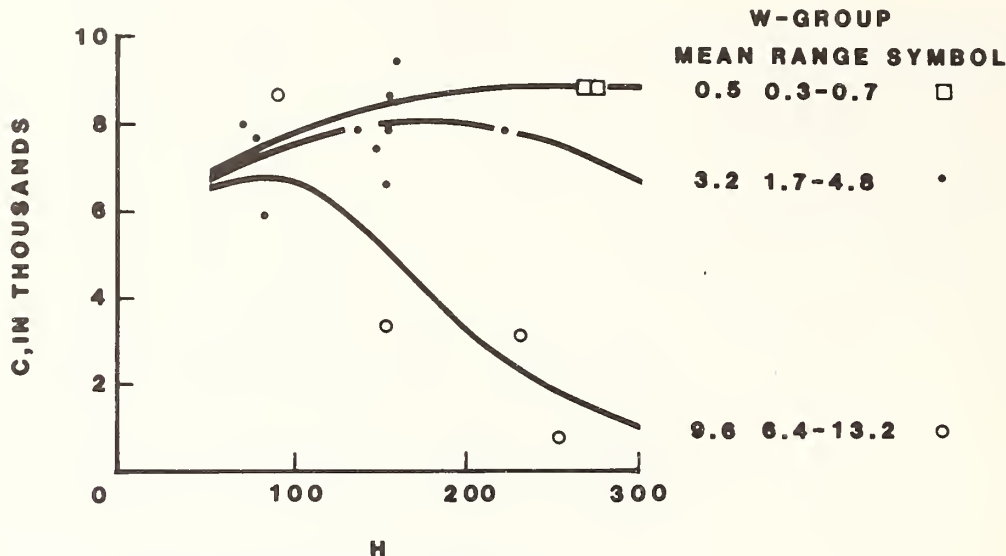

Figure 48.—Expected trends fitted through the data.

These curves, plotted at their respective W-means, were connected over W to form the implied surface, figure 49. And, it can be seen that major features of the expectation are reflected in the data—even within the limited range of H and W.
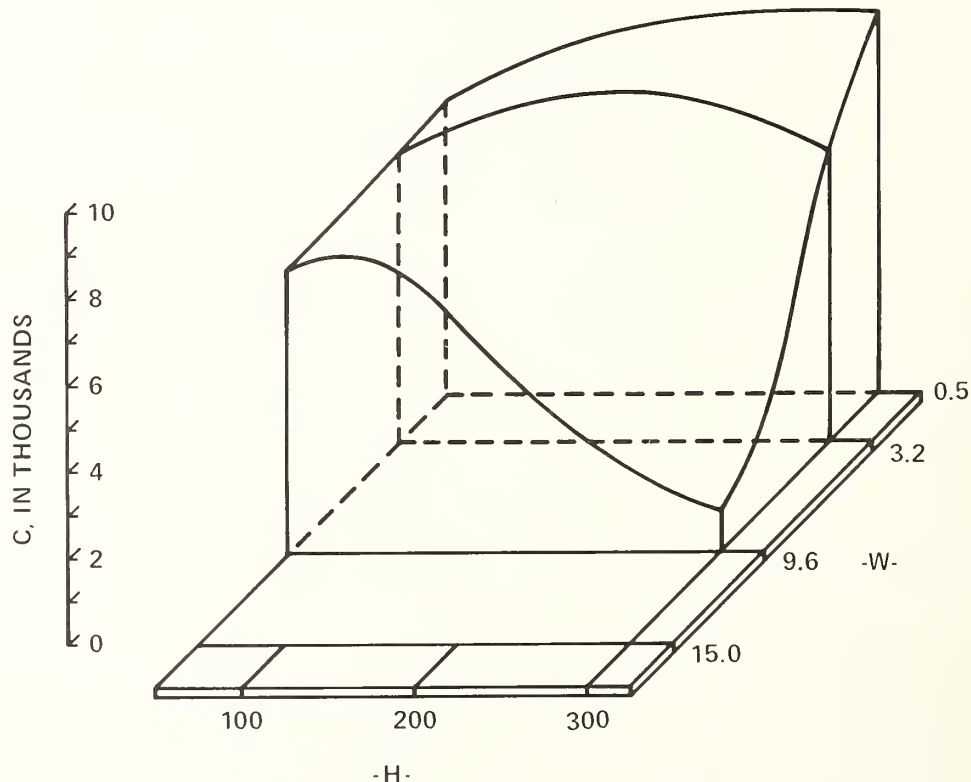

Figure 49.—The graphed hypothesis.

Figure 49, then, is the basic hypothesis for which a descriptor was developed. Assuming that the curves over H (fig. 48) could be suitably represented by segments of symmetrical bell-shaped forms, e^{-K} was deemed applicable and the identification of matching e-transforms was begun.

The e-transform is limited in that it will yield values of from zero to one in the full bell-shaped form only within the range $HP \pm HP$, where HP is the point in H at which the C-values peak. And, it was a unique feature of this example that the maximum H-values for all three curves of the set exceed $2HP$ (fig. 50).
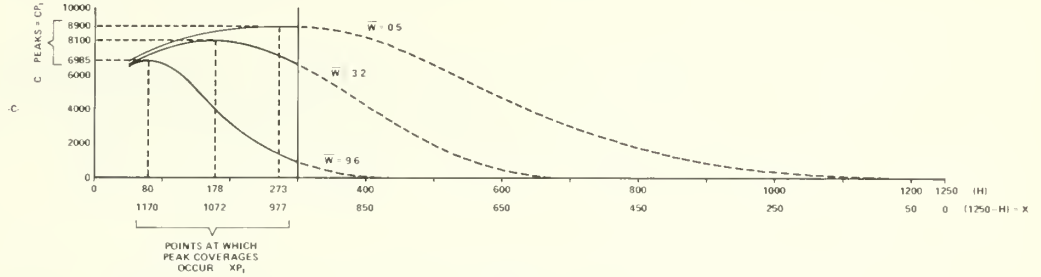

Figure 50.—Graphed trends from figures 49 and 50, extended.

The broadest curve (for $W = 0.5$) was estimated to peak at $H = 273$. In this case, a matching e-transform would have dropped below zero where H exceeded $2HP$, or $2(273) = 546$, long before the approximate graphed limit of $H = 1150$ was reached. One solution here is to reverse the H-scale using as a base, the largest H-value of the broadest sigmoid likely to be encountered in the set of interest. Since an even broader sigmoid than $W = 0.5$ is expected to exist at $W = 0$, the largest H-value is estimated at $1150 + 100 = 1250$. The H-axis is then reversed using $X1 = (1250 - H)$ where, as may be seen in figure 50, $XP1 = 977$, 1072, and 1170 for $W = 0.5$, $W = 3.2$, and $W = 9.6$, respectively. Now, as required for each sigmoid, $XP1 \pm XP1$ includes both the largest and smallest value of $X1$ that will be encountered, and $X1 = (1250 - X)$ is used as the basis for the bell-shaped H-effect descriptor (e^{-K}). The coverage estimator is then specified as,

$$\hat{C} = CP1 \left\{ \frac{e^{-\left| \frac{(X1/XP1) - 1}{1 - I} \right|^{n}} - e^{-(1/(1-I))^{n}}}{1 - e^{-(1/(1-I))^{n}}} \right\}$$

where,

$C =$ coverage in square feet (≥ 2 gal/100 ft)

$X1 = (1250\text{-}H)$

$XP1 =$ the point in $X1$ at which C peaks

$CP1 =$ coverage peak at $XP1$, scalar for the sigmoid

$I =$ the proportional point in $X1$ at which the inflection point of the bell-shaped curve occurs (a) in the range $X1 = 0$ to $XP1$ for the left half of the curve or (b) in the range $XP1$ to $2XP1$ for the right half (fig. 50).

$n =$ the power of the transform that dictates the degree of curvature above and below any inflection point.

Since the $XP1$- and $CP1$-values read from the three curves in figure 50 varied with wind in accord with expectation, they were each expressed as a suitable function of wind. Multiple-component X^n-descriptors were utilized.

$XP1$- and $CP1$- values from the foregoing equations along with representative paired $X1$- and C-values read from the left side of each bell-shaped curve were the basis for overlay curves. Standards for e^{-K} that were suitably similar to the overlay curves were identified, and the corresponding n (held constant) and I-values were recorded. Also, varying over wind in accord with expectation, I was described as a function of wind to complete the inputs to the coverage estimator. The details of these computations follow.

For $XP1 = f(W)$

Paired W- and $XP1$-values (0.5, 977; 3.2, 1072; and 9.6, 1170) were read from figure 50. These points were plotted and a smooth curve was drawn through them (fig. 51) that extended over the relevant range of W (0 – 15 mi/h).
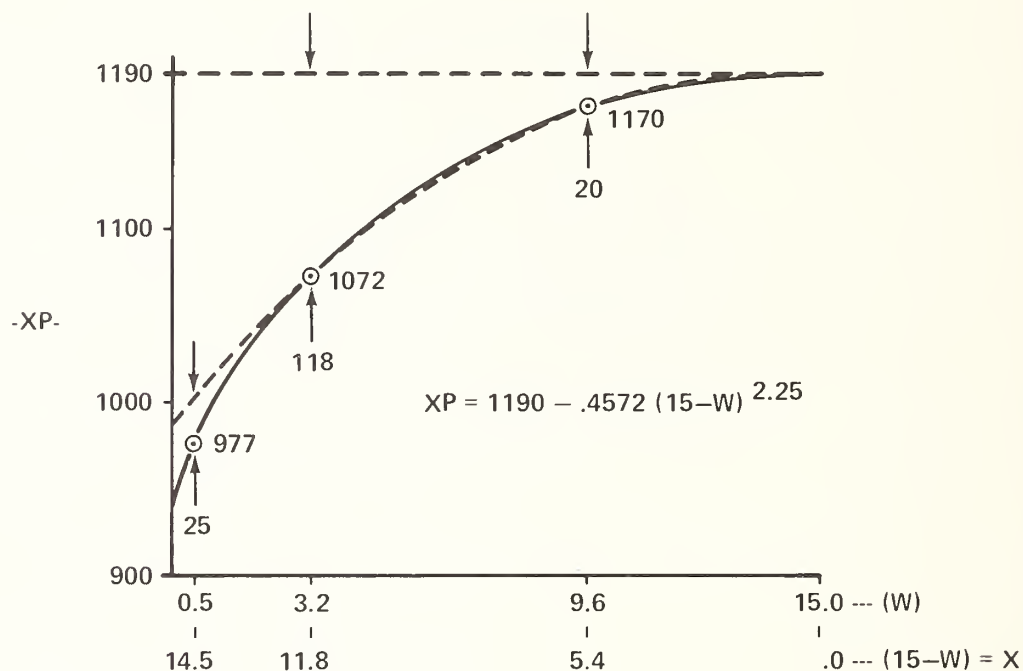

Figure 51.—Describing the XP-hypothesis.

The initial descriptor approach here was to subtract a single-component exponential curve on the reversed W-scale from the intercept, 1190 (table 17, columns 1–7). W was reversed in $X1 = (15 - W)$ to aline large values of the independent variable with those of $XP1$. Next, the three data point $X1$-values and associated coverage differences (absolute) from 1190 were scaled to 1.0 at $X1 = 14.5$. The overlay curve was not well matched by any curve in the X^n-Standards; so a two-component approach was adopted

Table 17.—Descriptor development for $XP1$

W =	$XP1$ =	$(15 - W)$ =	$(1190 - XP1)$ =	Overlay control points 1st segment		† $b(X1)^{2.25}$
X (1)	Y (2)	$X1$ (3)	$Y1$ (4)	$X1/XP1$ (5)	$Y1/YP1$ (6)	$\dot{Y}1$ (7)
0.0	—	15.0	—	—	—	—
.5	977	14.5	213	—	—	188
3.2	1072	11.8	118	1.00	1.00	118
9.6	1170	5.4	20	.46	.17	20
15.0	1190	.0	0	.00	.00	0

$(15 - W)$ =	$(\dot{Y}1 - Y)$ =	Overlay control points 2nd segment		†† $c(X1)^{20}$ =	††† $XP1$ =
$X1$ (8)	$X2$ (9)	$X1/XP2$ (10)	$Y2/YP2$ (11)	$\dot{Y}2$ (12)	(13)
15.0	—	—	—	—	936
14.5	25	1.00	1.00	25	977
11.8	0	.81	.00	0	1072
5.4	0	.37	.00	0	1170
.0	0	.00	.00	0	1190

† $b = 118/(11.8)^{2.25} = 0.4572$

†† $c = 25/(14.5)^{20} = 1.4811 \times 10^{-22}$

††† $XP1 = 1190 - bX1^{2.25} - cX1^{20}$—which gives a perfect match for the original $XP1$-values at control points 0–14.5 in wind.

(table 17, columns 8–13). This time, the differences were fitted at $X1 = 0$, 5.4, and 11.8 to start with (see the dotted line below the intercept, 1190, in figure 51). Then, the difference ($213 - 188 = 25$) between the first-component curve and the desired curve was added in a second component. Computations are summarized in table 17, columns 8–13, and overlay curves are shown in figure 52.
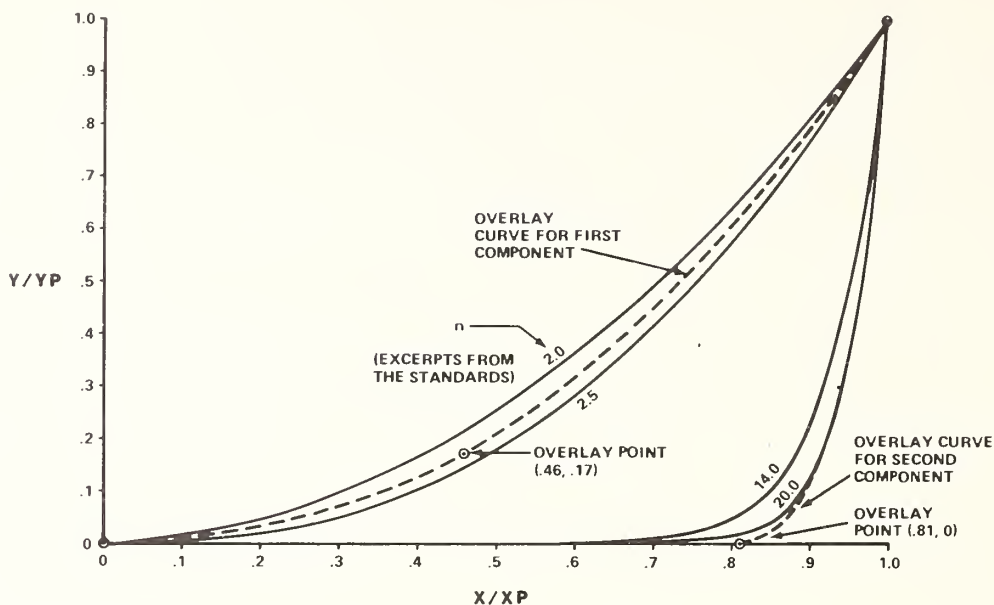
Figure 52.—First- and second-component overlay curves com-
pared to the X^n-Standards.

The completed function was then

$$\hat{X}P1 = 1190 - 0.4572(15 - W)^{2.25} - 1.4811 \times 10^{-22}(15 - W)^{20}, \ 0 \le W \le 15.$$

For $CP1 = f(W)$

Paired W- and $CP1$-values (0.5, 8900; 3.2, 8100; and 9.6, 6970) were read from figure
50. These points were plotted and a smooth curve was drawn through them (fig. 53)
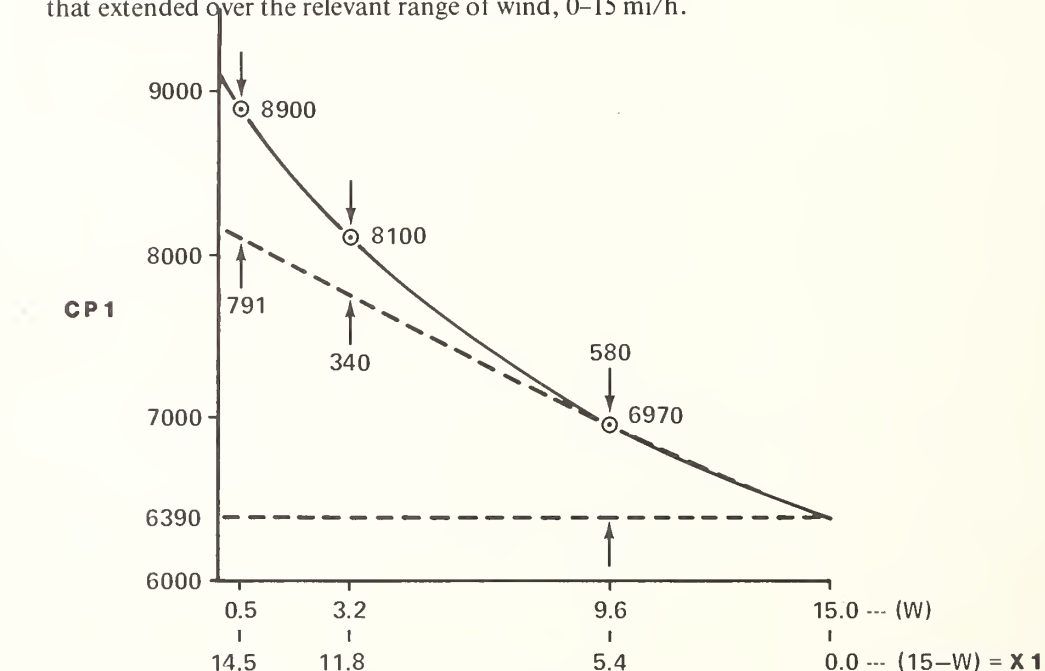that extended over the relevant range of wind, 0–15 mi/h.

Figure 53.—A flat curve, $X^{1.1}$, matches the lower end
$(9.6 \le W \le 15.0)$ of the graphed hypothesis.

Again, a single-component exponential was first tried for the descriptor here (table 18, columns 1–7). Reversing the W-axis to $X1 = (15 - W)$ to aline large values of the independent variable with those of $CP1$, the $X1$- and $CP1$-values were scaled to 1.0 at $X1 = 14.5$. An overlay curve was constructed and compared to the X^n-Standards. But, none of the Standards were acceptably close to the overlay, so a two-component model was tried next (table 18).

To start with, the lower end of the curve ($0.0 \le X1 \le 15.4$) was fitted with an intuitively selected flat form ($X1^{1.1}$); it was obvious without scaling and overlays that the curve was extremely flat in that range of $X1$ (fig. 53). The component $X1^{1.1}$ was then scaled to the difference (580) between the intercept (6390) and the desired curve height (6970) at $X1 = 5.4$. So this first component (table 18, column 7), along with the intercept, 6390, constitutes the partial descriptor:

$$\hat{CP}1 = 6390 + b(X1)^{1.1}.$$

Table 18.—Descriptor development for $\dot{CP}1$

W (1)	CP1 (2)	(15 − W) = X1 (3)	(CP1 − 6390) = Y1 (4)	Overlay control points 1st segment X1/5.4 (5)	Y1/580 (6)	† $bX^{1.1}$ = Ẏ1 (7)
0.0	—	—	—	—	—	—
.5	8900	14.5	2510	—	—	1719
3.2	8100	11.8	1710	—	—	1370
9.6	6970	5.4	580	1.00	1.00	580
15.0	6390	.0	0	.00	.00	0

(15 − W) = X1 (8)	(Y − Ŷ1) = Y1 (9)	Overlay control points 2nd segment X1/14.5 (10)	Y2/791 (11)	†† cX^4 = Ẏ2 (12)	††† $\dot{CP}1$ (13)
15.0	—	—	—	—	9080
14.5	791	1.00	1.00	791	8900
11.8	340	.81	.43	347	8107
5.4	0	.37	.00	15	6985
.0	0	.00	.00	0	6390

† $b = 580/(5.4)^{1.1} = 90.739$
†† $c = 791/(14.5)^4 = 0.017894$
††† $\hat{CP}2 = 6390 + bX1^{1.1} + cX1^4$

This is the dashed line above the intercept (6390) in figure 53. The remaining differences, 340 and 791, and the associated $X1$-values were listed and scaled to 1.0 at $X1 = 14.5$ (table 18, columns 8–11). The overlay curve was then plotted and compared to the X^n-Standards (fig. 54).
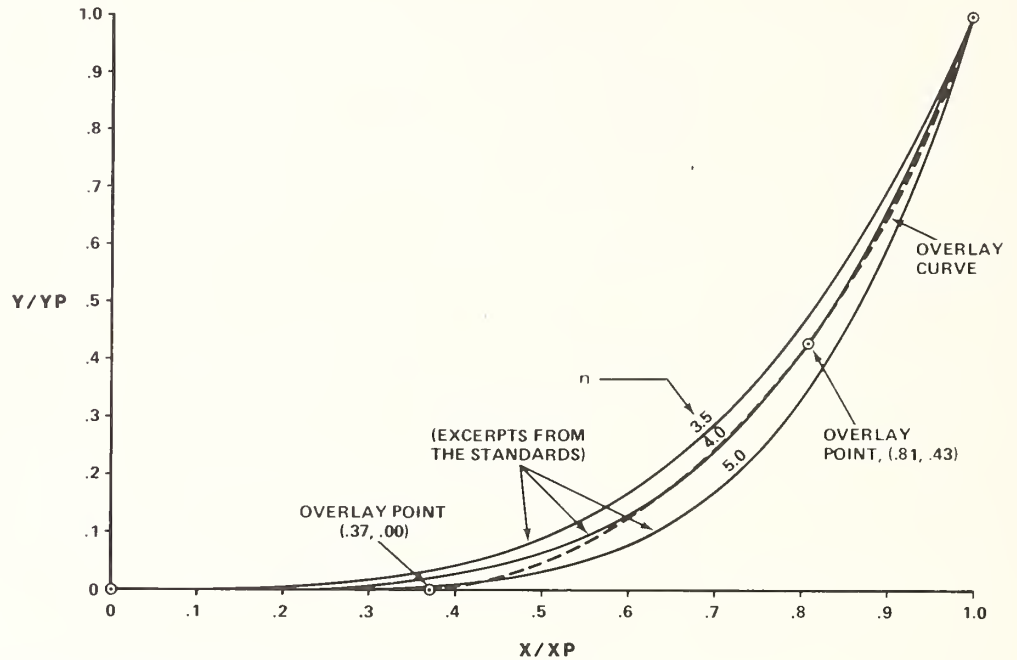

Figure 54.—Second component overlay curve compared to the X^n-Standards.

The curve $n = 4.0$ matched the overlay fairly well. So $(X1)^4$ was scaled to the difference, 791, at $X1 = 14.5$ (table 18, column 12). This was added to the intercept and the first component to arrive at the two-component descriptor, $\hat{C}P1 = 6390 + 90.739(15 - W)^{1.1} + 0.017894(15 - W)^4, \leq W \leq 15$. Note that the related estimates in table 18, column 13 were regarded as being satisfactorily close to the original objective values in column 2.

Matching the Bell-Shaped Curves

Tables 19 through 21 list $XP1$- and $CP1$-values from the equations developed in the foregoing sections along with some representative H- and C-values from the data-based portions of the bell-shaped curves in figure 50. Also listed are C-value estimates obtained by using matching e^{-K}-Standards (see the overlay curves in figure 55).

As may be seen in tables 19–21, the coverage values of the curve for each wind group were scaled to 1.0 by using the corresponding $\hat{C}P1$ as the maximum. The values of $X1$ or of $(2XP1 - X1)$ for each wind group were similarly scaled by using the corresponding $\hat{X}P1$ as the maximum. After the paired proportions for H-levels within each wind group were plotted and smoothed, the resulting overlay curves were compared to the e^{-K}-Standards for $n = 2$ (fig. 55). Although better matches for some of these overlays can be found in Standards that have n other than 2.0, it was decided to hold n constant

Table 19.—Descriptor development for C, W = 0.5

			† (1250 − H)	(2XP1 − X1)	†† (C − a)	Overlay control points		†††
W	H	C	X1	T	Y1	T/977	Y1/8900	Ŷ1
0.5	50	6860	1200	754	6860	0.77	0.77	7137
	100	7800	1150	804	7800	.82	.88	7793
	150	8450	1100	854	8450	.87	.95	8322
	200	8770	1050	904	8770	.93	.99	8692
	273	8900	977	977	8900	1.00	1.00	8900

† Temporary transform for plotting the overlay curve only. The temporary X1-values (T) must be in ascending order toward $XP1 = 977$ to match the position of the e^{-K}-Standards in two-space.
†† All sigmoids of the set are oriented at a = zero, so $(C − a) = C = Y1$.
††† Estimated coverage using e^{-K} with $X1 = (1250 − H)$, $I = 0.51$, $n = 2.0$, $XP1 = 977$, $CP1 = 8900$, and a zero intercept.
†††† Smoothed values from $\hat{X}P1$ and $CP1$, each a function of wind (shown earlier in the text).

Table 20.—Descriptor development for C, W = 3.2

			(1250 − H)	(2XP1 − X1)	(C − a)	Overlay control points		†Ŷ1
W	H	C	X1	T	Y1	T/1072	Y1/8107	
3.2	50	6730	1200	944	6730	0.88	0.83	6843
	100	7600	1150	944	7600	.93	.94	7612
	150	8040	1100	1044	8040	.97	.99	8042
	178	8107	1072	1072	8107	1.00	1.00	8107

† Estimated coverage using e^{-K} with $X1 = (1250 − H)$, $I = 0.71$, $n = 2.0$, $XP1 = 1072$, $CP1 = 8107$, and a zero intercept.

over wind. Then, the *I*-values corresponding to the best matching curve alternatives in this set, were estimated to be 0.51, 0.71, and 0.88 for $W = 0.5$, 3.2, and 9.6, respectively. On scaling and checking these and alternative curves (by means of a small computer) at the tabled *H*-values within *W*-group, some improvement was achieved with the final *I*-array, 0.51, 0.71, and 0.88. The last column in each of tables 19–21 shows the final scaled coverage estimates. There was close proximity of these values to actual coverage, *C*, so $I = f(W)$ was developed next.

Table 21.—Descriptor development for C, $W = 9.6$

W	H	C	† (1250 − H) X1	(C − a) Y1	Overlay control points		†† $\hat{Y}$
					X1/1170	Y1/6985	
9.6	80	6985	1170	6985	1.00	1.00	6985
	100	6820	1150	6820	.98	.98	6845
	150	5300	1100	5300	.94	.76	5448
	200	3270	1050	3270	.90	.47	3364
	250	1830	1000	1830	.85	.26	1612
	300	997	950	997	.81	.14	600

† Since the right half of this curve (fig. 50) was read, X1-values are already ascending toward $XP1 = 1170$ and no temporary transform of $X1$ is necessary for plotting the overlay curve.

†† Estimated coverage using e^{-K} with $X1 = (1250 − H)$, $I = 0.88$, $n = 2.0$, $XP1 = 1170$, $CP1 = 6985$, and a zero intercept.
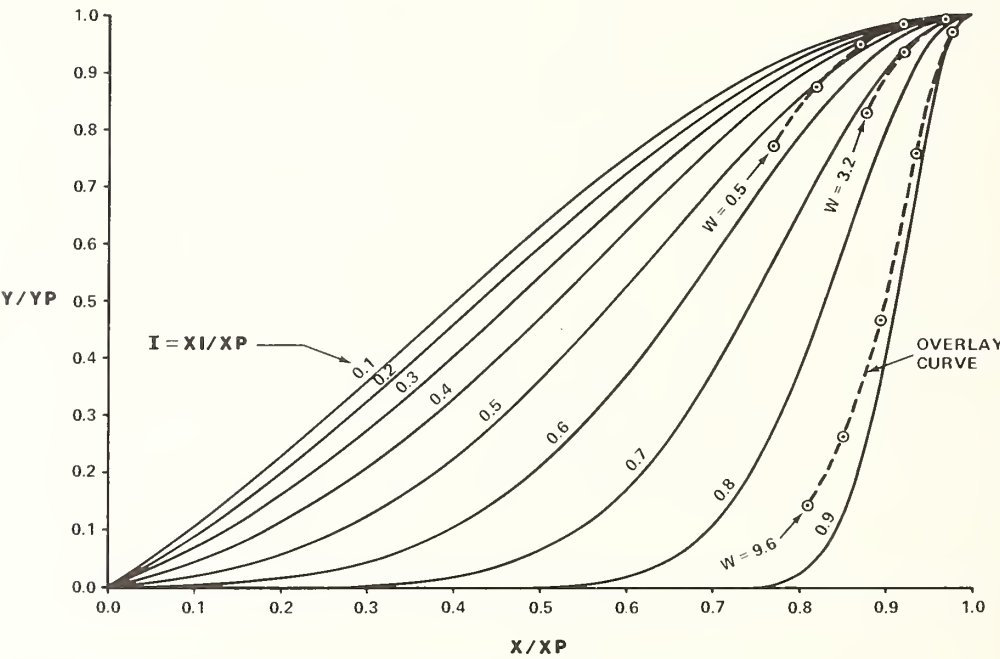

Figure 55.—Standards for $n = 2.0$ and proportional departure of inflection points in X, (XI), from XP, (XI/XP).
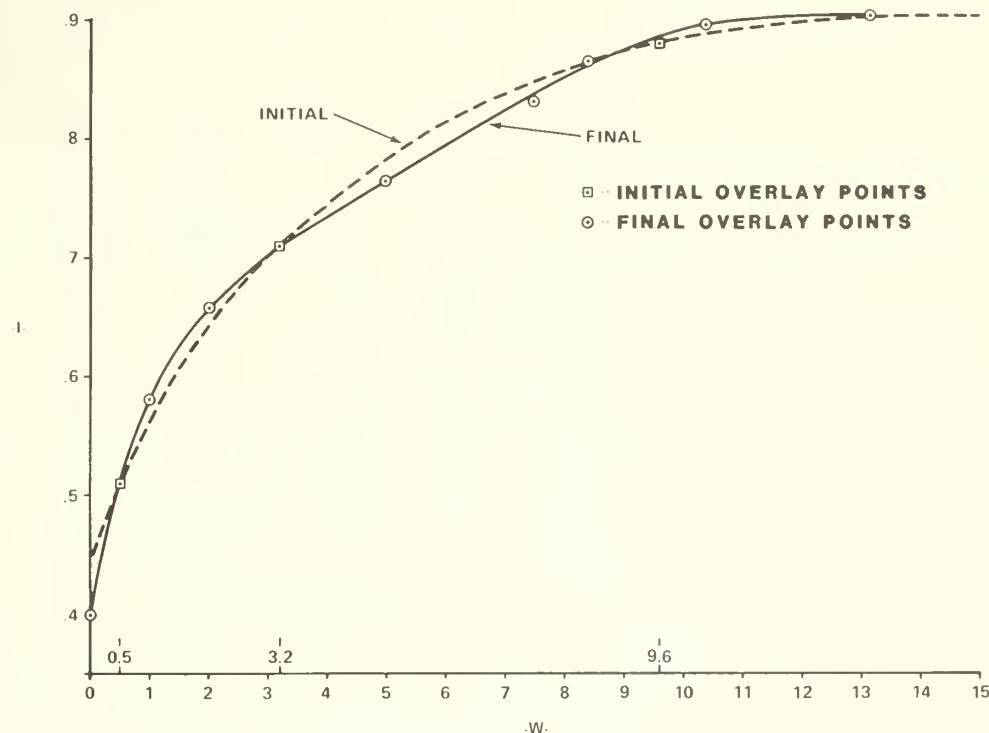
Figure 56.—Initial and final curves of *I* over *W*.

For $I = f(W)$

Using the paired wind and *I*-values just determined (0.5, 0.51; 3.2, 0.71; and 9.6, 0.88), *I* was plotted over *W* and a smooth *initial* curve drawn through the three data points (fig. 56).

On checking the performance of e^{-K} over the range of *W*, with smoothed *CP*-, *XP*-, and initial *I*-values, it was found that the left edge of the surface undulated unacceptably (at $H = 50$, $0 \le W \le 5$). *I*-values were adjusted iteratively to minimize the problem and the new (final) set of points shown in figure 56 were established. The smooth (final) curve through these points became the objective curve for which a descriptor was developed.

This curve was judged to require a multicomponent model because neither the sigmoids nor the exponentials have the flattened central segment found there. The flat segment was represented by a straight line; the negative differences at the left end by an exponential; and those at the right by the lower portion of a sigmoid (fig. 57).

The Flat Segment.—A straight line was drawn along the final curve. The intercept, $a = 0.62$, and values necessary to the coefficient for *W*, $(1.054 - 0.620)/15 = 0.0289$, were read directly from the graph. Then $\hat{Y}1$, the first descriptor component, $= 0.620 + 0.0289(W)$, (see table 22, column 3).

The Left End.—This residual portion of the curve ($Y2$) was satisfactorily matched by a single exponential of the reversed *W*-axis ($\hat{Y}2$), scaled at $X1 = 14.5$ (table 22, columns 4–8).

So the partial form at this point is:

$$\hat{Y}\,(\text{partial}) = 0.62 + 0.0289(W) - 4.3703 \times 10^{-21}(15 - W)^{16.75}.$$
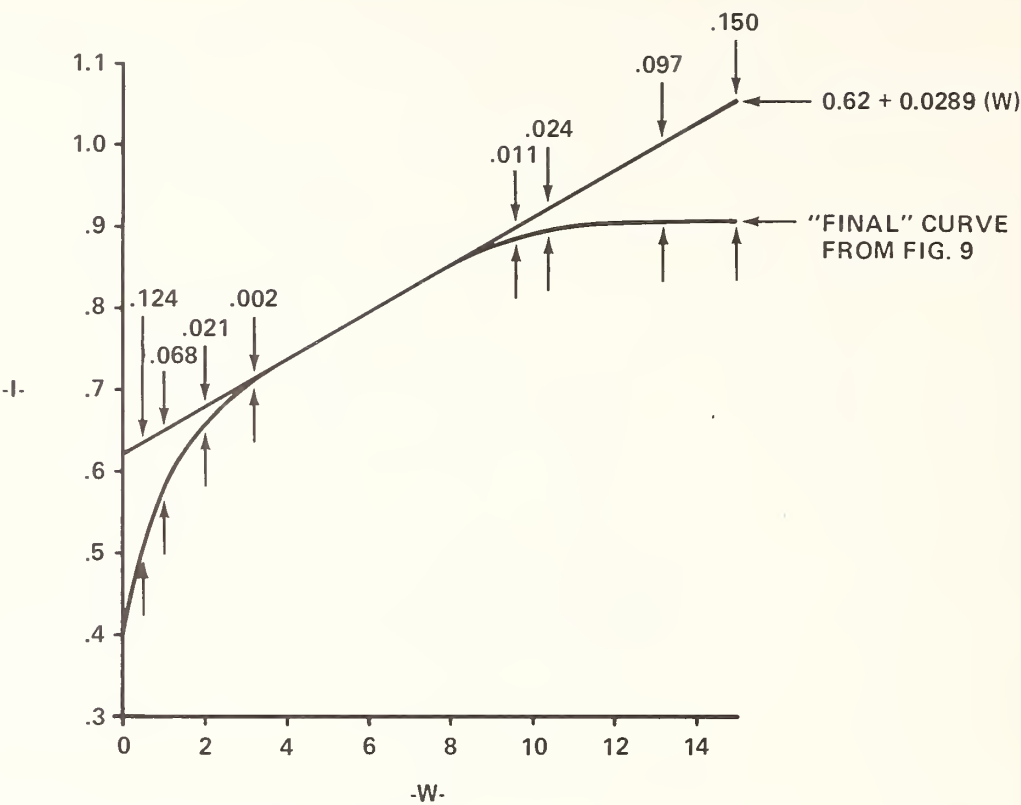
Figure 57.—Elements of $I = f(W)$, graphed.

Table 22.—Descriptor for $\hat{I}$, the *left end* and *central segment*

W (1)	I = Y1 (2)	$a + b(W)$ = $\hat{Y}1$ (3)	$(15 - W)$ = X1 (4)	$(\hat{Y}1 - Y1)$ = Y2 (5)	Overlay control points X1/14.5 (6)	Overlay control points Y2/0.124 (7)	† $cX^{16.75}$ $\hat{Y}2$ (8)
0.0	0.400	0.620	15.0	0.220	—	—	0.219
.5	.510	.634	14.5	.124	1.00	1.00	.124
1.0	.581	.649	14.0	.068	.97	.55	.069
2.0	.687	.678	13.0	.021	.90	.17	.020
3.2	.710	.712	11.8	.002	.81	.02	.004

† Although not shown in the text here, the curve implied by the overlay points matched $16 \leq n \leq 17$ in the X^n- Standards very well. Iterative checking showed $n = 16.75$ to perform best within that range. Then, $c = 0.124/(14.5)^{16.75}$ $= 4.3703 \times 10^{-21}$

The Right End.—For this portion of the curve, the differences ($Y3$) from the straight line and associated scaling information are listed in table 23. It is apparent in figure 58 (right side) that the objective curve is not well matched by any simple power of W. The same held true for a multiple-component descriptor that was subsequently developed. By

Table 23.—Descriptor for $\hat{I}$, the *right end*

		$a + b(W)$ $=$	$(\hat{Y}1 - I)$ $=$	Overlay control points [†]	
W (1)	I (2)	$\hat{Y}1$ (3)	Y3 (4)	W/15 (5)	Y3/0.150 (6)
8.4	0.863	0.863	0.000	0.56	0.00
9.6	.886	.897	.011	.64	.07
10.4	.897	.921	.024	.69	.16
13.2	.904	1.001	.097	.88	.65
15.0	.904	1.054	.150	1.00	1.00

[†] The overlay curve is compared to the X^n-Standards at the right side of figure 58.

reorienting the exponential curve in space, however, reversing W to $X1 = (15 - W)$ and inverting $Y3$ to $Y4 = (0.15 - Y3)$, the curve becomes convex-upward with increasing values of $X1$. Also, it is at least roughly matched by the sigmoid Standard, $n = 8$ and $I = 0.108$ (see table 24 and the left overlay curve in fig. 58). This sigmoid was the result of an interpolation between the two Standards $I = 0.1$ and 0.2 at $n = 8$.
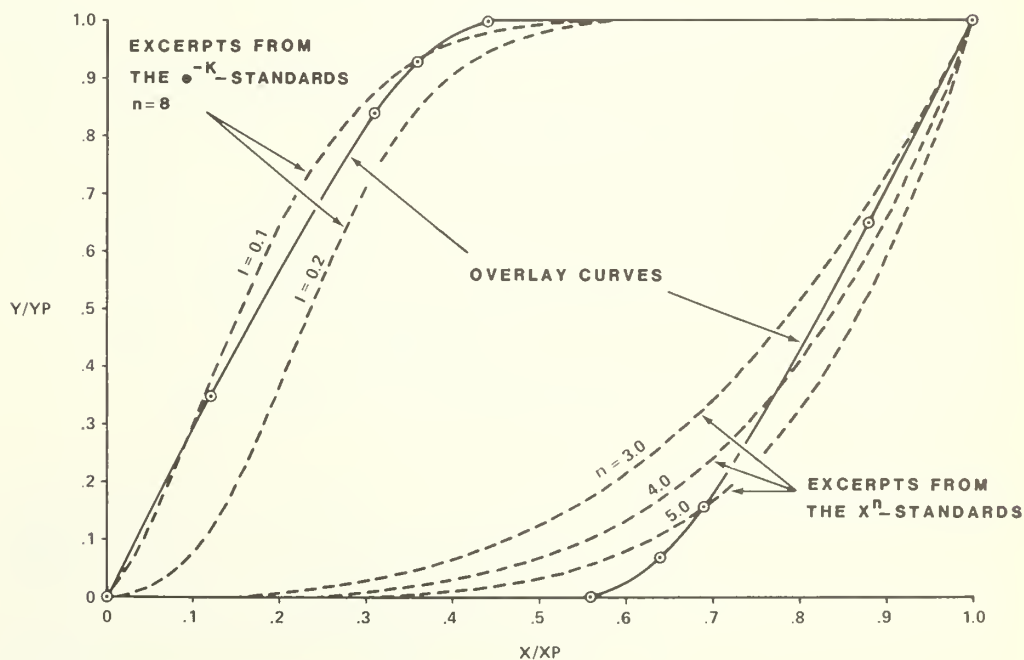

Figure 58.—Overlay curves compared to the Standards.

Table 24.—Descriptor (continued) for $\hat{I}$, the right end

W (1)	$(15-W)$ = X1 (2)	† $(\hat{Y}1-I)$ = Y3 (3)	$(0.150-Y3)$ = Y4 (4)	Overlay control points X1/15 (5)	Overlay control points Y4/0.150 (6)	†† de^{-K} = $\hat{Y}4$ (7)
0.0	15.0	—	0.150	1.00	1.00	0.150
8.4	6.6	0.000	.150	.44	1.00	.146
9.6	5.4	.011	.139	.36	.93	.139
10.4	4.6	.024	.126	.31	.84	.130
13.2	1.8	.097	.053	.12	.35	.053
15.0	.0	.150	.000	.00	.00	.000

† From table 23, column 4.
†† e^{-K} using X1, $n=8$, $I=0.108$, $XP1=15.0$, $YP=0.150$, and the intercept, $a=0$.

Then, the right end was specified as:

$$\hat{Y}4 = (0.15 - Y3) = 0.150(e^{-K})$$
$$\hat{Y}3 = 0.150 - 0.150(e^{-K})$$

$$\hat{Y}3 = 0.150 - 0.150 \left\{ \frac{e^{-\left|\frac{\frac{(15-W)}{15}-1}{1-0.108}\right|^8} - e^{-\left\{\frac{1}{1-0.108}\right\}^8}}{1 - e^{-\left\{\frac{1}{1-0.108}\right\}^8}} \right\}$$

and simplified:

$$\hat{Y}3 = 0.16349 e^{-\left|\frac{\frac{(15-W)}{15}-1}{0.892}\right|^8}.$$

The three components were assembled for $\hat{I}$.—

$$\hat{I} = 0.62 + 0.0289(W) - 4.3703 \times 10^{-21}(15-W)^{16.75} - 0.16349 e^{-\left|\frac{\frac{(15-W)}{15}-1}{0.892}\right|^8}.$$

The overall performance of this descriptor can be seen from the tabulation of the objective and estimated I in table 25, where I and $\hat{I}$ were suitably close over the range of W, as already verified by segment during development.

Table 25.—The performance of $\hat{I}$

W	Objective I	$\hat{I}$
0.0	0.400	0.401
.5	.510	.510
1.0	.581	.580
2.0	.657	.658
3.2	.710	.709
5.0	.766	.764
7.5	.838	.835
8.4	.863	.859
9.6	.886	.886
10.4	.897	.900
13.2	.904	.905
15.0	.904	.904

Summary for C′

At this point, all necessary inputs have been derived and the complete hypothesis is:

$$C' = CP1 \left\{ \frac{e^{-\left|\frac{(X1/XP1)-1}{1-I}\right|^2} - e^{-(1/(1-I))^2}}{1 - e^{-(1/(1-I))^2}} \right\}$$

where:

C' = coverage in square feet, estimated from the preleast squares fit motel

$CP1$ = coverage peak for any specified windspeed, W, and

$\hat{CP1}$ = $6390 + 90.739(15-W)^{1.1} + 0.017894(15-W)^4$, $0 \le W \le 15$

$X1$ = $(1250 - H)$

H = drop height, $50 \le H \le 300$

XPI = point in $X1$ at which $CP1$ occurs, or

$\hat{XP1}$ = $1190 - 0.4572(15-W)^{2.25} - 1.4811 \times 10^{-22}(15-W)^{20}$

I = inflection point in X expressed as a proportion of XP, ($X1/XP$ in Matcha-curve-1, Jensen and Homeyer 1970),

$\hat{I}$ = $0.62 + 0.0289(W) - 4.3703 \times 10^{-21}(15-W)^{16.75} - 0.16349 e^{-\left|\frac{\frac{(15-W)}{15}-1}{0.892}\right|^8}$.

The hypothesis was then adjusted back to the data from which it was partially derived following the fitting procedures discussed under 2-D, X^n and e^{-K}, where $C' = X$ and the simple least squares adjustment coefficient for the entire hypothesis,

$$b = \Sigma XY / \Sigma X^2 = 1.000569 \text{ and } \hat{C} = bC' .$$

The coefficient, b, is very near 1.0000; so it is evident that even before least-squares adjustment, the original hypothesis was well alined with the data spatially. But, in checking the form of the hypothesis by comparing predicted ($\hat{C}$) and actual (C) coverages in figure 59, at least one anomaly appears. Actual coverage data points for the three high-wind points ($W = 8.4$, 10.4 and 13.2) probably lie too close to the surface since substantial variation occurs about the surface at lower wind levels; i.e., reasonable variance about the surface would be expected at high-wind levels also.
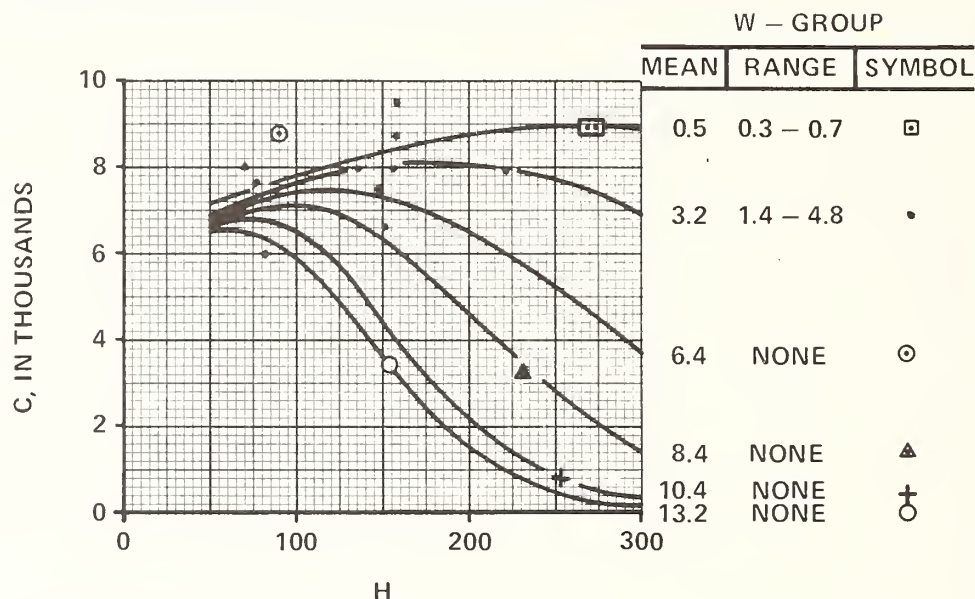
Figure 59.—Hypothesis performance by wind group.

W — GROUP		
MEAN	RANGE	SYMBOL
0.5	0.3 – 0.7	▣
3.2	1.4 – 4.8	•
6.4	NONE	☉
8.4	NONE	▲
10.4	NONE	☦
13.2	NONE	○

Recall that through the use of controlled I-values (fig. 56) for curves passing close to the three high-wind points, low variation of these points from the surface was assured. Alternative I-values could be used that would allow for variation from the surface, in accord with some assumed variance criteria. This refinement was not attempted and the model was adopted as developed. Predicted values (table 26) and the associated surface (fig. 60) for the model are as shown below.

Table 26.—Model values

	Drop height					
Wind	50	100	150	200	250	300
mi/h	---------------------------- *Feet* ----------------------------					
0	7,198	7,804	8,316	8,710	8,969	9,081
5	6,830	7,525	7,707	7,337	6,491	5,338
10	6,617	6,707	4,925	2,619	1,009	282
15	6,345	5,663	3,460	1,447	414	81
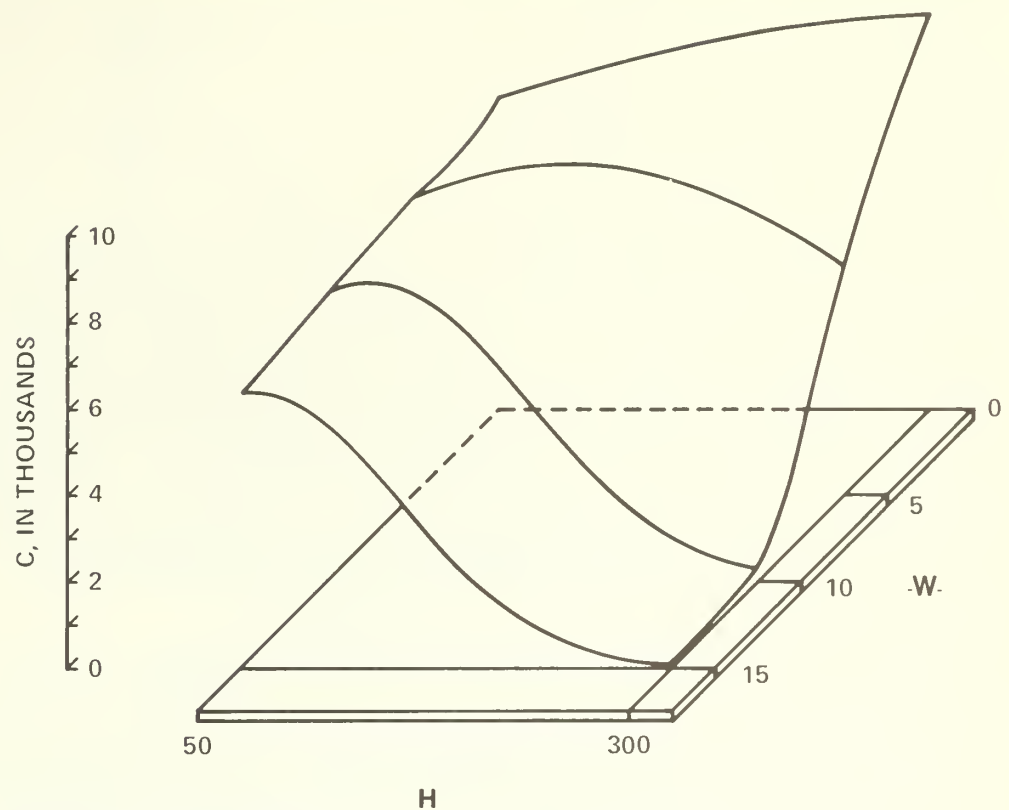
Figure 60.—The 3-D hypothesis.

It is appropriate to review the imposing list of constraints that can be met in models like this one. Controllable items include: the intercept for the whole surface; the elevation, breadth, and positioning of the peaks over the interacting independent variables; the trend in coverage at the truncated left edge of the surface; the magnitude of curvature above and below the inflection points in the bell-shaped curves; and the positioning of the inflection points themselves within the range of the independent variables.

Asymmetrical Bell-Shaped Ridge over $X1$, with Moving Peak in $X2$. This is Described in Two Segments and Interacts with a Sigmoidal $X2$-Effect

Live Data Example

In this hypothesis from Klein, Parker, and Jensen 1978, tree mortality percent in a western forest is characterized by tree diameter (d.b.h.) over the course of a beetle epidemic (fig. 61).

The graphed hypothesis is applicable only at discrete points in time and at the midpoints of 2-inch d.b.h. classes, but both variables are treated as continuous. As was evident in the original data, the more-or-less bell-shaped trends over time differ substantially on either side of the central ridge. For example, observe strong asymmetry at
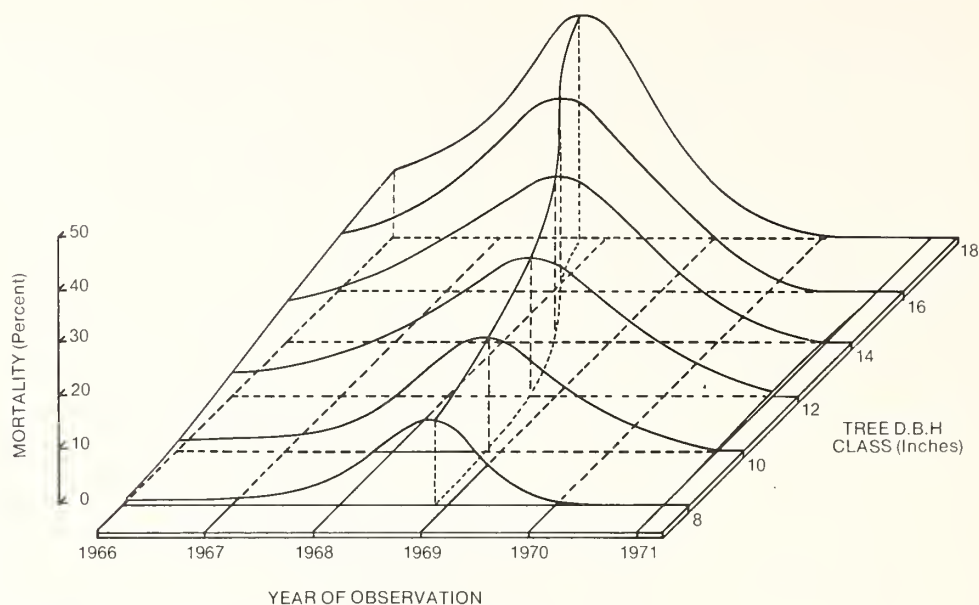
Figure 61.—Tree mortality over the course of a beetle epidemic.

d.b.h. = 12 to 18 inches, made most noticeable perhaps by elevational differences in the curves at their left and right extremes. See also the dwindling breadth of curve crowns above and below 15 inches d.b.h., an interactive change included in the descriptor along with asymmetry.

To assemble descriptor components, left and right sides of the ridge were described separately (fig. 62 and 63), using sigmoids from the e^{-K}-Standards that varied in shape and scale according to data trends over d.b.h. Because the lower portion of curves of the left half were asymptotic at values larger than zero, it was necessary to include the left-edge intercept, *Int*, or floor, upon which the left-side sigmoids rested conceptually. *Int* is a function of d.b.h., as is *XP*, the location of the ridge in time.
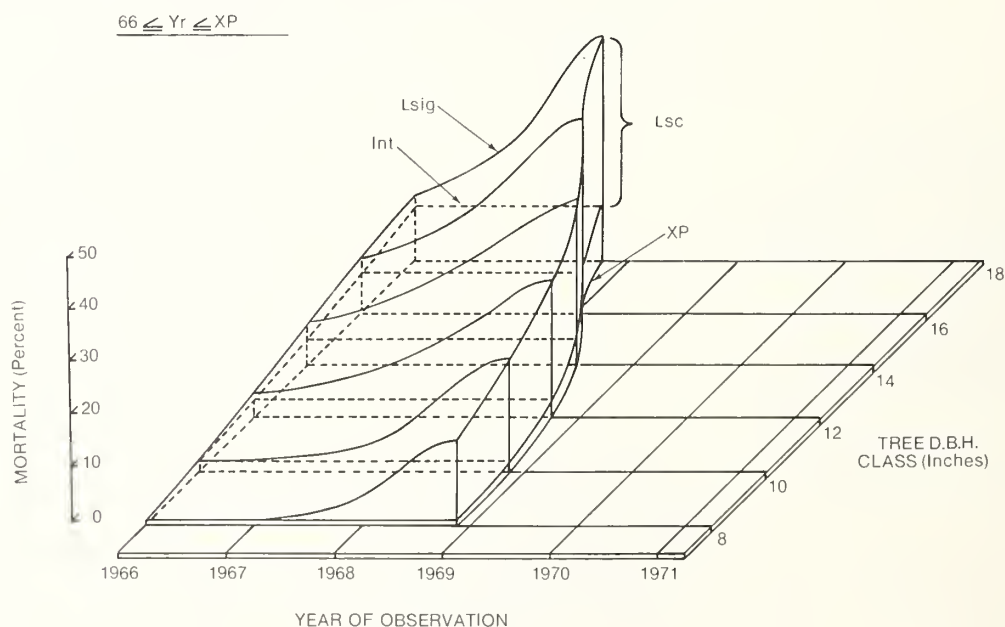
Figure 62.—Tree mortality over the course of a beetle epidemic, *left segment*.

$XP \leq Yr \leq 71$
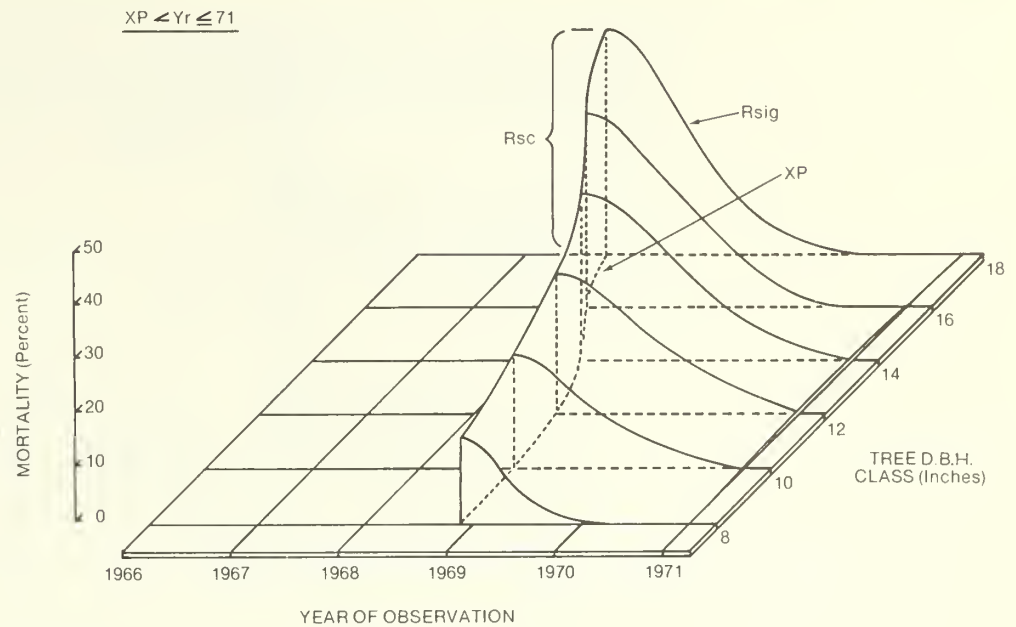
Figure 63.—Tree mortality over the course of a beetle epidemic, *right segment*.

Sigmoids are described within the range $XP \pm 5$ years (Yr), since all sigmoids are estimated to be fully expressed therein. Use of a constant maximum range, such as $XP \pm 5$ years, keeps descriptor components to a minimum for the sigmoidal time effects, yet permits satisfactory matching of the objective curves in this case. Restated in general terms, the whole descriptor is as follows:

Mortality percent $= Int + Lsc(Lsig) + Rsc(Rsig)$
where
$Lsig =$ left sigmoid $= f_L(Ln, LI, XP, Yr)$. See the basic sigmoid parameters defined in Jensen 1979.
$Ln = Lsig$ power $= f_1$(d.b.h.)
$LI = Lsig$ inflection point as a proportion of the range in years from $XP - 5$ to XP, $= f_2$(d.b.h.)
$XP =$ point in time where surface peaks $= f_3$(d.b.h.)

$Rsig =$ right sigmoid $= f_R(Rn, RI, XP, Yr)$
$Rn = Rsig$ power $= f_4$(d.b.h.)
$RI = Rsig$ inflection point as a proportion of the range in years from $XP + 5$ to XP, $= f_5$(d.b.h.)
$Int =$ intercept, left edge $= f_6$(d.b.h.)
$Rsc = Rsig$ scalar $=$ ridgetop $= f_7$(d.b.h.)
$Lsc = Lsig$ scalar $=$ (ridgetop) $- (Int)$
Segmental constraints:
Left side; $66 \leq Yr \leq XP$, discrete values only
Right side; $XP \leq Yr \leq 71$, discrete values only
Either side; $8 \leq$ d.b.h. ≤ 18, midpoints of 2-inch d.b.h.
               class only . . . 8, 10, 12, etc.
The model, refitted by least squares to smoothed mortality percent at 36 control points on the original data cross sections over time resulted in an R^2 of 0.96. Used as a

goodness-of-fit index, this high R^2-value attests to the fact that the descriptor duplicates the objective graph with reasonable accuracy.

The explicit hypothesis and moderate developmental detail follow:

Mortality percent $= K(Int + Lsc[Lsig] + Rsc[Rsig])$

where

$K =$ least-squares coefficient $= 0.9877$

$Int = 1 + 0.2321(\text{d.b.h.} - 8)^{1.63}$

$Rsc = 2.6429(\text{d.b.h.}) - 5.157$

$Lsc = Rsc - Int$

$$Lsig = \left\{ \frac{e^{-\left|\dfrac{\dfrac{5 - |Yr - XP|}{5} - 1}{1 - LI}\right|^{Ln}} - e^{-\left(\dfrac{1}{1 - LI}\right)^{Ln}}}{1 - e^{-\left(\dfrac{1}{1 - LI}\right)^{Ln}}} \right\}$$

$$XP = 67.65 + 1.2257 e^{-\left|\dfrac{\dfrac{20 - \text{d.b.h.}}{12} - 1}{0.65}\right|^{3.9}}$$

$$LI = 0.851 - 0.1531 e^{-\left|\dfrac{\dfrac{7 - |\text{d.b.h.} - 13.5|}{7} - 1}{0.45}\right|^{2}}$$

$Ln = 1.5$

$Rsig =$ as for $Lsig$, but using RI and Rn

$RI = 0.752 + 7.8173 \times 10^{-4} |\text{d.b.h.} - 14|^{2.8}$

$Rn = 2$

Limits

$66 \leq Yr \leq 71$, discrete units only

$66 \leq Yr \leq XP$, for Int, Lsc, $Lsig$

$XP < Yr \leq 71$, for Rsc, $Rsig$

$8 \leq \text{d.b.h.} \leq 18$.

Supplementary Explanatory Detail

Int was estimated from leftward extension (from the ridge) of the mortality trend indicated by data in each of six 2-inch d.b.h. groups. All six trends reached lower asymptotes by 1963 and, at that point, suggested a flat, concave-upward curve over d.b.h. (fig. 64). This was satisfactorily described by using the X^n-Standards.

Rsc is simply the height of the ridge above zero (no intercept) and serves as the scalar for the right-half sigmoids. *Rsc* is a linear function of d.b.h. adopted to represent the somewhat irregular pattern of ridge values for the six d.b.h. groups (fig. 65). Note that the ridge line in figure 62 only appears to be sigmoidal by reason of the sigmoidal change of point-of-peaking in time with a change in diameter.

Lsc $= (Rsc - Int)$ and is the scalar for the left-half sigmoids.

XP, the point in time at which the bell-shaped curves peaked, was estimated from the *XP*'s for the six data-group cross sections (fig. 66). This curve was estimated to asymptote at 68.88 for lower diameters and 67.75 for higher diameters. A suitable match was
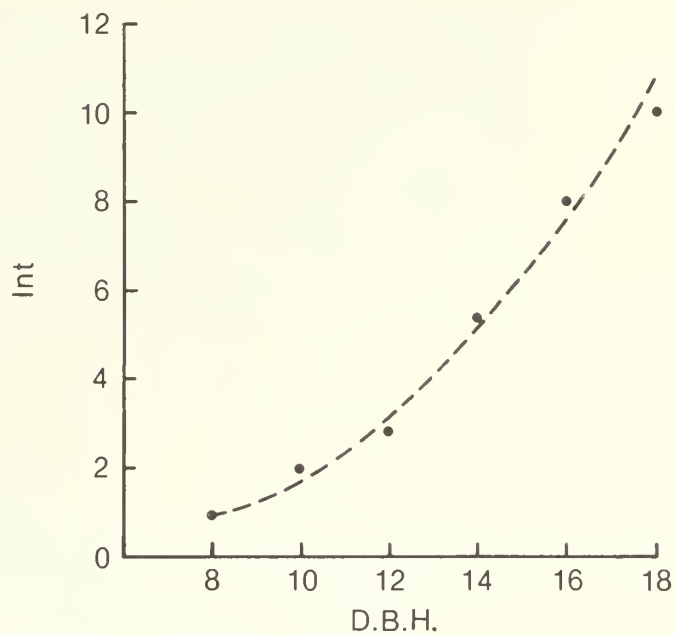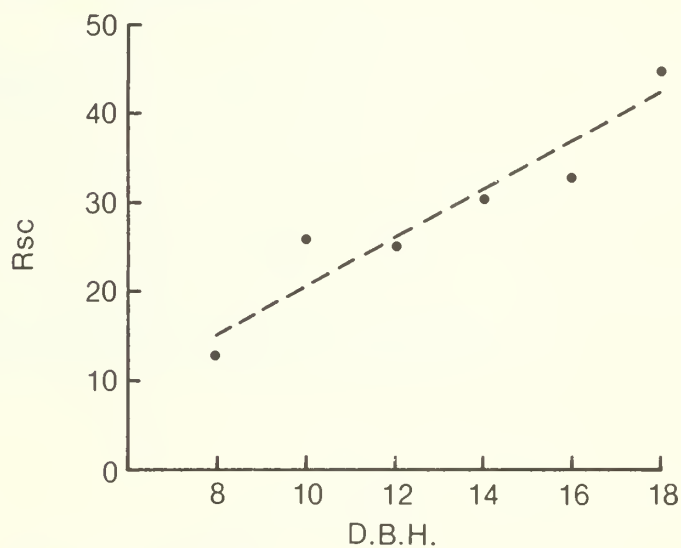
Figure 64.—*Int* smoothed.

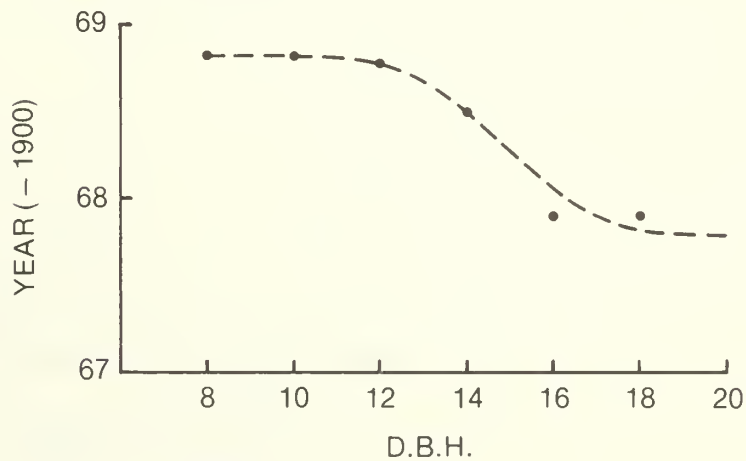

Figure 65.—*Rsc* smoothed.

Figure 66.—*XP* smoothed.

found in the e^{-K}-Standards when the d.b.h. scale was reversed to 20-(d.b.h.).

Lsig specifies the sigmoidal shape of the left side (fig. 62). After transforming Year to $5 - |Yr - XP|$ to create X-values ranging from zero at $XP - 5$ to 5 at XP, the six d.b.h. group cross sections (left halves) were each scaled to 1.0 in X and Y at critical points in X. Overlay curves were plotted for these cross sections (fig. 67). The pattern was one of wider sigmoidal crowns near d.b.h. = 14 inches, narrowing with departure from that d.b.h. This is reflected in the bell-shaped function for the inflection points, LI. Also, the e^{-K}-Standards with $n = 1.5$ were found to represent this curve array with reasonable accuracy, so *Ln* was set at the constant, 1.5.
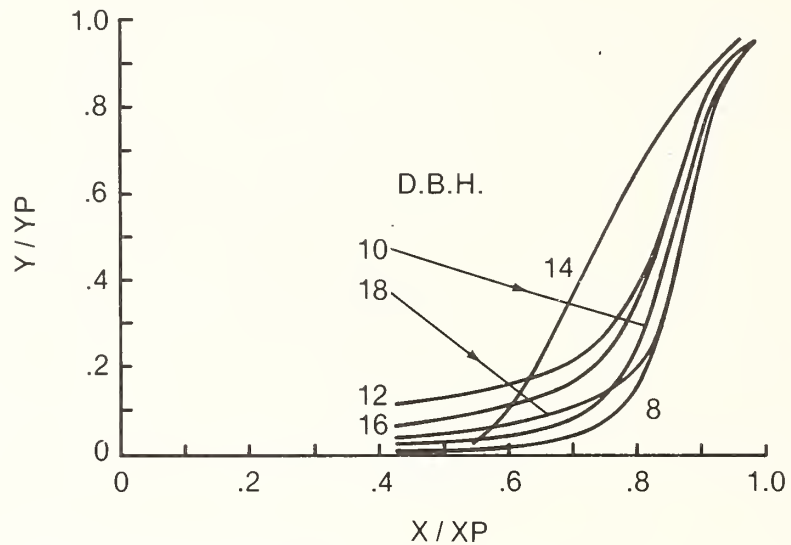
Figure 67.—The overlay curves.

LI, the function for the inflection points, is the dashed line in figure 68 and represents the inflection points adopted and plotted for each overlay curve. *LI* reflects the width-of-curve-crown trend noted under *Lsig* and in the text.
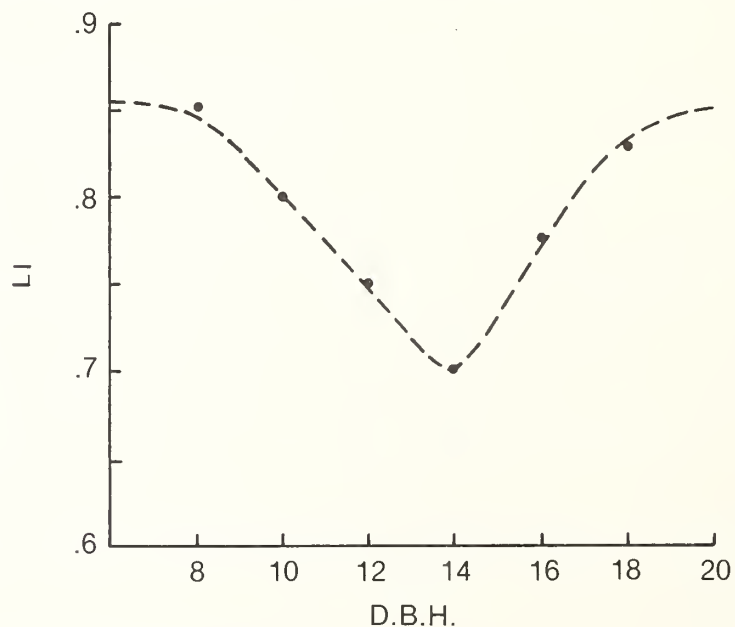
Figure 68.—*LI* smoothed.

Rsig, *RI*, and *RN* were obtained in a similar fashion. The Year transform again was $5 - |Yr - XP|$ and ranged in value from 5.0 at *XP* to zero at $XP + 5$. The right-side cross sections were fairly well matched by e^{-K}-Standards with $n = 2$, so *Rn* was set constant at $Rn = 2$. *RI* showed the same general widening of curve crown at d.b.h. = 14 inches.

Asymmetrical Bell-Shaped Ridge over $X1$, with Moving Peak in $X2$. This is described in Three Segments and Interacts with a Sigmoidal $X2$-Effect

Live Data Example

Quality score (t) was originally described as an aggregate of 11 planar regions over flow (F) and stability (S) of gap-graded road materials, a strongly segmented descriptor (fig. 69, from Lee and others 1973). The objective here was to smooth the figure mathematically. Although the problem is an unusual one, its solution serves admirably to demonstrate descriptor segmentation.

From figure 69, it can be seen that opposite sides of the ridge differ substantially in slope so that an symmetrical, flat-topped, bell-shaped curve would be required to describe the cross section at any point in S while rounding the junctures of planes. A relatively simple descriptor alternative involves segmentation of the (S) and (F) regions as shown, with left and right orientation lines. Note that the lines are parallel to their respective sides of the ridge and lie one unit in F closer to the ridge center. This permits use of a single, but different, sigmoid cross section to represent and smooth the corners of each segment, left and right. The sigmoids will peak at their respective orientation lines and will be functional over a constant distance from them (left or right as appropriate). The constant will vary by side as needed. Since the ridge is flat topped, it will have a value of $t = 10$ everywhere in the center segment.
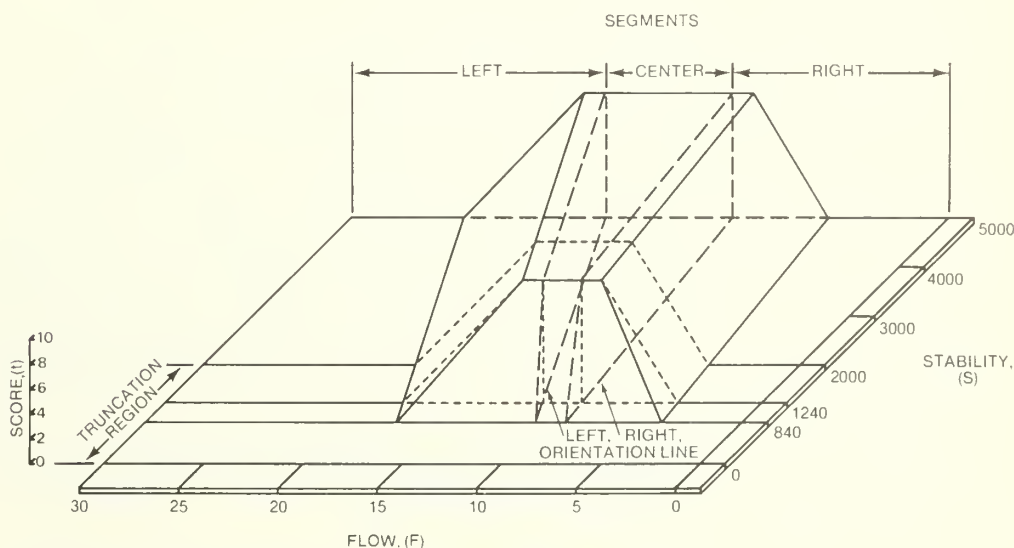

Figure 69.—Quality of gap-graded road materials: segmented planar form.

Then, to this point, we have described a ridge with three segments specified in terms of S and F; the sigmoidal effect to the left of the left orientation line; the sigmoidal effect to the right of the right orientation line; and the flat ridge area between these lines at a value of $t = 10$.

Finally, a sigmoidal truncation of the front end of this ridge is achieved through multiplication of all components of the descriptor by an appropriate sigmoid, changing in value from zero to one within the range $0 \leq S \leq 2000$, and being applicable for $0 \leq S \leq 5000$.

In general terms, we have:

$Lsig$ and $Rsig$ = left- and right-segment sigmoids, respectively

LO, RO = left- and right-orientation lines, respectively

CC = center segment, constant

$Tsig$ = truncator sigmoid

Then

$$t = Tsig(Lsig + CC + Rsig)$$

and

$Tsig = f(S)$

$Lsig = f(LO, F)$

$Rsig = f(RO, F)$

$LO = f(S)$

$RO = f(S)$

Limits

For $Lsig$, $\quad LO < F \leq 28$

For $Rsig$, $\quad 0 \leq F \leq RO$

For CC, $\quad LO \leq F \leq RO$

and, $\qquad 0 \leq S \leq 5000$.

The final descriptor form is shown in figure 70 along with the original planar form for comparison. It can be seen that the descriptor does a creditable job of emulating the planar form while smoothing the corners, all with three segments in place of the original 11 segments.
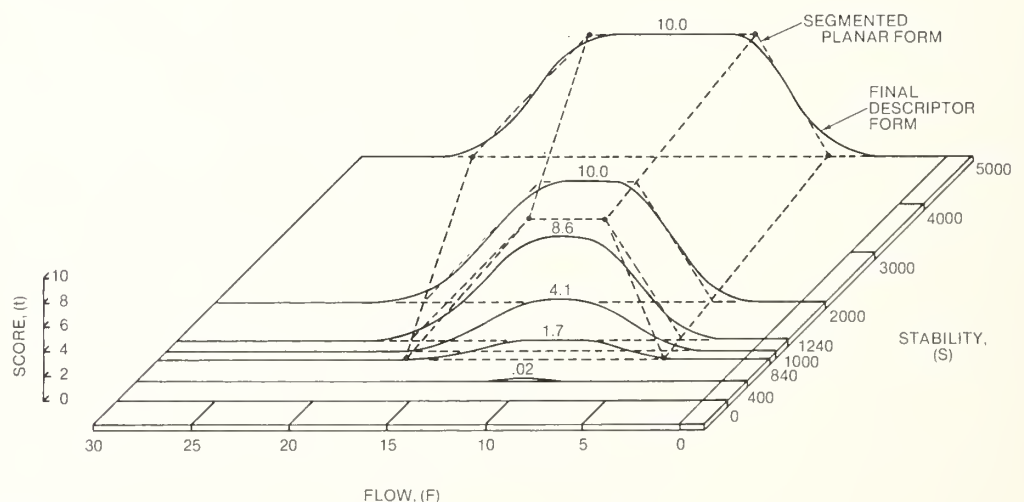
Figure 70.—Quality of gap-graded road materials: segmented planar and final descriptor forms.

Explicit hypothesis and moderate developmental detail follow:

If

$$F > LO, \; t = Tsig(Lsig)$$
$$LO \leq F \leq RO, \; t = 10(Tsig)$$
$$F < RO, \; t = Tsig(Rsig)$$

where

$$F = \text{soil flow}$$
$$LO = 8.888 + 0.0017036(S)$$
$$RO = 8.404 + 0.00048076(S)$$
$$S = \text{soil stability}$$

$$Lsig = 10\,e^{\displaystyle -\left|\frac{\dfrac{(LO + 20 - F)}{20} - 1}{0.23}\right|^{2.2}} \; ,$$

$$Tsig = 1 - e^{\displaystyle -\left|\frac{\dfrac{(6000 - S)}{6000} - 1}{0.185}\right|^{6}} \; ,$$

$$Rsig = 10\,e^{\displaystyle -\left|\frac{\dfrac{|RO - 11| + F}{11} - 1}{0.30}\right|^{2.4}} \; .$$

Limits
$$0 \leq F \leq 28,$$
$$0 \leq S \leq 5000.$$

Supplementary Explanatory Detail

Lsig, the left segment of figure 69, has a constant cross section over F for $1240 \leq S \leq 5000$, approximated in the descriptor by a sigmoid oriented at $F = LO$ and extending leftward a distance of 20 units in F. This is about the minimum operational span for the sigmoids here. At the upper extreme of S, ($S = 5000$), the left-segment sigmoid is expected to be completely specified in the range $27 \geq F \geq LO$, as in figure 70. Setting 28 as the upper level of F within which all left-segment sigmoids must be completely specified, we turn to the limiting case at $S = 0$. Here, $LO = 8.888$ and the sigmoidal range must then be at least $(28 - 8.888) = 19.112$; so 20 was adopted as the operational span. Note that a larger span could have been adopted.

The F-scale is reversed to $(LO + 20 - F)$, as shown in figure 71, to associate the largest value of the sigmoidal span, 20, with the peak of the sigmoid at LO. By scaling control points from the left cross section at $S = 1240$ (fig. 71) to 1.0 in X, $(LO + 20 - F)$, and Y, (score, t), and making an overlay curve, an appropriate sigmoid was identified from the e^{-K}-Standards.
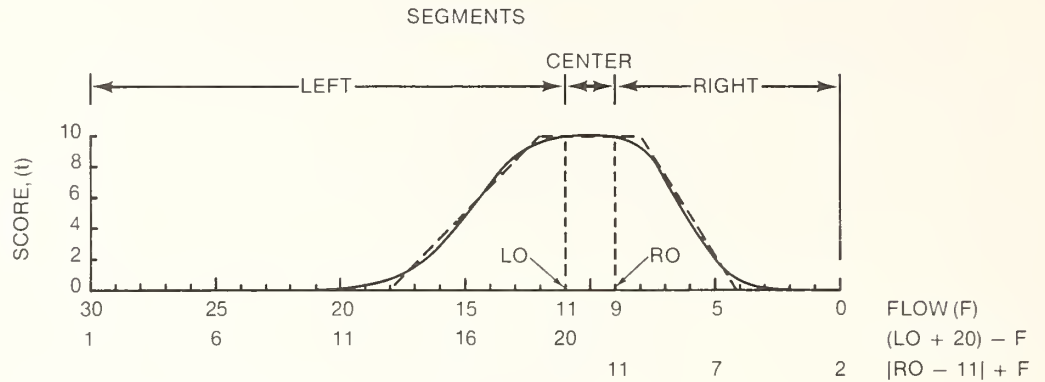
Figure 71.—A *t*-cross section over *F* at *S* = 5000. Note: the cross-sectional shape of the left segment is constant in the range $1240 \leq S \leq 5000$; the right segment, although different in cross-sectional shape, is also constant in shape over the range $1240 \leq S \leq 5000$.

Tsig, from (fig. 72), the planar ridge truncation ranges from $t = 0$ at $S = 840$ to $t = 10$ at $S = 1240$. This plane, scaled to 1.0, is matched and smoothed by *Tsig*, as is shown in figure 72. Note from the explicit *Tsig* formula that the inverted sigmoid to the left of the truncation plane (with base = 1.0 and peaking at 0, 0) was described on the reversed S-axis, $(6000 - S)$, and subtracted from 1.0 to arrive at *Tsig*. This provided a more accurate duplication of the truncator plane than did other sigmoid alternatives in this case.

Although a maximum of $S = 6000$ appears in *Tsig*, the applicable range is still limited to $S = 5000$ based on the original figure (fig. 69).
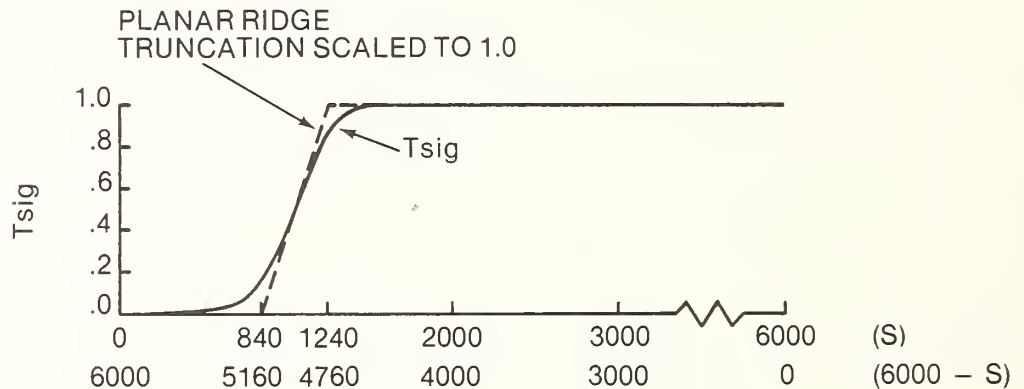
Figure 72.—Ridge truncation sigmoid, *Tsig*.

Rsig, the right segment of figure 69, has a constant cross section over F for $1240 \leq S \leq 5000$, approximated in the descriptor by a sigmoid oriented at RO and extending to the right for a distance of 11 units in F. Eleven is about the minimum operational span for the right-segment sigmoids. RO ranges from 8.404 at $S = 0$ to 10.808 at $S = 5000$. A range of 11 includes F = zero at both extremes and so was adopted. The *Rsigs* were described as a function of the F-transform $|RO - 11| + F$, as shown in figure 71. Thus, the maximum value of 11 always occurred at the sigmoidal peak, $F = RO$, and *Rsig* functioned over the range zero to 11 of the F-transform.

Summary

The final surface, then, is simply the sum of the three contiguous ridge segments, all of which are truncated at appropriate points in S through multiplication by the proportional values of *Tsig*.

**Symmetrical, Inverse
Bell-Shaped Ridge
over $X1$, with
Constant Point of
Minimum in $X1$ and
Interacting with a
Concave-Upward
$X2$-Effect**

Live Data Example

Here, the amount of natural reproduction (number of lodgepole pine seedlings per acre) over the Sleeping Child burn was expected to be affected by both azimuth and slope (data from Lyon 1976). Further, azimuth and slope were expected to interact strongly, the magnitude of response to azimuth being dependent on slope percent.

A small data set was used to develop a graphic hypothesis consistent with these expectations. It was very close to the mathematical hypothesis pictured in figure 73.
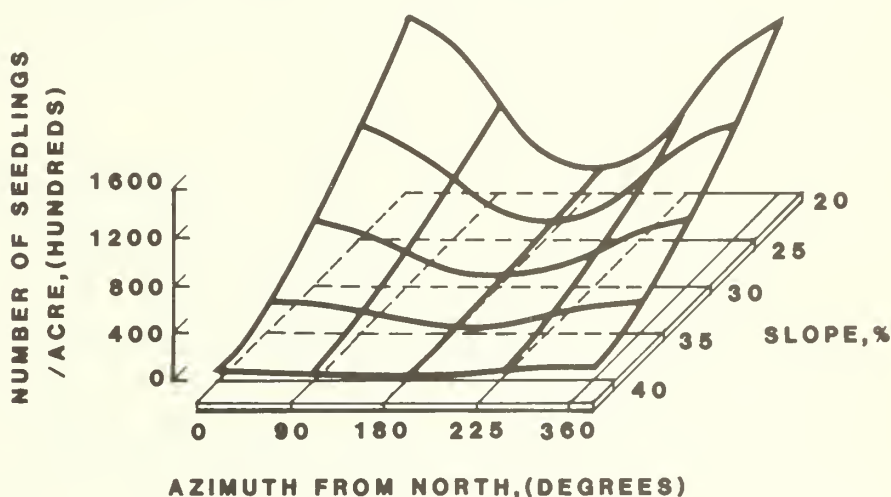
Figure 73.—The mathematical hypothesis.

**Descriptor Development
for Figure 73**

The **Azimuth (A)-effect** may be seen as cross sections over AZ at slope percent $(SL) = 20$, 30, 35, and 35. These were screened for shape using the e^{-K}-Standards. Note that, since the bell-shaped curves were symmetrical, either sigmoidal half would be representative of the whole (the left-half was used). Also, negative departures from either edge could be used to specify the depth of the sigmoids (these negative values were ignored in the screening, but were accounted for in the final mathematical hypothesis). Sigmoids were found to be sufficiently similar at different SL-levels to adopt the common form,

$$e^{-K} = 1.0675 * e^{-\left|\dfrac{\frac{AZ}{180} - 1}{0.655}\right|^{2.4}} - 0.0675,$$

where the trough is at a fixed point in AZ ($XP = 180$, here).

And, given the subtraction of suitably scaled sigmoids from either edge (*EDGE*),

$$\text{Number of seedlings} = EDGE - YP\left(1.0675 * e^{-\left|\frac{\frac{AZ}{180} - 1}{0.655}\right|^{2.4}} - 0.0675\right),$$

where *EDGE*, was better matched by the lower 85 percent of a sigmoid on the reversed slope scale with a maximum value of 100 than by a simple X^n-form. Thus,

$$EDGE = 2400 * e^{-\left|\frac{\frac{(100 - SL)}{100} - 1}{0.255}\right|^{2.6}}.$$

The trough of the objective figure (*MIN*) was expressed as the height of the negative bell-shaped (or sigmoidal) peaks above the 3-D base. As with *EDGE*, this was described as the lower 85 percent of a sigmoid on the reversed slope scale with a maximum value of 100. And,

$$MIN = 250 * e^{-\left|\frac{\frac{(100 - SL)}{100} - 1}{0.29}\right|^{2.3}}.$$

Then, $YP = EDGE - MIN$

LIMITS: $0 \le AZ \le 360$, $20 \le SLOPE \le 45$.

Note that inverse asymmetrical bell-shaped functions, often typical of azimuth effects on plant growth, can be described roughly as above, but in two segments. Each segment then has its own sigmoidal shape. Also, it could easily be that the trough, which was at a fixed point in AZ ($XP = 180$), in the foregoing example, changes in AZ depending on slope. In such a case, $XP = f(SL)$ in the sigmoidal effect of AZ.

Concave-Upward Relation in Two Dimensions, with Constant Point of Peaking in $X1$ Over $X2$.

Live Data Example

Soil temperatures (*ST*) at various depths and percent of duff reduction were studied on a clearcut area that had been subjected to a controlled burn. A data set (from Shearer 1974 and 1975) was devoted to hypothesis development as shown below.

Data were grouped into duff-reduction (DR) classes and trends over "depth in soil" (DS) were smoothed in accord with expectation. These were screened over the reversed DS-scale in the X^n-Standards and were all reasonably represented by $b_i(7 - DS)^6$. Then,

$$ST = 45 + (YP/(7)^6)(7 - DS)^6.$$

And, YP, the smoothed curve of scaling heights for the individual DS-curves (at the scaling point $[7 - DS] = 7$), was concave-upward over DR and could have been described as an exponential function of DR. The lower half of a sigmoid, however, was found to mimic the objective curve more closely so,

$$YP = 365.171 \left(e^{-\left| \dfrac{\frac{DR}{200} - 1}{0.56} \right|^{2.2}} \right) - 10.171,$$

thus producing figure 74. Limits of use for this hypothesis are: $0 \le DR \le 100$ and $0 \le DS \le 7$.
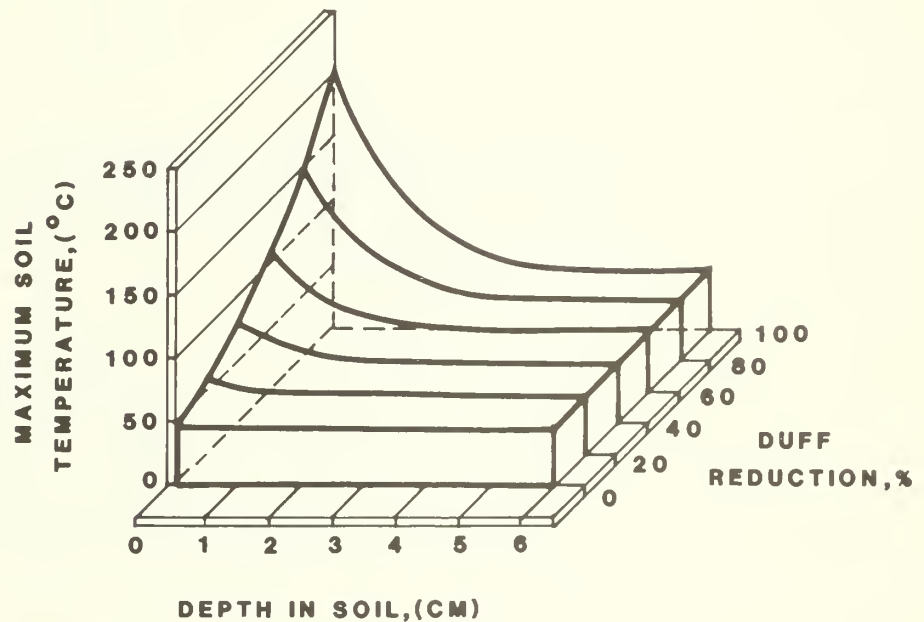
Figure 74.—The mathematical hypothesis.

Note that only the lower (left) half of the YP-sigmoid is utilized in this relation as the result of doubling the DR-scale ($XP = 200$) and the ST scale as well ($YP + $ intercept $= 400$, or $YP = 355$). In the last case, it would have been more consistent to have used $YP = 400$, but a suitable e^{-K} was found with 355; so 355 was retained.

76

Asymmetrical Bell-Shaped $X1$-Effect with Point of Peaking Moving in $X2$. The $X1$-Effect is Described in Two Segments and Interacts with the Bell-Shaped $X2$-Effect and the Concave-Upward $X3$-Effect

Contrived Example

Assume that finite curve forms and scales for a 4-D relation have been developed (within gross constraints of the expected relation) from trend information contained in half of a current data set, partitioned over the ranges of the three independent variables. The most prominent feature of the resulting curve array is the asymmetric nature of the $X1$-effect. This is displayed in figure 75 at three levels of $X2$, within each of three levels of $X3$.
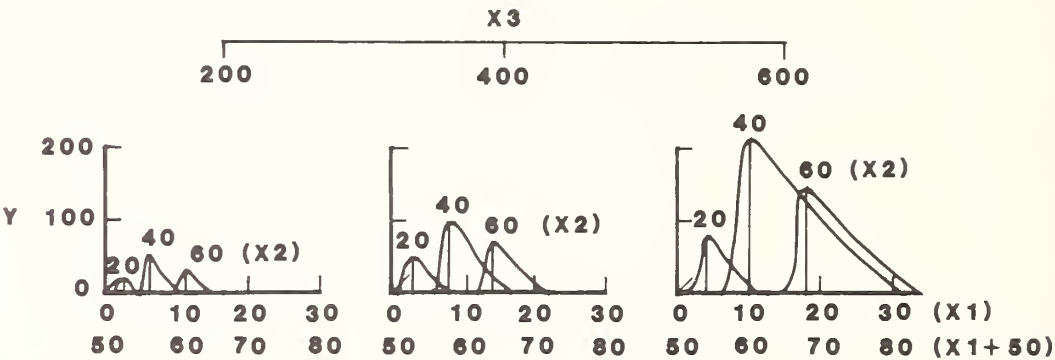
Figure 75.—The partial graphed hypothesis.

Also prominent, is the $X2$-effect, bell shaped, but truncated at the high end of the $X2$ scale. This is perhaps more fully appreciated in figure 76.
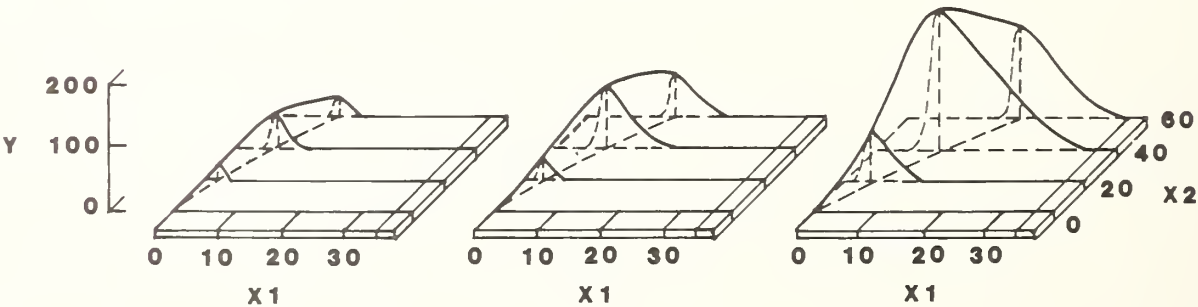

Figure 76.—The complete graphed hypothesis.

The number of $X2$- and $X3$-partitions are kept to a minimum to simplify the presentation of associated descriptive methods. More partitions would probably be desirable in a live data application.

Descriptor methods involved are identical to those shown earlier for 2- and 3-D hypotheses and are simply expanded to accommodate another independent variable. From figure 76 we can anticipate a reasonable mathematical hypothesis to be as shown below.

$X1$-**Effect.**—Since the bell-shaped curves are asymmetric, it would be efficient to create a sigmoidal descriptor for the left and right sides separately. They would be joined at $XP1$ and would be scaled to a common height, $YP1$. Thus, with $X1$ adjusted to $X1 + 50$ to accommodate the curve-breadth limit, $XP \pm XP$, the hypothesis for say, the left half, would be:

$$\hat{YL} = YP1(e^{-K}) \text{ left}$$

or,

$$\hat{YL} = YP1 \left\{ \frac{e^{-\left| \frac{\frac{(X1+50)}{XP1} - 1}{1 - IL} \right|^{nL}} - e^{-\left\{ \frac{1}{1 - IL} \right\}^{nL}}}{1 - e^{-\left\{ \frac{1}{1 - IL} \right\}^{nL}}} \right\}$$

where $YP1$, $XP1$, IL, and nL may change over the range of $X2$, $X3$, or both.

$YP1$.—Plotting the heights of the nine curves from figure 76 in figure 77 and smoothing over these points, $YP1$ varies as a symmetrical bell-shaped curve (e_2^{-K}) over $X2$, changes in height ($YP2$), and perhaps changes in shape (n and I) over $X3$. Then, $\hat{YP1} = YP2(e_2^{-K})$.
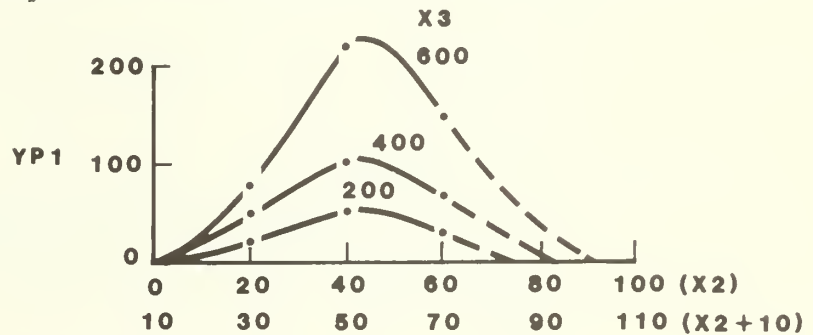

Figure 77.— YP1 smoothed.

$YP2$.—From figure 78, the plotted heights of these curves appear to follow an exponential function of X. Let us assume that we have made and compared an overlay curve with the X^n-Standards and that we have found a suitable descriptor in $\hat{YP2} = b_3(X3)^{n3}$.
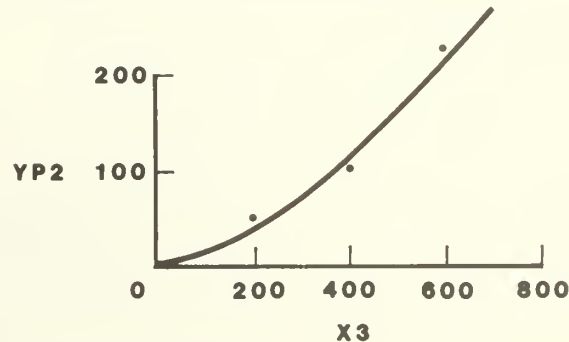

Figure 78.— YP2 smoothed.

$X2$ in e_2^{-K}.—The largest sigmoid of the set (for $X3 = 600$) reaches $X2 = 90$. Since $XP2 = 45$ here, all sigmoids fall within the required limits, $XP \pm XP$. But, it might be reasonable to extrapolate to $X3 = 700$ where the expected maximum might be say 100. In which case, a constant can be added to $X2$ in e^{-K} to accommodate the $(XP \pm XP)$-requirement, using $(X2 + 10)$ in place of $X2$, $XP2 = 55$, and $2XP2 = 110$. Then, the broadest curve will fall within $XP2 \pm XP2$.

$XP2$ in e_2^{-K}.—As may be seen in figure 77, $\hat{XP2} = 45$ in $X2$ for all levels of $X3$. And, since $(X2 + 10)$ is to be used in place of $X2$, $\hat{XP2} = 55$.

n_2 in e_2^{-K}.—Assume that overlay curves have been made for the left half of the three symmetrical bell-shaped curves in figure 77 and that comparison with the e^{-K}-Standards resulted in $n = 1.7$, 2.0, and 2.5 for $X3 = 200$, 400, and 600, respectively. Without the formality of plotting, n_2 will be assumed to be an exponential function of $X3$ so that: $\hat{n}_2 = a_4 + b_4(X3)^{n_4}$.

I_2 in e_2^{-K}.—Along with n_2, above, assume that appropriate I_2-values have been iden- tified as 0.50, 0.45, and 0.40 for $X3 = 200$, 400, and 600, respectively. By inspection, I_2 is a negative linear function of $X3$ so that $\hat{I}_2 = a_5 - b_5(X3)$.

In summary,

$$\hat{YP1} = YP2 \left\{ \frac{e^{-\left| \frac{\frac{(X2+10)}{XP2} - 1}{1 - I_2} \right|^{n_2}} - e^{-\left\{ \frac{1}{1-I_2} \right\}^{n_2}}}{1 - e^{-\left\{ \frac{1}{1-I_2} \right\}^{n_2}}} \right\}$$

where,
$\hat{YP2} = b_3(X3)^{n_3}$
$\hat{XP2} = 55$
$\hat{n}_2 = a_4 + b_4(X3)^{n_4}$
$\hat{I}_2 = a_5 + b_5(X3)$.

$X1$ in $(e^{-K})_{\text{left}}$.—Revision of $X1$ is necessary, since the smallest XP (from figure 76) approaches zero and the broadest curve reaches $X1 = 35$ at $X3 = 600$. Assuming ex- trapolation to $X3 = 700$, we might expect the broadest curve to reach no more than say $X3 = 50$.

To meet the constraint that all curves of the set be within $XP \pm XP$, $(X1 + 50)$ was used in place of $X1$. Then, where $XP1 = $ zero, $(X1 \pm 50) = 50$ and, at the high extreme where $X1 = 35$, $(X1 + 50) = 85$. And, using $(X1 + 50)$ in e^{-K}, all curves will be within the minimum $XP1 = 50$, since $\pm 2XP1 = 100$.

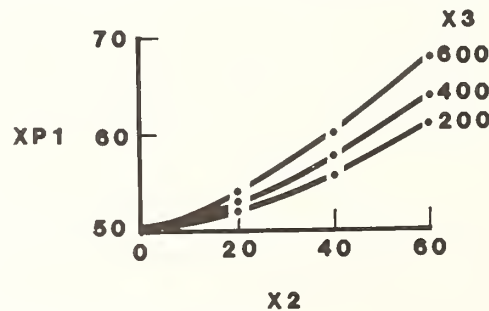$XP1$ in $(e^{-K})_{\text{left}}$.—$XP1$-values read from figure 76 are plotted and smoothed in figure 79.

Figure 79.—$XP1$ smoothed.

We will assume by inspection, that $XP1$ is an exponential function of $X2$ and that

$$X\hat{P}1 = (YP3/(60)^{n6}(X2)^{n6}.$$

YP3.—At the scaling point, $X2 = 60$, the heights ($YP3$) of the three curves in figure 77 are read as 11, 14, and 18, for $X3 = 200$, 400, and 600, respectively. Plotting these points in figure 80 and smoothing, $YP3$ can be seen to be a very flat exponential function of $X3$ so that
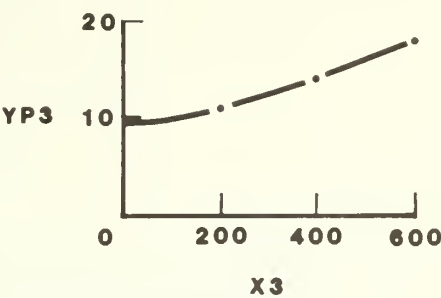
$$Y\hat{P}3 = a + b_7(X3)^{n7}.$$

Figure 80.—YP3 smoothed.

Also, we will assume that the shapes of the three curves in figure 77 have been compared with the X^n-Standards and have been found to have a constant n.

Then, $X\hat{P}1 = (YP3/(60)^{n6})(X2)^{n6}$
where $Y\hat{P}3 = a_7 + b_7(X3)^{n7}$.

nL and IL in $(e^{-K})_{left}$.—We will assume that the left sides of the nine curves in figure 75 have been screened for matching e^{-K}-Standards with the results shown in tables 27 and 28.

Table 27.—nL in $(e^{-K})_{left}$

X2	X3		
	200	400	600
	----------------- n ------------------		
20	2	2	2
40	2	2	2
60	2	2	2

Table 28.—IL in $(e^{-K})_{left}$

X2	X3		
	200	400	600
	------------------ IL ------------------		
20	0.970	0.965	0.938
40	.965	.959	.943
60	.973	.955	.940
average	0.969	0.960	0.940

nL.—Referring to table 27, the set of e^{-K}-Standards with $n = 2$ was deemed appropriate for the set, all levels of $X2$ and $X3$ included. So, $NL = 2$, a constant.

IL.—The I-values in table 28 are quite large since the left-side curves have very steep slopes and are proportionally far to the right in the $(X1 + 50)$ range. Systematic variation is associated primarily with changes in $X3$ as indicated by the average IL-values. These are plotted and smoothed in figure 81.
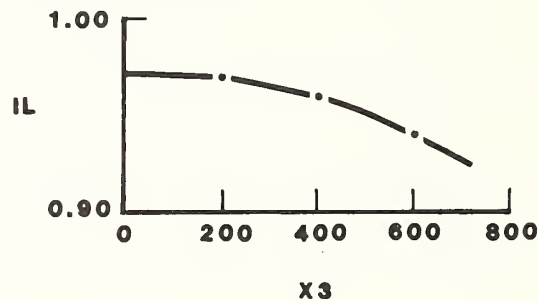
Figure 81.—IL smoothed.

And, again assuming this relation can be satisfactorily expressed by an exponential, we have:

$$\hat{IL} = 0.971 - b_7(X3)^{n7}.$$

Then, to summarize, the entire left side of the hypothesis may be specified as:

$$\hat{YL} = YP1(e^{-K}) \text{ left}$$

or,

$$\hat{YL} = YP1 \left\{ \frac{e^{-\left| \frac{\frac{(X1+50)}{XP1} - 1}{1 - IL} \right|^{nL}} - e^{-\left\{ \frac{1}{1-IL} \right\}^{nL}}}{1 - e^{-\left\{ \frac{1}{1-IL} \right\}^{nL}}} \right\}$$

where $YP1$, $XP1$, IL, and nL may change over the range of $X2$, $X3$, or both.

$$Y\hat{P}1 = YP2 \left\{ \frac{e^{-\left| \frac{\frac{(X2+10)}{XP2} - 1}{1-I_2} \right|^{n_2}} - e^{-\left\{ \frac{1}{1-I_2} \right\}^{n_2}}}{1 - e^{-\left\{ \frac{1}{1-I_2} \right\}^{n_2}}} \right\}$$

and

$$\begin{aligned}
YP2 &= b_3(X3)^{n_3} \\
XP2 &= 55 \\
n_2 &= a_4 + b_4(X3)^{n_4} \\
I_2 &= a_5 + b_5(X3) \\
XP1 &= (YP3/(60)^{n_6})(X2)^{n_6} \text{ and} \\
&\quad YP3 = a_7 + b_7(X3)^{n_7} \\
nL &= 2 \\
IL &= 0.971 - b_7(X3)^{n_7}.
\end{aligned}$$

Description of the right side of the hypothesis would be approached in the same fashion as above, to provide the unknowns in:

$$\hat{Y}R = YP1 \left\{ \frac{e^{-\left| \frac{\frac{X}{XP1} - 1}{1-IR} \right|^{nR}} - e^{-\left\{ \frac{1}{1-IR} \right\}^{nR}}}{1 - e^{-\left\{ \frac{1}{1-IR} \right\}^{NR}}} \right\}.$$

Note that $X1$ for the right side curves could be set $= (50 - X1)$ and $YP1$ and $XP1$ are the same for the right side as for the left.

Asymmetrical Bell-Shaped $X1$-Effect, with Constant Point of Peaking in $X2$. The $X1$-Effect is Described in Two Segments and Interacts with Concave-Upward $X2$- and $X3$-Effects

Live Data Example

The relation between total terpene content of lodgepole pine phloem by d.b.h. (D) phloem thickness (P), and 5-year radial growth (G) (from W. E. Cole and others 1981) was hypothesized graphically very nearly as in figure 82.

In explaining descriptor development here, we will focus on generalities. The details of formulating the graphed hypothesis, selecting control points, making overlay curves and comparing them to the Standards are assumed to be known from earlier text.
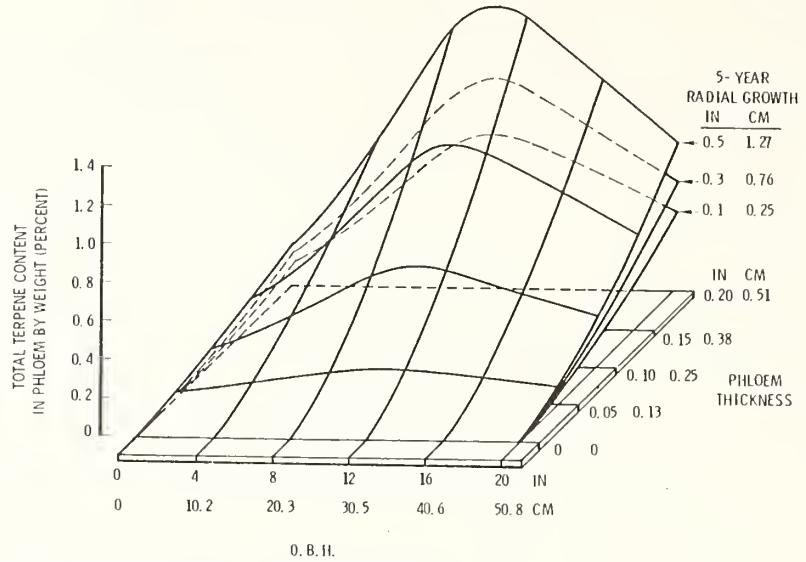
Figure 82.—The mathematical hypothesis.

In this example, the phloem thickness (P) effect was strong in both expectation and data trends (after testing more modest hypotheses, a data set was exploited for interactive hypothesis development). Its effect in the data was clearly exponential within d.b.h./growth data groups and appeared to be reasonably constant at about $n = 1.55$. Then, where the scaling point in P was at $G = 0.14$ (the approximate upper limit of the data over G),

$$\text{percent terpene content} = \left\{ \frac{YPP}{(0.14)^{1.55}} \right\} P^{1.55} \quad .$$

The heights of the peaks (YPP) of the asymmetrical bell-shaped curves over d.b.h. (D), at the constant point of peaking (XP), 10.5 inches, are specified as:

for $D \leq 10.5$

$$YPP = YPD(1.00165\, e^{-\left| \frac{\frac{D+8.5}{19} - 1}{0.395} \right|^2} - 0.00165),$$

for $D > 10.5$

$$YPP = YPD(1.07092\, e^{-\left| \frac{\frac{38.5-D}{28} - 1}{0.490} \right|^{1.4}} - 0.07092),$$

where

$$YPD = 0.38 + 1.0292(G)^{1.4}.$$

Note that sigmoids over D, while having a different shape on opposite sides of the peak, were identified as having consistent shapes for the three growth levels.

This completes the formulation applicable in the range $0 \le P \le 0.20$, $0 \le D \le 25$, and $0 \le G \le 0.35$, but explanation of the D-transforms for the sigmoids may be helpful here. The broadest bell-shaped curve expected (at $P = 0.20$) ranges from about $D = -8.5$ on the left side to $D = 38.5$ on the right. With $XP = 10.5$, the D scale for the left side is changed to $(D + 8.5)$ and that for the right is $(38.5 - D)$, as shown in figures 83 and 84.
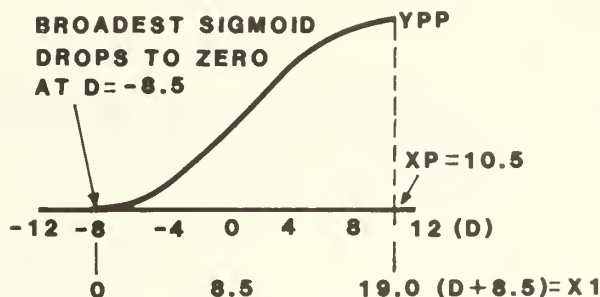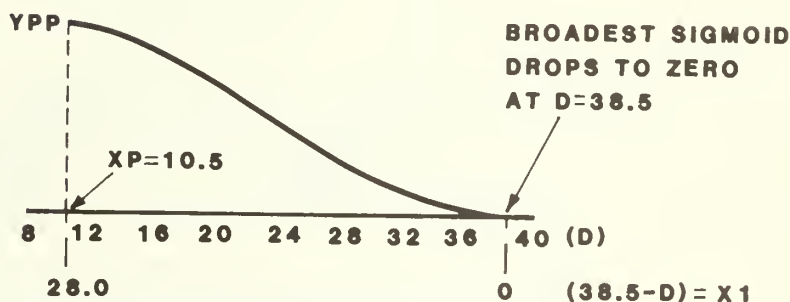
Figure 83.—D-transform for the left side.

Figure 84.—D-transform for the right side.

Again, these transforms of D insure that all points of the sigmoids are within the range $XP1 \pm XP1$.

The foregoing hypothesis was ultimately refitted to the data from which it was largely derived. This provided the most realistic appraisal of scale available at the moment for the relation characterized.

Given that total terpene estimated from the model $= X$ and that terpene content actually measured in the data $= Y$, the least squares coefficient, b, was

$$b = \Sigma XY / \Sigma X^2 = 1.10301.$$

This corrects for underscaling in the hypothesis insofar as the data set utilized is concerned. Slight improvement in R^2 was noted for the interactive hypothesis over that for the simple additive model with only linear effects of D, P, and G: $R^2 = 0.39$ versus 0.35, respectively. So, no potentially great advantage of the interactive over the additive model appears to exist in this data set. But, the hypothesis still provides new insights for the area of interest that should be of value in planning new studies.

Convex-Upward
$X1$-Effect with Peak
Moving in $X2$,
Interacting with
Concave-Upward
$X2$-Effects and Slight
Convex-Upward
$X3$-Effects

Live Data Example

Laboratory-controlled calibration data for Peltier thermocouple psychrometers were assembled by Brown and Bartos, 1981, and are shown smoothed over water potential in figure 85.
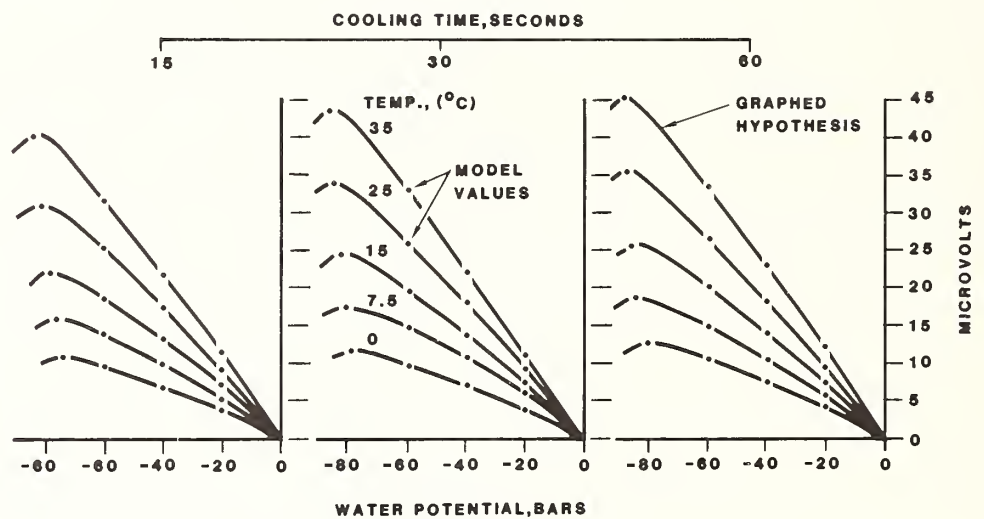

Figure 85.—The graphed hypothesis and model performance.

The combination of strong expectations for the relation, a well-conceived laboratory study, and strong data-group means left little doubt as to the form and scale of the relation between microvolt output and the independent variables, water potential in negative bars, temperature of the measured medium and the cooling time. The smoothed curves represent an exceedingly strong hypothesis and, with one additional variable, formed the basis for a published mathematical model intended for adjustment to other psychrometers of the same design. The four dimensional relation pictured, in fact, was described mathematically before including the effects of the fifth dimension and provides a unique opportunity to study four dimensional descriptor methods.

The strategy here was to describe microvolt output (MW) as a function of water potential (WP), temperature (T), and cooling time (CT), solving the resulting equation for (WP).

It was noted at the outset that interest in WP was limited to $XP \leq WP \leq 0$, where XP is the point in WP where microvolts peak. Also, it can be seen in figure 85 that XP changes over both T and CT. The heights of the curves, called upper intercepts (UI) here, change with both T and CT, and all curves over WP are oriented at zero. The general form of the relation is estimable from figure 85 as:

$$MV = UI1 - (UI1/|XP|^{n_1})|XP - WP|^{n_1}.$$

This is an exponential in the reversed WP-scale, $|XP - WP|$, scaled to the difference between $UI1$ and zero ($= UI1$) at $WP =$ zero, and subtracted from $UI1$. Smoothed values of XP and $UI1$ were established and described first, since they were subsequently used in place of actual XP and $UI1$-values to smooth XP-effects.

XP.—Within each of the three cooling times, the negative XP-values were read from figure 85 for each of the five temperature curves. The absolute values of these were plotted and smoothed over T within CT-groups, with the results shown in figure 86 as
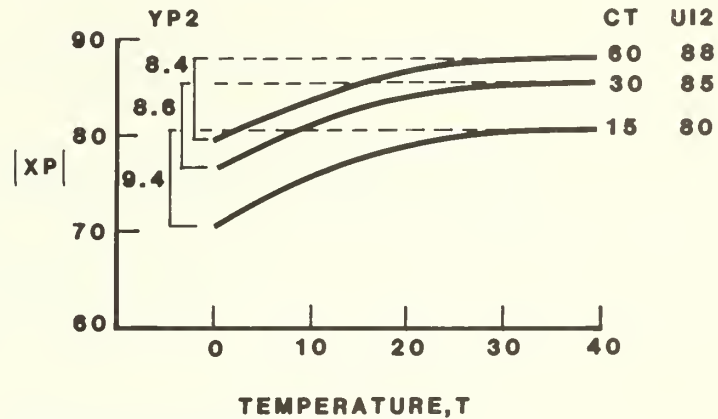
Figure 86.—$|XP|$ smoothed.

an exponential effect in the reversed T-scale, $(40 - T)$, scaled to the difference between an upper intercept ($UI2$), and scaled to the absolute difference between $UI2$ and the curve at $T =$ zero. Then, multiplying by (-1) to return $|XP|$ to its original negative state,

$$XP = (-1)(UI2 - (YP2/(40)^{n2})(40 - T)^{n2}).$$

UI2.—The $UI2$-values were plotted over CT and smoothed as shown in figure 87.
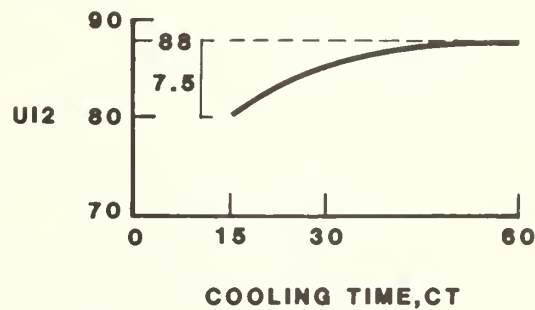
Figure 87.—$UI2$ smoothed.

This was described as an exponential in the reversed CT scale, $(60 - CT)$, subtracted from the upper intercept of 88.0, and scaled to the drop (7.5) at $CT = 15$. The resulting form was

$$UI2 = 88 - (7.5/(45)^{2.7})(60 - CT)^{2.7}$$
$$= 88 - 0.0002579 (60 - CT)^{2.7}.$$

YP2.—Similarly, the $YP2$-values were plotted over CT and smoothed (fig. 88).
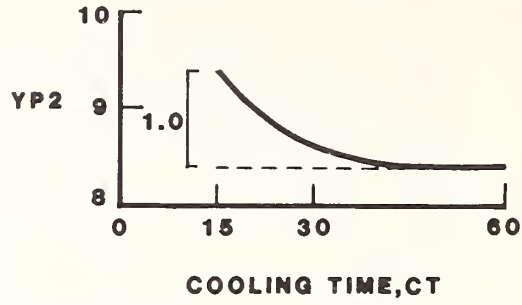
Figure 88.—*YP2* smoothed.

The resulting curve was described as an exponential in the reversed CT scale, $(60 - CT)$, scaled to the difference, 1.0, from the intercept at $CT = 15$, and added to the intercept. In this case,

$$YP2 = 8.4 + (1.0/(45)^{3.97})(60 - CT)^{3.97}$$
$$= 8.4 + 2.734 \times 10^{-7}(60 - CT)^{3.97}.$$

The shapes of the curves over T in figure 86 were determined through overlay curves and the X^n-Standards to be virtually constant at $n_2 = 2.35$. Then

$$XP = (-1)(UI2 - (YP2/(40)^{2.35})(40 - T)^{2.35}).$$

UI1.—Following the analytical pattern for XT, peak values ($UI1$) of the 15 curves in figure 85 were read, plotted, and smoothed over T within each of three CT-groups. Comparison of overlay curves with the X^n-Standards led to adoption of a constant flat form ($n = 1.1$) for all three curves. Intercepts and scaling heights changed over CT so that

$$UI1 = INT3 + (YP3/(40)^{1.1})(T)^{1.1}$$

where

$$INT3 = 12.1 - 0.003475(60 - CT)^{1.63}$$
$$YP3 \ = 39.2 - 0.0004346(60 - CT)^{2.45}.$$

n_1.—After graphically adjusting the figure 85 curves over WP for smoothed values of XP and $UI1$, absolute differences between the $UI1$ and the associated curves were read for seven points in WP ($XP \le WP \le$ zero). The resulting control points were normalized, plotted, and compared to the X^n-Standards. From this, n_1 varied sigmoidally over both T and CT such that

$$n_1 = 1.18 + 0.185 \left\{ \frac{e^{-\left| \frac{\frac{(40 - T)}{40} - 1}{1 - I} \right|^m} - e^{-\left\{ \frac{1}{1 - I} \right\}^m}}{1 - e^{-\left\{ \frac{1}{1 - I} \right\}^m}} \right\}$$

where

$$I = 0.45 + 0.000333(T) + (1.9846 \times 10^{-19})(CT)^{10}$$

$$m = 2.5 + e^{-\left| \dfrac{\dfrac{(60-CT)}{60} - 1}{0.405} \right|^3}.$$

So, with the foregoing inputs and as originally formulated,

$$MV = UI1 - (UI1/|XP|^{n_1})|XP - WP|^{n_1}$$

can now be estimated with the foregoing inputs. Performance of the model is shown on figure 85 where it may be seen that the model is an excellent reproduction of the graphed hypothesis. Modest smoothing effects over CT exist near the peaks at 30 and 60 seconds. The resulting four dimensional model is presented in figure 89 at two points in the fourth dimension ($CT = 15,60$).
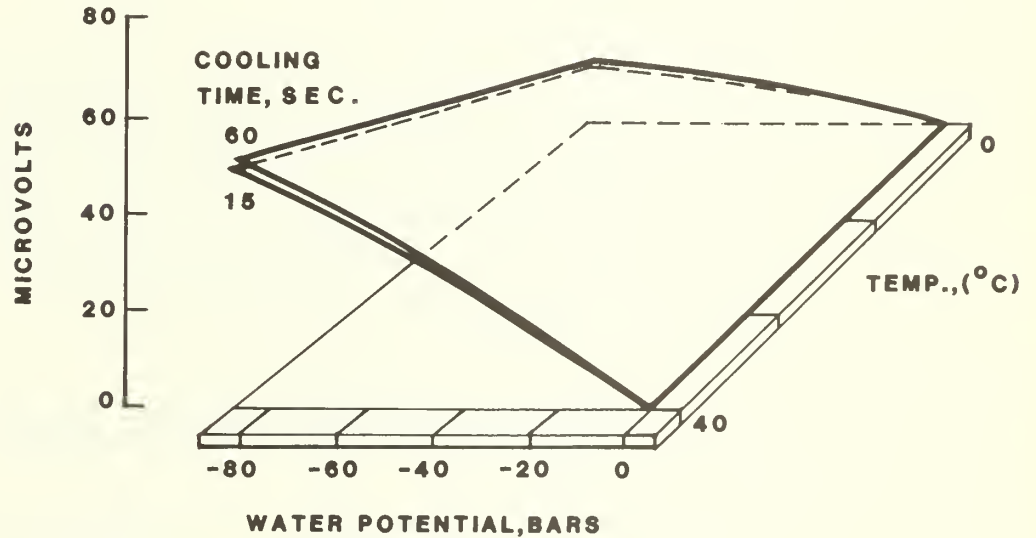
Figure 89.—The mathematical hypothesis for micro-volts.

Solution for WP.—As stated previously, interest here focused on $WP = f(CT, T,$ and $MV)$. Solving the MV estimator for WP, we have

$$WP = \left\{ \left\{ \frac{|XP|^{n_1}(UI1 - MV)}{UI1} \right\}^{1/n_1} + XP \right\} *(-1), \ XP \le WP \le 0.$$

**Concave-Upward
$X1$-Effects, with
Constant Point of
Peaking in $X2$ and
Interacting with
Convex-Upward
$X2$-Effects; Fourth
Dimension Discrete**

Live Data Example

Here, phloem thickness (P) in lodgepole pine was expressed as a function of electrical resistance of cambium (R), d.b.h. (D) and of three discrete points in time, May, July, and October. The hypothesis (fig. 90) was based on a fairly large data set from a period of active tree growth (July) and was developed within the constraints of prior knowledge (data from D. M. Cole and Jensen 1980).
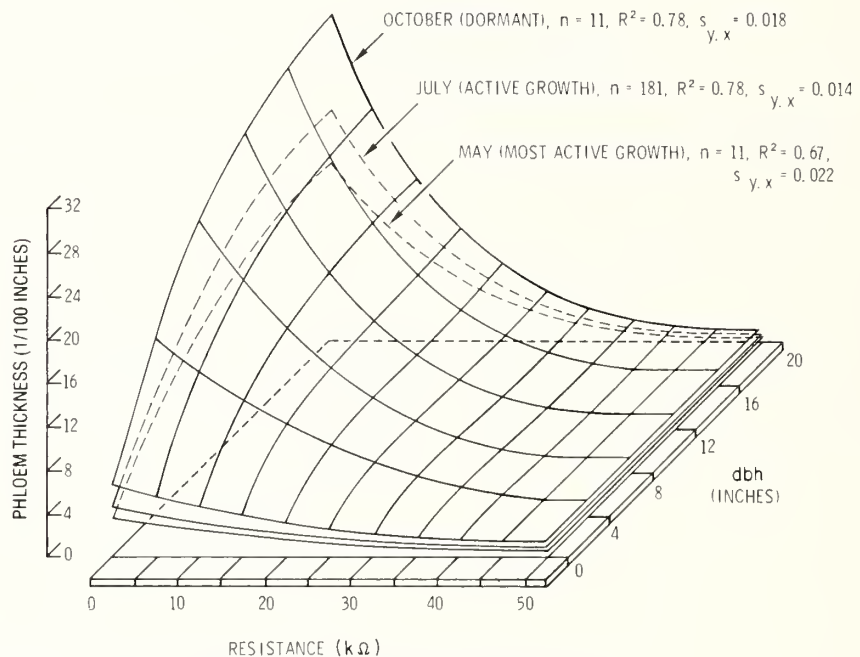
Figure 90.—Phloem thickness of lodgepole pine in relation to d.b.h. and electrical resistance of cambium, the mathematical hypothesis.

Data for May and October were subsequently obtained and appeared to be fairly well represented by the July surface. When the hypothesis was fitted to each of the new data sets independently, the resulting surfaces bracketed that for July as expected. The hypothesis was subsequently tested with new, small data sets.

Explanations of descriptor development that follow, assume familiarity with 2-D descriptor methods discussed earlier.

The July data were sorted into d.b.h.-groups. Within each d.b.h.-group, smoothed trends over R were estimated in accord with expectation (shown schematically in figure 91).

The negative relation of P to R was strongly displayed in the data, so this was the starting point for the descriptor using the reversed R-scale on an estimated intercept of 0.01. Then
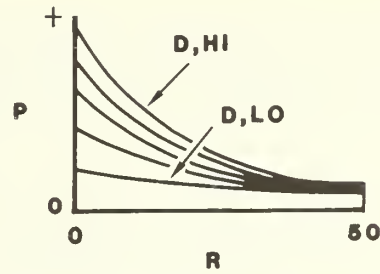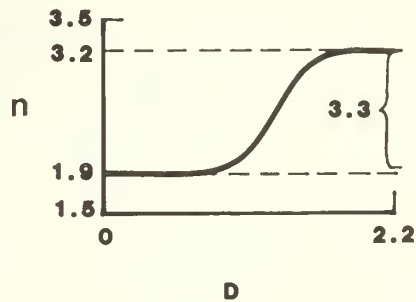
$$P = 0.01 + (YP/(45)^n)(50 - R)^n.$$

Figure 91.—The schematic trends.

Screening the resulting curves for n in the X^n-Standards, n varied sigmoidally from 1.9 at smaller diameters to about 3.2 at larger ones. The trend was estimated to be as shown in figure 92 where,

Figure 92.—n smoothed.

$$n = 1.9 + (1.3)e^{-\left|\dfrac{\frac{D}{22}-1}{0.7}\right|^{7}}$$

The R-effect was scaled at $R = 5$ or $(50 - R) = 45$, since this was the lower limit of the data over R. The height of the July surface at this point minus the intercept of $0.01 = YP$. YP varied positively (convex upward) with D as shown on the July surface (fig. 90) at $R = 5$. This effect (fig. 93) was described as a double component X^n-function of the re-
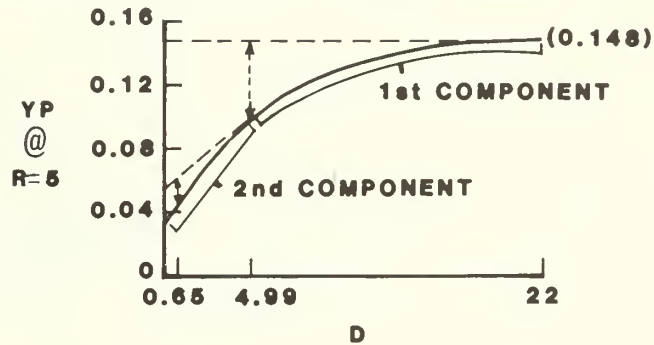
Figure 93.—YP smoothed.

versed D-scale, subtracted from the uppermost YP, ($YP = 0.158 - 0.010 = 0.148$). The first component was scaled at $D = 4.99$, the second at 0.65. And

$$YP = 0.148 - (2.2687 \times 10^{-5})(22 - D)^{2.72}$$
$$- (1.2694 \times 10^{-14})(22 - D)^{9},$$

thus completing the inputs for the hypothesis pictured in figure 90. Limits of application are: $0 \leq D22$; $0 \leq R \leq 50$. For $D > 22$, $n = 3.2$ and for $R > 50$, $P = 0.01$.

Based on performance of the hypothesis for the May and October data sets, $R^2 = 0.67$ and 0.78, $s_{y.x} = 0.22$ and 0.018, respectively, the July hypothesis appears to represent other months within reason.
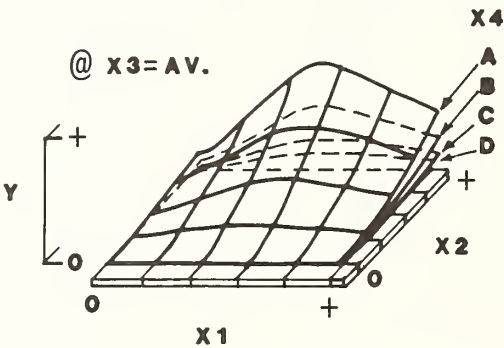
91

MATHEMATICAL DESCRIPTION OF GRAPHED
HYPOTHESES – FIVE DIMENSIONS
Outline for "FIVE DIMENSIONS"

**Extension of the
4-D Psychrometer
Example
(Pages 86–89) to
Include the Linear
Interactive Effects of
X3 and X4**

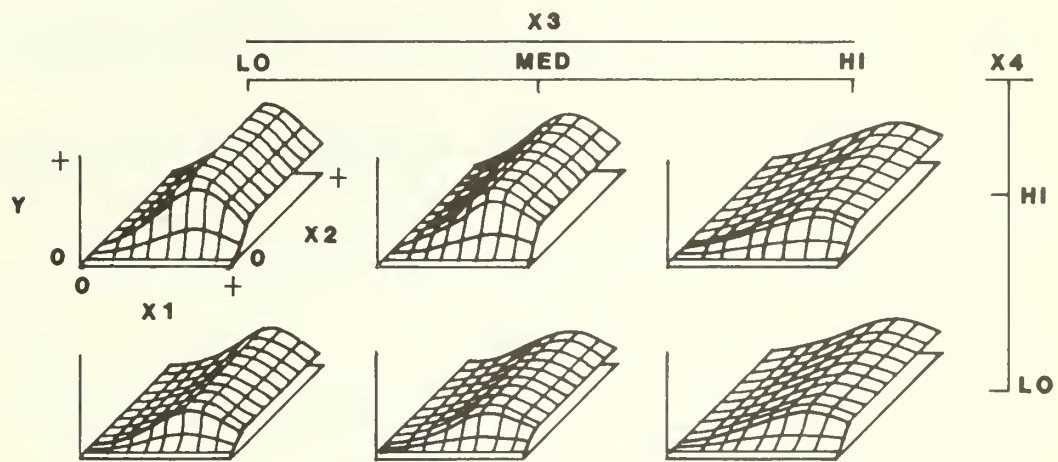**Live Data Example**

The Brown and Bartos (1981) four-dimensional thermocouple example (fig. 89 and 94), ultimately had a fifth dimension. It consisted of the variable, zero-offset microvolts
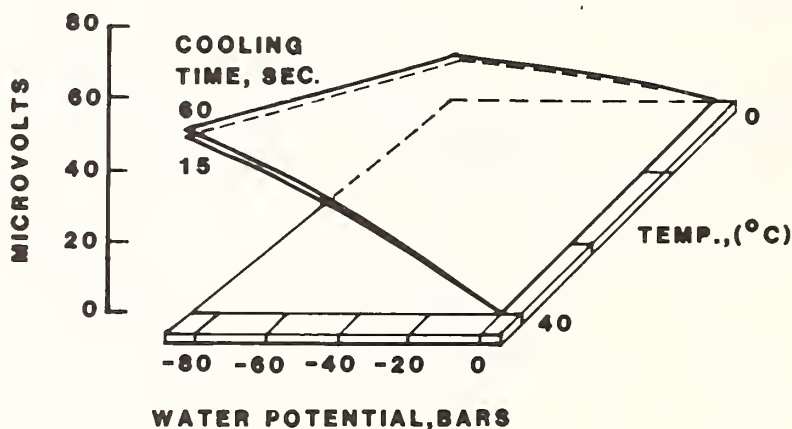

Figure 94.—The 4-D microvolt mathematical hypothesis.

(ZOM), and is an index of the temperature differential between the thermocouple sensor tips. Such differential has an effect, zero-offset error (ZOE), on the microvolt output that changes depending on the average temperature level of the measured medium and on the direction of the temperature difference between the tips, as indicated in figure 95.
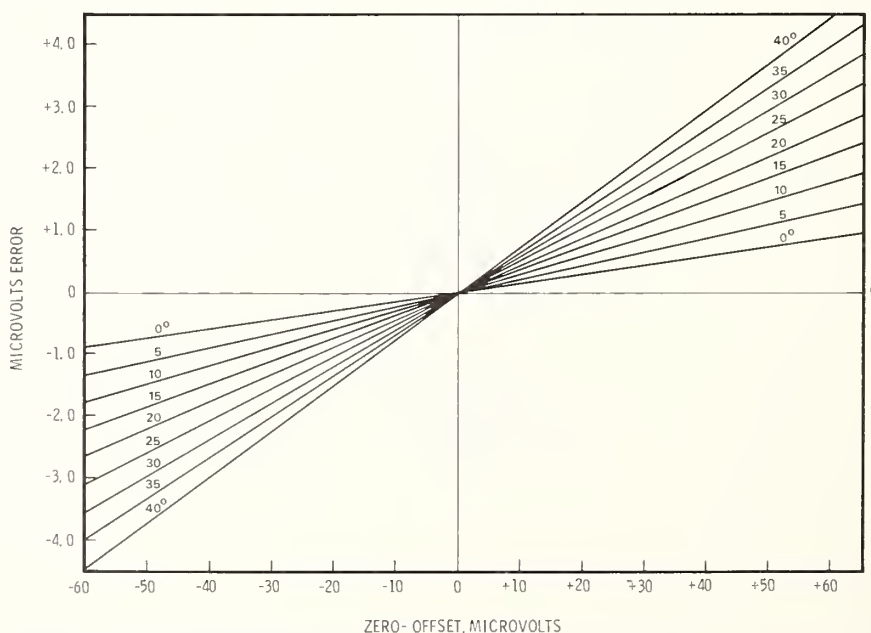

Figure 95.—Zero-offset error source information.

ZOE is quantified in figure 95 only at $CT = 15$ seconds and $WP = -22.5$. A proportional ratio of change, C, for microvolts estimated in the four-dimensional model ($MV4$) is derived from MV-readings at $WP = -22.5$, as specified below:

$$C = \frac{MV_s + (MV_s/MV_{15})ZOE}{MV_s} ,$$

where

$MV_s = MV$ at specified average temperature, ZOM, and $15 \leq CT \leq 60$

$MV_{15} =$ as above, but with $CT = 15$.

Then,

$MV5 = MV4(C)$

where

$MV4 = f(CT, T, WP)$, as previously specified, and

$ZOE = b_1(ZOM) + b_2(ZOM)(T)$

where

b_1 and b_2 are estimable directly from figure 96, an annotated version of the right side of the three-dimensional form implied in figure 95.
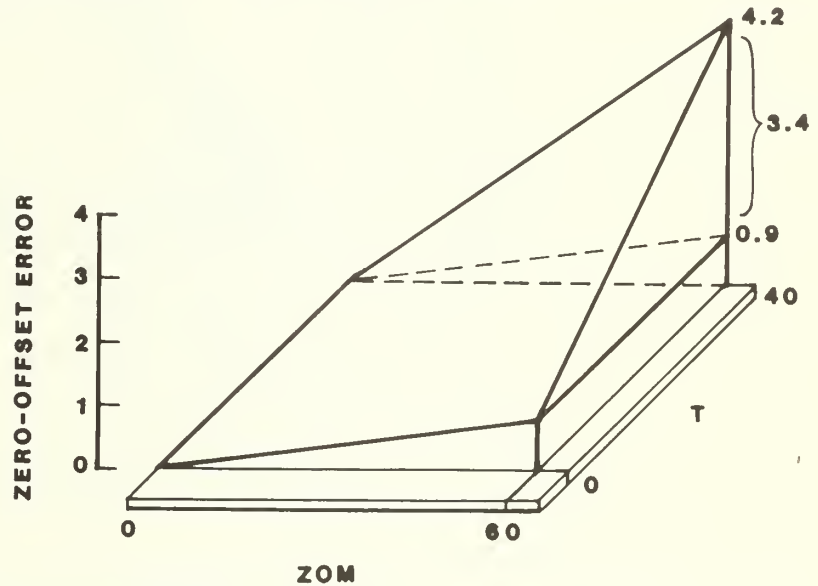

Figure 96.—Zero-offset error in 3-D.

From figure 96,

$b_1 = (0.9/60)(ZOM) = 0.015(ZOM)$
$b_2 = (3.4/60 \times 40))(ZOM)(T) = 0.001471(ZOM)(T)$.

Note that the formula for the right side of figure 95 applies to the left side also, since the sign of ZOM and C both become negative there.

This completes the five-dimensional relation, where $MV5 = MV4(C)$ and

$$MV5 = (UI1 - (UI1/|XP|^{n_1})|XP - WP|^{n_1})C.$$

Again, with interest focused on WP and solving $MV5$ for WP, we have

$$WP = \left\{ \left\{ \frac{|XP|^{n_1}(UI1 \times C - MV)}{UI1 \times C} \right\}^{1/n_1} + XP \right\} *(-1),\ XP \leq WP \leq 0.$$

**Discrete-Variable
Extension of the
4-D Terpene Model**

Live Data Example

Given the 4-D relation already established for total terpenes (fig. 82 and 97), the residual problem of estimating such a relation for each of three component or component groups of the total (beta-phelandrene, beta-pinene + 3-carene + myrcene, and alpha-pinene) was approached. The associated data were screened graphically over D, P, and G, and were found to contain more relative variability than existed with analysis of total terpenes. There did not appear to be, however, any recognizable departure of basic forms from those estimated to exist for total terpenes.
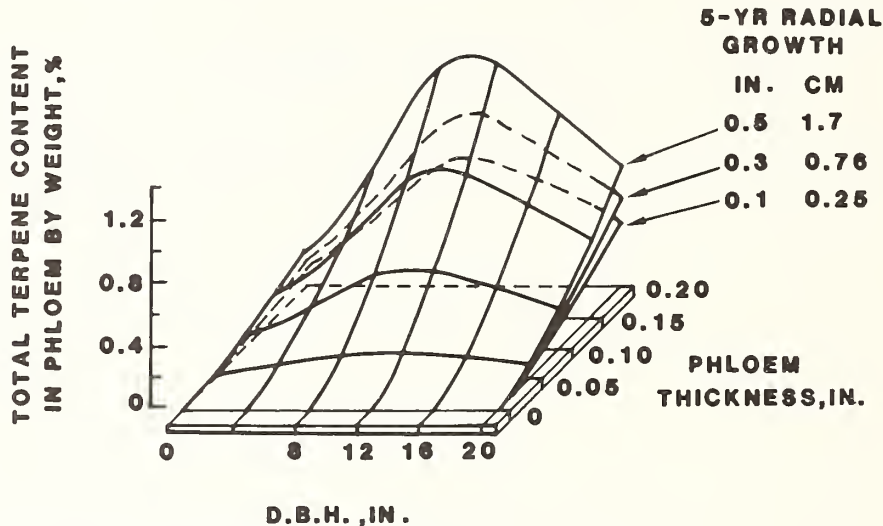

Figure 97.—The 4-D mathematical hypothesis.

Then, the obvious alternative of fitting the relation developed for total terpenes to that for each component or component group by least squares was adopted. That is, where estimated total terpene $(T) = X$ and measured component terpene $= Y$, the least squares coefficient, b, was

$$b = \Sigma XY / \Sigma X^2.$$

The expected sum of the three coefficients independently obtained was the b of 1.10301 determined for total terpenes (from the 4-D terpene example). So, the three b values were adjusted by the simple ratio of

$$\left\{ \frac{b \text{ for total terpenes}}{\Sigma b_i \text{ for components}} \right\}.$$

Final component coefficients (and associated R^2's) are shown in table 29. Holding G at its average, 1.59, the resulting surfaces appear as in figure 98.

These surfaces would vary jointly as a rather flat concave-upward curve over G since, from the 4-D terpene example,

$$YPD = 0.38 + 1.0292(G)^{1.4}.$$

Table 29.—4-D coefficients and R^2's for terpene components

	b	R^2
Beta-phelandrene	0.64292	0.402

Beta-pinene +
   3-carene +
     myrcene ....
	.30222	.352

Alpha-pinene	.15787	.213
Total terpenes (sum)	1.10301	0.387

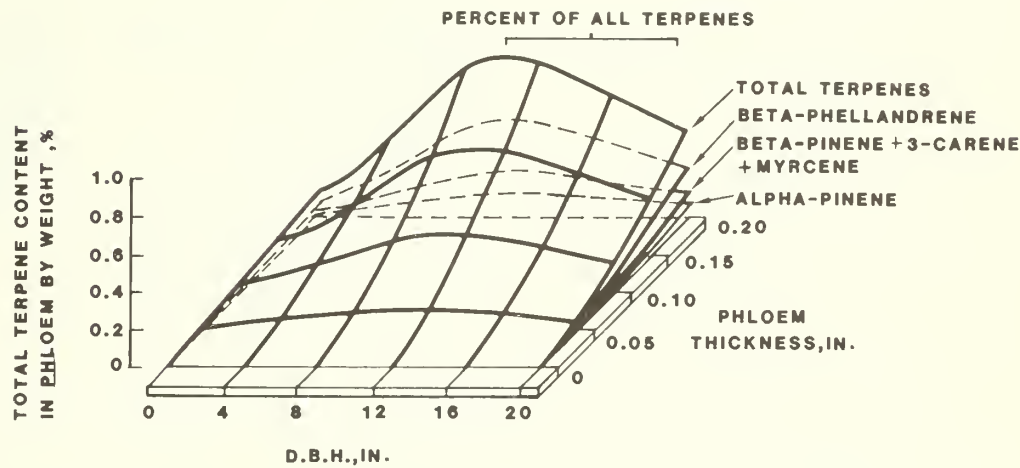Figure 98.—Discrete partitions for the 4-D terpene hypothesis.

Also, since the form of the relation is identical for each component terpene and the total and since component scales sum to that for the total, components will always sum to the total at any point in the relation.

Symmetrical Bell-Shaped $X1$-Effect with Moving Peak in $X3$; $X2$, a Sigmoid, Interacts with $X1$ to Form the Ridge Shown, Which Changes in Height Sigmoidally Over the Ranges of $X3$ and $X4$

Live Data Example

Our hypothesis development here, involves a small data set (from Lee and others 1973) associated with the gap-graded road materials problem discussed under 3-D, asymmetrical bell-shaped ridges. These data were exhausted of information graphically under constraints of expectation to arrive at the mathematical hypothesis shown in figure 99.
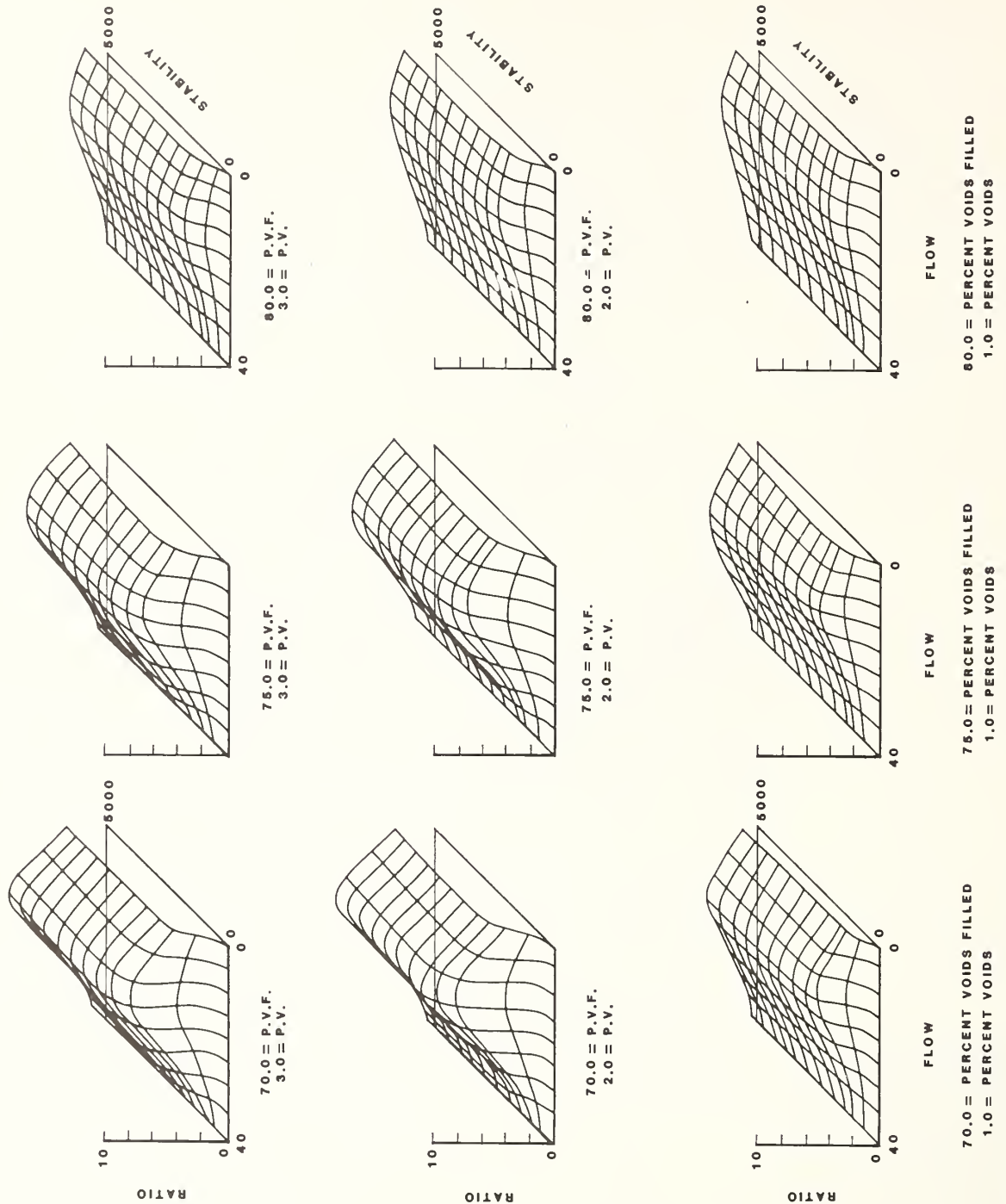
Figure 99.—The mathematical hypothesis.

The explanations of descriptor development that follow presume familiarity with the methods presented in the TWO DIMENSIONS section.

The effect of stability (S) on the dependent variable, ratio (R), was strongly expressed in the data and so was the first effect specified in the descriptor. S appeared to have a consistent sigmoidal shape within partitioned data groupings (some missing because of the small data set) of the remaining three independent variables, flow (F),

percent voids (V), and percent voids filled (VF). This is shown schematically in the top two graphs in figure 100. The starting point in the descriptor is

$$\text{RATE} = (YP)e^{\displaystyle -\left| \frac{\dfrac{S}{5000} - 1}{0.9} \right|^{35}},$$

a sigmoid upward to the right over S with zero intercept whose vertical scale, YP, is dependent on the remaining three variables.
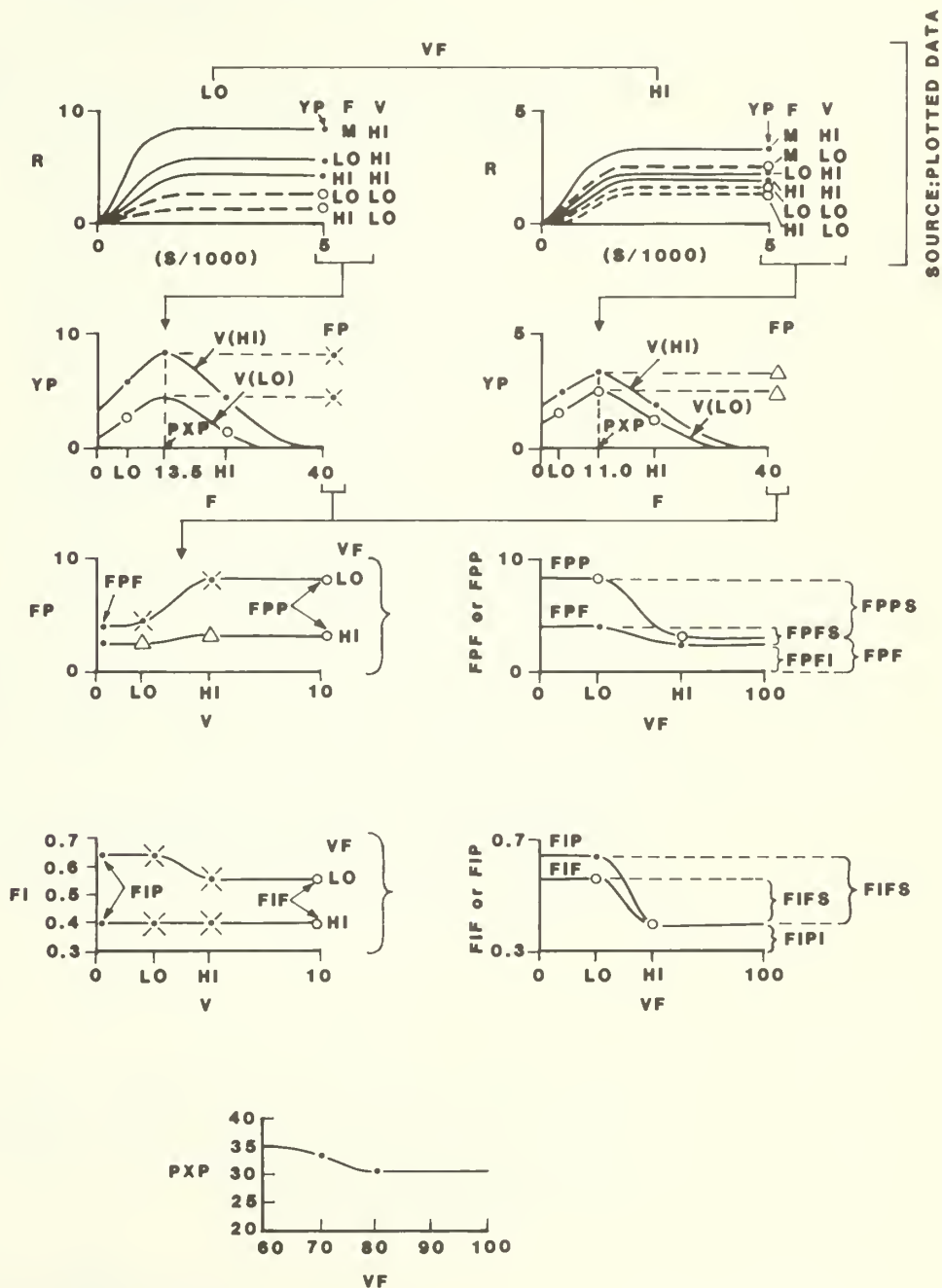

Figure 100.—Sequential development of forms and scalars.

The scalar effect of F at $S = 5000$ is bell shaped and symmetrical as may be seen in the two graphs (second pair from the top) in figure 100. Adding 20 to F to accommodate the broadest curve of the set under the constraint that e^{-K} functions only between zero and $2XP$, these curves are described by

$$YP = FP \left\{ \frac{e^{-\left|\frac{\frac{(F+20)}{PXP} - 1}{1 - FI}\right|^{1.6}} - e^{-\left\{\frac{1}{1-FI}\right\}^{1.6}}}{1 - e^{-\left\{\frac{1}{1-FI}\right\}^{1.6}}} \right\}.$$

where

FP, the scalar for YP, is estimated (conservatively) to vary sigmoidally with both V and VF, as shown in the third tier of graphs from the top of figure 100. The descriptor is

$$FP = FPF + (FPP)e^{-\left|\frac{\frac{V}{10} - 1}{0.78}\right|^{50}}$$

and

$$FPF = 2.4 + (1.8)e^{-\left|\frac{\frac{(100 - VF)}{40} - 1}{0.42}\right|^{9}}$$

$$FPP = 0.8 + (2.9)e^{-\left|\frac{\frac{(100 - VF)}{40} - 1}{0.42}\right|^{9}}$$

where FPP adds $(3.2 - 2.4 =)0.8$ at $VF = 100$, and $(7.9 - (2.4 + 1.8 + 0.8) =)2.9$ at $VF = 0$. PXP is mobile and is assumed to be sigmoidal as shown in the graph at the bottom of figure 100. PXP changes with VF only and can be identified as

$$PXP = 31 + (2.8)e^{-\left|\frac{\frac{(100 - VF)}{40} - 1}{0.42}\right|^{9}}.$$

And the inflection points (FI) for the bell-shaped YP-curves vary with V, as shown in the left graph of the two just above the one for PXP. The graph to the right of that shows associated sigmoidal trends (assumed) over VF for intercepts (FIF) and peaks (FIP). All told, the descriptor for FI is as follows

$$FI = FIF + (FIP)e^{-\left|\frac{\frac{(10 - V)}{10} - 1}{0.27}\right|^{10}}$$

where

$$FIF = 0.41 + (0.15)e^{-\left|\dfrac{\dfrac{(100 - VF)}{40} - 1}{0.42}\right|^{9}}$$

$$FIP = (0.08)e^{-\left|\dfrac{\dfrac{(100 - VF)}{40} - 1}{0.42}\right|^{9}}.$$

This chain of descriptor components is converted to the Fortran IV statements shown below:

$T = (EXP(-(ABS(((100 - VF)/40 - 1)/.42)**9)))$
$PXP = 31 + 2.8*T$
$FPF = 2.4 + 1.8*T$
$FPP = .8 + 2.9*T$
$FIF = .41 + .15*T$
$FIP = .08*T$
$FP = FPF + FPP*(EXP(-(ABS((V/10 - 1)/.78)**50)))$
$FI = FIF + FIP*(EXP(-(ABS(((10 - V)/10 - 1)/.27)**10)))$
$LN = EXP(-(ABS(((F + 20)/PXP - 1)/(1 - FI))**1.6))$
$RN = EXP(-((1/(1 - FI))**1.6))$
$YP = FP*((LN - RN)/(1 - RN))$
$RATE = 1.0315*YP*(EXP(-(ABS((S/5000 - 1)/.9)**35)))$

Note that the coefficient of 1.0315 resulted from the refitting of the mathematical model back through the data from which it was derived by least squares. Given that modeled rates $= X$ and actual rates $= Y$, $b = \Sigma XY/\Sigma X^2$. Then bX (or $RATE$) is the model submitted to electronic computer/plotter processing that resulted in the graphic presentation of the mathematical hypothesis in figure 99.

It is of interest that the additive model with linear effects of S, F, V, and VF, reached an R^2 of only 0.42 under least squares fit, while, for the model just derived, $R^2 = 0.80$. There would appear to be substantial benefit from utilizing all information at hand for developing the hypothesis in this case.

Symmetrical Bell-Shaped $X1$-Effect with Constant Point of Peaking in $X2$. The Interacting Effect of $X2$ is Concave-Upward and Those of $X3$ and $X4$ are Sigmoidal

Live Data Example

The flexibility of e^{-K} in representing a complex relation is again evident in the five-dimensional interaction pictured in figure 101.
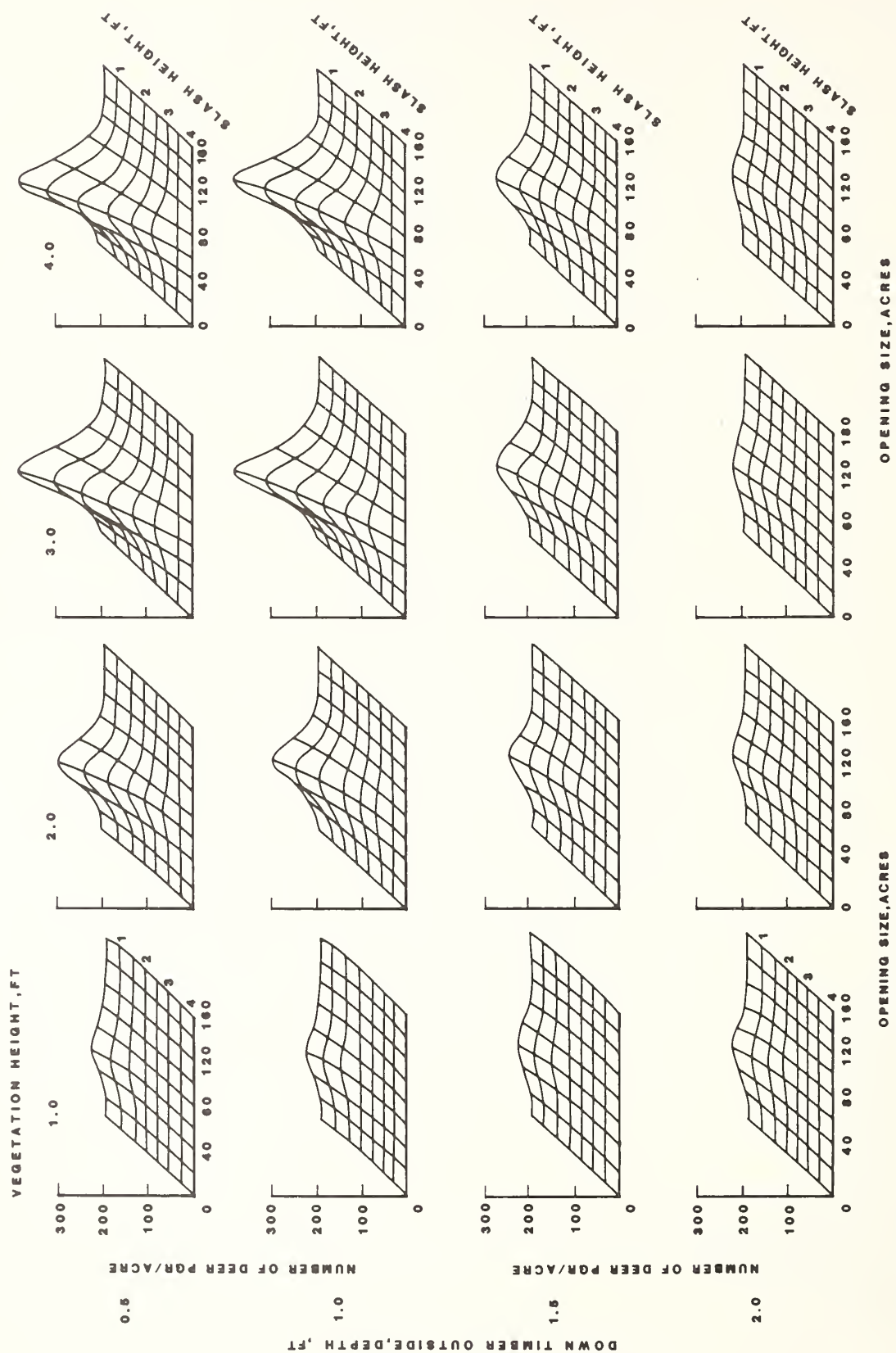
Figure 101.—Deer pellet groups as five-dimensional function of clearcut opening characteristics.

Here, data from Lyon 1976 and Lyon and Jensen 1980 were the basis for an index to intensity of deer use of forest openings created by clearcutting in western Montana. The index is expressed as a function of opening size, height of new vegetation, depth of slash in the opening, and depth of dead and down timber adjacent to the opening.

The data at hand were initially committed to statistical evaluation of the linear effects of the above variables and other independent variables on the intensity index. These were virtually the simplest regression hypotheses that could have been adopted. In this case, the evaluation provided only weak support for expected results and yielded little new information.

To exploit the data further, a hypothesis was developed for the set of four independent variables above. Prior knowledge of the forms of the relations, including interactions, between these variables was summarized. Subject to these constraints, the limited data were then partitioned and graphically exhausted of associated curve-form and scaling information. Data appeared to provide strong support for the dynamic interaction anticipated. Procedures specified here were used to develop a functional form, XT, for the graphed interaction. This was refitted to the data by least squares in the model $PGR = b(XT)$ and $b = 0.9721$. The adjusted model is specified below:

$$PGR = f(VI, SI, SO, \text{Acres})$$

where,

PGR = number of deer pellet groups per acre inside the opening.
VI = height of vegetation in feet, inside the opening.
SI = depth of logging slash in feet, inside the opening.
SO = depth of dead and down timber, in feet, outside the opening.
Acres = size of opening in acres.

If $SI < PO$

$$PGR = \left\{ \frac{YP}{(PO - 0.6)^{1.55}} \{PO - SI\}^{1.55} \right\} (0.9721)(50)$$

where

$$YP = YPS \left\{ \frac{e^{-\left| \frac{\frac{\text{Acres} + 200}{260} - 1}{1 - I} \right|^{1.75}} - e^{-\left\{ \frac{1}{1-I} \right\}^{1.75}}}{1 - e^{-\left| \frac{1}{1-I} \right|^{1.75}}} \right\} + 0.23$$

$$YPS = 0.57 + 3.23 \left\{ e^{-\left| \frac{\frac{VI}{8} - 1}{0.76} \right|^{20}} \right\} \left\{ e^{-\left| \frac{\frac{3 - SO}{3} - 1}{0.4942} \right|^{10}} \right\}$$

$$PO = 6.289 e^{-\left| \frac{\frac{VI}{10} - 1}{0.999} \right|^{10.5}} - 2.289$$

$$I = 0.897 - 0.067e^{\displaystyle -\left| \frac{\frac{VI}{8} - 1}{0.404} \right|^{3.5}}.$$

If $SI > PO$

$PGR = 0$

Limits

$0 \le SI \le 4$, $0 \le SO \le 3$, $0 \le VI \le 8$, $0 \le$ Acres ≤ 300.

Graphic development of the model described by this function apparently resulted in great sensitivity to the interaction information contained in the data. But, since the degrees of freedom thereby sacrificed were unknown, conventional statistical parameters were not estimable. Some indication as to the goodness-of-fit of the functional form to the data set from which it was largely derived is provided by the proportion of the total sum of squares explained by the model, $R^2 = 0.71$ here.

Contrast this with the R^2 of 0.21 achieved with a minimum-effort additive regression model where linear effects of the same four independent variables have been fitted to the data by least squares. It would appear that sharp focus on interaction formulation was justified.

At this point in the paper, it is assumed that only a minimum of explanatory information will be necessary to clarify descriptor development.

The expected negative SI effect was strongly apparent in the data and so was used as the starting point for the descriptor. This effect was exponential over the reversed SI-axis where $0.6 \le SI \le PO$. The lower extreme of the data in SI, 0.6, was adopted as the scaling point (largest PGR-values) in the reversed SI-scale. PO, a variable over VI, represented the point in SI where the PGR-curves reached zero (fig. 102).

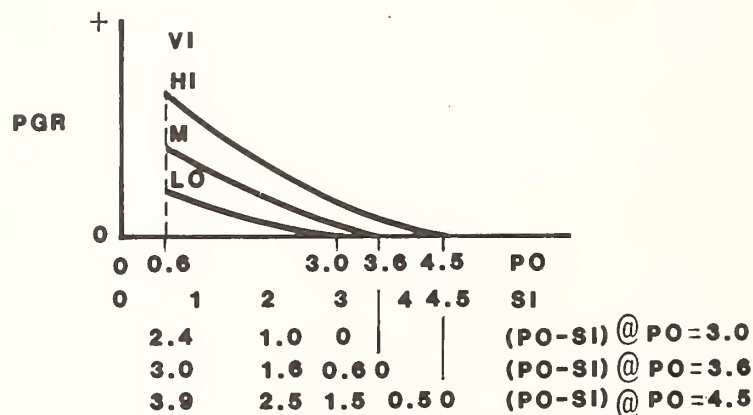|	0.6		3.0	3.6	4.5	PO		
0	1	2	3		4	4.5	SI	
	2.4	1.0	0				(PO-SI) @ PO = 3.0	
	3.0	1.6	0.6	0			(PO-SI) @ PO = 3.6	
	3.9	2.5	1.5	0.5	0		(PO-SI) @ PO = 4.5	

Figure 102.—The *SI*-effect with changing points of origin, *PO*.

When the point of exponential origin was allowed to vary, n in X^n approached a constant (1.55) over SI, but the scaling heights of these curves ($@SI = 0.6$) varied over $ACRES$, VI and SO.

Then,

$$PGR = (50 \times b)(YP/(PO-0.6)^{1.55})(PO - SI)^{1.55}, \quad SI \le PO$$

where

50 is the constant necessary to the conversion of data units to acres;

b is the least squares coefficient fitting the derived model back through the source data.

Note that segmentation is employed in the exponential variable here, since beyond PO in SI, PGR is specified as zero. PO varied sigmoidally over VI and

$$PO = 6.289\, e^{-\left|\frac{\frac{VI}{10} - 1}{0.999}\right|^{10.5}} - 2.289$$

$$YP = 0.23 + YPS \left\{ \frac{e^{-\left|\frac{\frac{Acres + 200}{260} - 1}{1 - I}\right|^{1.75}} - e^{-\left\{\frac{1}{1-I}\right\}^{1.75}}}{1 - e^{-\left\{\frac{1}{1-I}\right\}^{1.75}}} \right\}.$$

XP appeared constant at 260 acres and, from the e^{-K}-Standards, $n = 1.75$ was reasonably representative for all curves. I, however, varied sigmoidally over VI and

$$I = 0.897 - 0.067\, e^{-\left|\frac{\frac{VI}{8} - 1}{0.404}\right|^{3.5}}.$$

YPS, the heights of the bell-shaped curves over $ACRES$, varied as an interaction of sigmoids, a new descriptor feature. YPS varied sigmoidally over VI as

$$YPS = 0.57 + 3.23\, e^{-\left|\frac{\frac{VI}{8} - 1}{0.76}\right|^{20}},$$

but only achieved this magnitude of effect at smaller SO-values. The VI-effect became sigmoidally smaller as SO increased. Noting that the unscaled sigmoid over the reversed SO-axis $(3 - SO)$ ranges in value from zero to one, the SO-effect,

$$e^{-\left|\frac{\frac{3 - SO}{3} - 1}{0.492}\right|^{10}},$$

becomes a convenient multiplier with which to achieve the appropriate sigmoidal reduction of the maximum VI-effect.

All curve-form estimates were derived from data-based graphic hypotheses, normalized control points, overlay curves, and comparison to either the X^n- or e^{-K}-Standards. While

the foregoing mathematical specifications may seem voluminous, they are quite easily specified in a short Fortran IV program for computer processing, as shown:

$$PO = 6.289*(EXP(-(ABS((VI/10-1)/.999)**10.5))) - 2.289$$
$$IF(SI.GT.PO)GO\ TO\ 1$$
$$A = EXP(-(ABS(((3-SO)/3-1)/.492)**10))$$
$$B = EXP(-(ABS((VI/8-1)/.76)**20))$$
$$YPS = 3.23*A*B + .57$$
$$I = .897 - .067*(EXP(-(ABS((VI/8-1)/.404)**3.5)))$$
$$LN = EXP(-(ABS(((ACR+200)/260-1)/(1-I))**1.75))$$
$$RN = EXP(-((1/(1-I))**1.75))$$
$$YP = YPS*((LN-RN)/(1-RN)) + .23$$
$$PGR = (YP/(PO-.6)**1.55)*((PO-SI)**1.55)*(0.9721)*50$$
$$X(5) = PGR$$
$$RETURN$$
$$1\ X(5) = 0$$
$$RETURN$$
$$END$$

Note that figure 102 was plotted electronically using a program that incorporated the above statements.

PUBLICATIONS CITED

Bartlett, M.S.

1947. The use of transformations, Biometrics 3:39–52.

Box, G.E.P., W. G. Hunter, and J. S. Hunter.

1978. Statistics for experimenters. Wiley & Sons, New York.

Brown, R. W., and D. L. Bartos.

1981. A calibration model for screen-caged Peltier thermocouple psychrometers. USDA For. Serv. Res. Pap. INT–293, 155 p. Intermt. For. and Range Exp. Stn., Ogden, Utah.

Cole, D. M., and C. E. Jensen.

1980. Estimating phloem thickness in lodgepole pine stands using electrical resistance measurements. Can. J. For. Res. 10(1):102–106.

Cole, D. M., and C. E. Jensen.

1981. Models for describing vertical crown development of lodgepole pine stands. USDA For. Serv. Res. Pap. INT–292, 10 p. Intermt. For. and Range Exp. Stn., Ogden, Utah.

Cole, W. E., E. P. Guyman, and C. E. Jensen.

1981. Terpene content of lodgepole pine phloem and its relation to mountain pine beetle. USDA For. Serv. Res. Pap. INT–281, 14 p. Intermt. For. and Range Exp. Stn., Ogden, Utah.

Damaerschalk, J. P., and A. Kozak.

1977. The wholebole system – a conditioned dual equation system for precise prediction of tree profiles. Can. J. For. Res. 7(3):488–497.

Draper, N. R., and W. C. Hunter.

1969. Transformations: some examples revisited. Technometrics 11:23–40.

Draper, N. R., and H. Smith.

1966. Applied regression analysis. Wiley and Sons, New York. p. 277–280.

George, C. W., and A. D. Blakely.

1973. An evaluation of the drop characteristics and ground distribution patterns of forest fire retardants. USDA For. Serv. Res. Pap. INT–134, 60 p. Intermt. For. and Range Exp. Stn., Ogden, Utah.

Jensen, C. E.

1979. e^{-K}, a function for the modeler. USDA For. Serv. Res. Pap. INT–240, 9 p. Intermt. For. and Range Exp. Stn., Ogden, Utah.

Jensen, C. E.

1976. Matchacurve–4: segmented mathematical descriptors for asymmetric curve forms. USDA For. Serv. Res. Pap. INT–182, 16 p. Intermt. For. and Range Exp. Stn., Ogden, Utah.

Jensen, C. E.

1973. Matchacurve–3, multiple-component and multidimensional mathematical models for natural resource models. USDA For. Serv. Res. Pap. INT–146, 42 p. Intermt. For. and Range Exp. Stn., Ogden, Utah.

Jensen, C. E., and J. W. Homeyer.

1971. Matchacurve–2 for algebraic transforms to describe curves of the class X^n. USDA For. Serv. Res. Pap. INT–106, 39 p. Intermt. For. and Range Exp. Stn., Ogden, Utah.

Jensen, C. E., and J. W. Homeyer.

1970. Matchacurve–1 for algebraic transforms to describe sigmoid- or bell-shaped curves. 22 p. USDA For. Serv., Intermt. For. and Range Exp. Stn., Ogden, Utah.

Karst, O. J.

1958. Linear curve fitting using least deviations. J. Am. Stat. Assoc. 53:118–132.

Lee, D-Y, H. T. David, and R. W. Mensing.
  1973. Evaluation of gap-graded asphalt concrete mixtures. Part 1: Mechanical properties. Eng. Res. Inst., Iowa State Univ.
Lyon, L. J.
  1976. Big game use of clearcuts in western Montana. Printed by USDA For. Serv., Wildlife and Fisheries Div. To be used as an interim guide for timber production—big game management decisions by National Forest Supervisor and Rangers in R-1.
Lyon, L. J., and C. E. Jensen.
  1980. Management implications of elk and deer use of clearcuts in Montana. J. Wildl. Manage. 44(2):352–362.
Mead, R., and D. J. Pike.
  1975. A review of response surface methodology from a biometrics viewpoint. Biometrics. 31–803–851.
Mosteller, F., and J. W. Tukey.
  1977. Data analysis and regression, a second course in statistics. Addison–Wesley, Reading, Mass.

ADDITIONAL REFERENCES

Baker, B. H., and G. C. Trostle.
  1973. Douglas-fir beetle attraction and tree-group response. J. Econ. Entomol. 66: 1002–1005.
Bartos, D. L., and R. S. Johnston.
  1978. Biomass and nutrient content of quaking aspen at two sites in the western United States. For. Sci. 24(2):273–280.
Basile, J. V., and C. E. Jensen.
  1971. Grazing potential on lodgepole pine clearcuts in Montana. USDA For. Serv. Res. Pap. INT–98, 11 p. Intermt. For. and Range Exp. Stn., Ogden, Utah.
Clary, W. P., and C. E. Jensen.
  1981. Mathematical hypothesis for herbage production potential on pinyon-juniper areas. USDA For. Serv. Res. Pap. INT–279, 8 p. Intermt. For. and Range Exp. Stn., Ogden, Utah.
Clayton, J. L., and C. E. Jensen.
  1973. Water retention in granitic soils of the Idaho batholith. USDA For. Serv. Res. Pap. INT–143, 23 p. Intermt. For. and Range Exp. Stn., Ogden, Utah.
Clendenen, G. W.
  1979. Gross cubic volume and equations and tables, outside bark, for pinyon and juniper trees in northern New Mexico. USDA For. Serv. Res. Pap. INT–228, 32 p. Intermt. For. and Range Exp. Stn., Ogden, Utah.
Cole, W. E.
  1976. Mathematical models for the mountain pine beetle-lodgepole pine interaction. *In* Proc. XVI IUFRO World Congr., Norway.
Cole, W. E., G. D. Amman, and C. E. Jensen.
  1976. Mathematical models and for the mountain pine beetle-lodgepole pine interaction. Environ. Entomol. 5(1):11–19.
George, C. W.
  1975. Fire retardant ground distribution pattern from the CL–215 air tanker. USDA For. Serv. Res. Pap. INT–165, 67 p. Intermt. For. and Range Exp. Stn., Ogden, Utah.

ADDITIONAL REFERENCES

George, C. W.
    1973. Use of forest fire retardants. *In* Proceedings of the Canadian International Sym-
    posium on Aerospace Services to Conservation of the Environment, Vancouver, B.C.
Hann, D. W., and B. B. Bare.
    1978. Comprehensive tree volume tables for major species of New Mexico and Arizona:
    1. Results and methodology. USDA For. Serv. Res. Pap. INT–209, 43 p. Intermt.
    For. and Range Exp. Stn., Ogden, Utah.
Harniss, R. O., and R. B. Murray.
    1976. Reducing bias in dry leaf weight estimates of big sagebrush. J. Range Manage.
    29(5):430–432.
Kilkki, P., and M. Siitonen.
    1975. Simulation of artificial stands and derivation of growing stock models from this
    material. Acta For. Fenn. 145, 33 p. Helsinki.
Klein, W. H., D. L. Parker, and C. E. Jensen.
    1978. Attack, emergence, and stand depletion trends of the mountain pine beetle in a
    lodgepole pine stand during an outbreak. Environ. Entomol. 7(5):732–737.
Kotok, E. S., D. P. Lowery, and C. E. Jensen.
    1969. Surface temperature as an indicator of wood moisture content during drying.
    For. Prod. J. 19(9):80–82.
Lyon, L. J.
    1976. Elk use related to characteristics of clearcuts in western Montana. *In* Proceedings,
    Elk—Logging—Roads Symposium (University of Idaho, Moscow). p. 69–72.
Packer, P. E., C. E. Jensen, E. L. Noble, and J. A. Marshall.
    1979. A prediction model to estimate revegetation potential of land surface mined for
    coal in the West. *In* Proceedings of the International Congress of Energy and
    Ecosystems (University of North Dakota, 1978).
Packer, P. E., C. E. Jensen, E. L. Noble, and J. A. Marshall.
    1982. Models to estimate revegetation potentials of land surface mined for coal in the
    west. USDA For. Serv. Gen. Tech. Rep. INT–123, 25 p. Intermt. For. and Range
    Exp. Stn., Ogden, Utah.
Stermitz, J. E., M. G. Klages, and J. E. Lotan.
    1974. Soil characteristics influencing lodgepole pine regeneration near West Yellow-
    stone, Montana. USDA For. Serv. Res. Pap. INT–163, 16 p. Intermt. For. and
    Range Exp. Stn., Ogden, Utah.
Shearer, R. C.
    1974. Early establishment of conifers following prescribed broadcast burning in west-
    ern larch/douglas-fir forests. *In* Proceedings of Fire and Land Symposium, (Univer-
    sity of Montana).
Shearer, R. C.
    1975. Seedbed characteristics in western larch forests after prescribed burning. USDA
    For. Serv. Res. Pap. INT–167, 26 p. Intermt. For. and Range Exp. Stn., Ogden,
    Utah.
Stevens, R. A., P. Plummer, C. E. Jensen, and B. C. Guinta.
    1974. Site productivity classification for selected species on winter big game ranges for
    Utah. USDA For. Serv. Res. Pap. INT–158, 24 p. Intermt. For. and Range Exp.
    Stn., Ogden, Utah.

APPENDIX-A: e^{-K} DERIVATION

e^{-K}: Its Derivation, Potentials, and Limitations

The new function, simply identified as e^{-K}, provides the analyst with a finite source of versatile transformations for use when it is inefficient to search for alternatives or when alternatives are inadequate. While e^{-K} is not a panacea for all the problems modelers face in developing functional relationships, it along with curves of the class $X^n (n \geq 1)$ does serve a broad spectrum of transformation needs with no particular limitations as to curve shapes for which it is most useful. Methods for developing mathematical descriptors using these functions have been treated by Jensen and Homeyer (1970, 1971) and Jensen (1973, 1976, and 1979) and are summarized and updated in this paper.

A variant of the Normal function e^{-K} is defined as:

$$e^{-K} = \left\{ \frac{e^{-\left|\frac{(X/XP)-1}{(1-I)}\right|^n} - e^{-\left\{\frac{1}{(1-I)}\right\}^n}}{1 - e^{-\left\{\frac{1}{(1-I)}\right\}^n}} \right\}, \quad 0 \leq X \leq 2Xp$$

where,

- e = natural logarithm base.
- XP = pivot point in X for e^{-K} and is the point in X at which the bell-shaped curve peaks.
- XI = point of sigmoidal inflection in X.
- I = proportional departure of XI from zero to XP or from $2XP$ to XP.
- n = power of negative exponents for e.

The left numerator, like the Normal function, generates a system of bell-shaped curves about a central point in X, XP in this case. These curves reach the maximum value of 1.0 at XP and then decline sigmoidally and symmetrically on either side of XP with increasing departure of X from XP.

User control of the curve system is enhanced if all curves of the set range in value from zero to one within a finite domain of X. To achieve this property, curves generated by the left numerator have been forced through zero at $XP \pm XP$ as follows:

Let the left numerator $= e^{-T}$ and let $e^{-T_0} = e^{-T}$ at $X = 0$ or $2XP$. Consider the residuals generated by $1 - e^{-T}$. Expanded by the inverse $(1 - e^{-T_0})^{-1}$ and subtracted from one, we have

$$e^{-K} = 1 - (1 - e^{-T_0})^{-1}(1 - e^{-T}),$$

which simplifies to the final form

$$e^{-K} = (e^{-T} - e^{-T_0})(1 - e^{-T_0})^{-1}.$$

Then the right numerator and the denominator serve to force curves of the left numerator through zero at $XP \pm XP$. This domain, along with XP, can be altered to accommodate the needs of individual conceptual models by adding constants ($+$ or $-$) to the X-scale. The apparent complexity of e^{-K} is much reduced by the fact that in application, the right numerator and the denominator simplify to constants or approach zero and can be deleted.

APPENDIX A (con.)

Sigmoids on either side of XP are forced into different areas of two-dimensional space by shifting I, the proportional point of inflection in X, and the slope of the sigmoidal face at I changes with n.
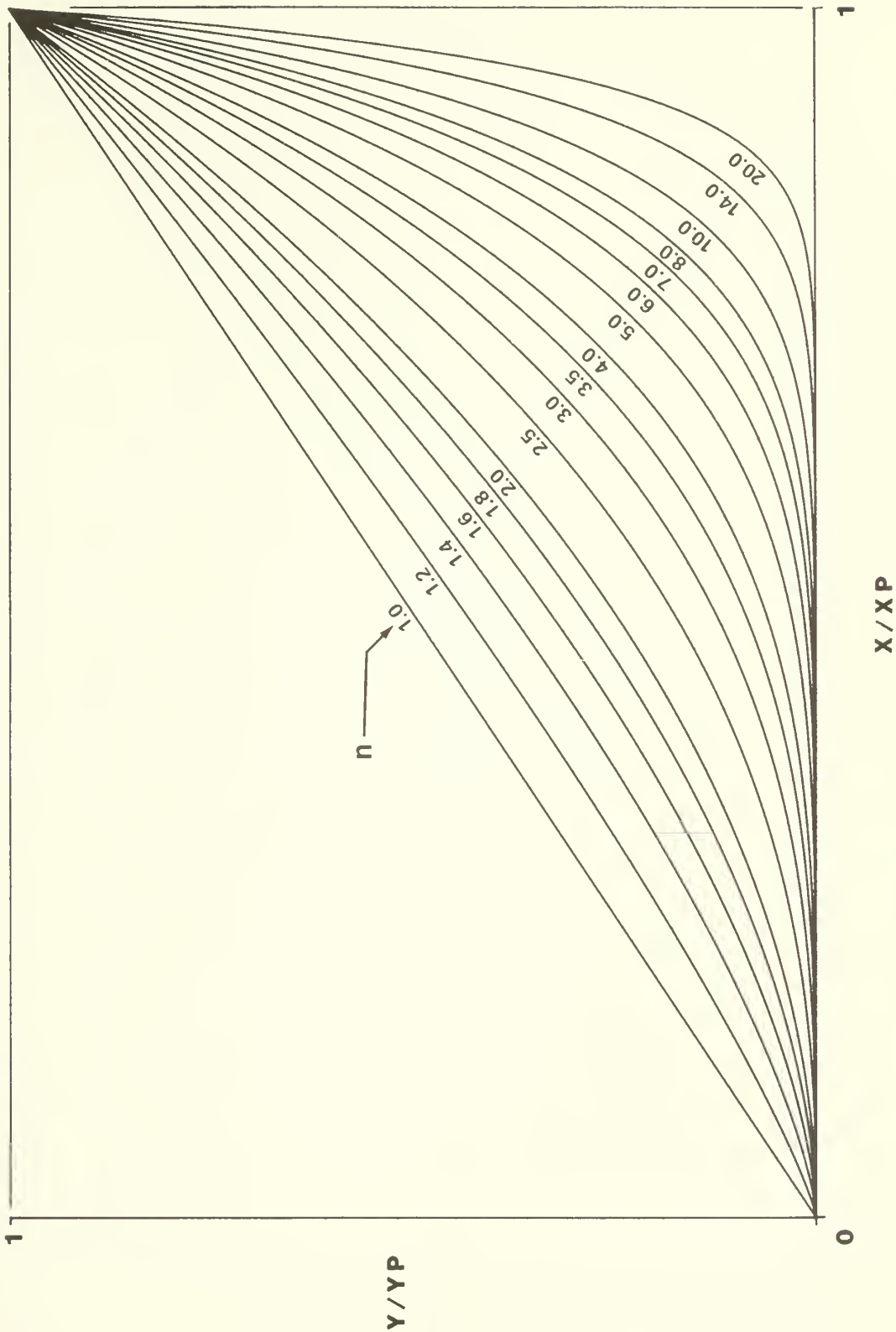
Arrays of curves from the left half of this function (a mirror image of the right half) are shown in the e^{-K}-Standards that follow. Sets are given for commonly used increments of n, $1.2 \leq n \leq 10.0$. Each set has curves progressing from $I = 0.1$ at the left to 0.9 at the right. These curves or any portions thereof provide an almost endless potential for matching graphed curves and describing them mathematically. Given that YP is the peak value of Y (the dependent variable) on the objective curve, the selected e^{-K}-function (e^{-K} ranges from zero to one) may be scaled to that curve through multiplication by YP.

While the controllable parameters I, n, XP, and YP provide exceptional descriptive power in two dimensions, such power is magnified manyfold for hypotheses involving three or more dimensions, as well as strong interactions. For example, the location of peaks Y that move across the independent variables in any fashion can be described with $XP = f_1(X_i)$. The heights of these peaks in any pattern and changing sigmoidal shapes leading up to them can again be pictured as functions of the independent variables $YP = f_2(X_i)$, $n = f_3(X_i)$, and $I = f_4(X_i)$. Additionally, asymmetry in bell-shaped hypotheses is easily accounted for by describing sigmoids on either side of XP independently (segmented descriptors), while scaling both to the same height at XP.

A descriptor (XT), adopted as a hypothesis in its entirety, may be fitted to pertinent data by least squares in the simple model, $Y = \beta XT + \epsilon$, where the ϵ are $NID\,(0, \sigma^2)$, constant variance, and $\beta = \Sigma XTY / \Sigma XT^2$.

Weighted regression procedures are recommended where the variance about regression is not uniform over the ranges of the independent variables. In such cases, reasonable success in achieving constant variance has been obtained by solving for departures $(Y_i - \hat{Y}_i)^2$ or d_i^2 as a suitable function of the related $\hat{Y}_i$ in $d_i^2 = b\,\hat{Y}^n$. Then the weight, w, for each observation is set equal to $1/\hat{Y}^n$ and a weighted β in $Y = \beta\,\hat{Y}$ is estimated as $\beta = \Sigma w \hat{Y} Y / \Sigma w \hat{Y}^2$.

More complex, generally iterative fitting procedures, such as the Newton–Raphson methods, can be used to arrive at statistical estimates of internal model parameters (see Damaerschalk and Kozak 1977; Draper and Smith 1966).
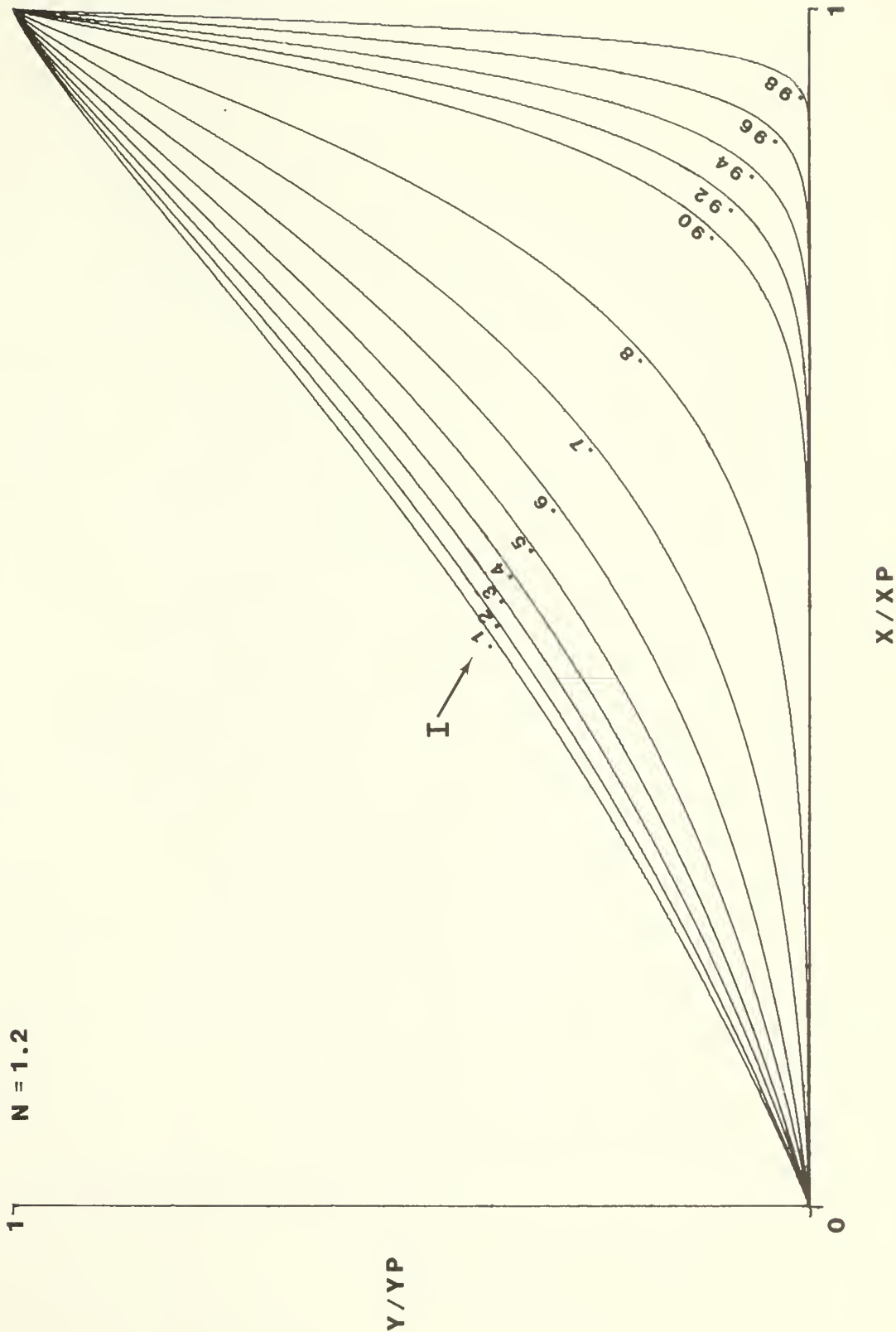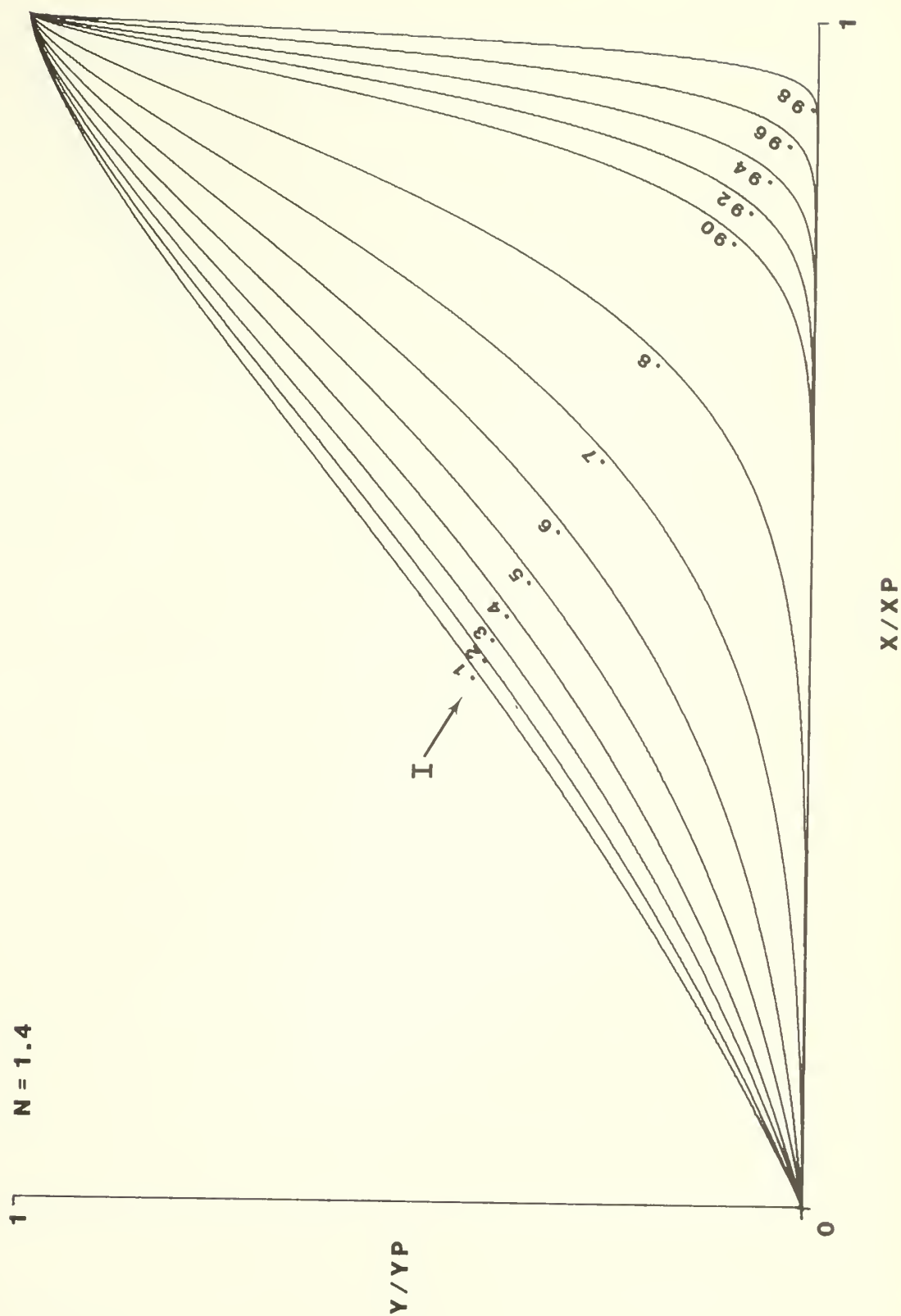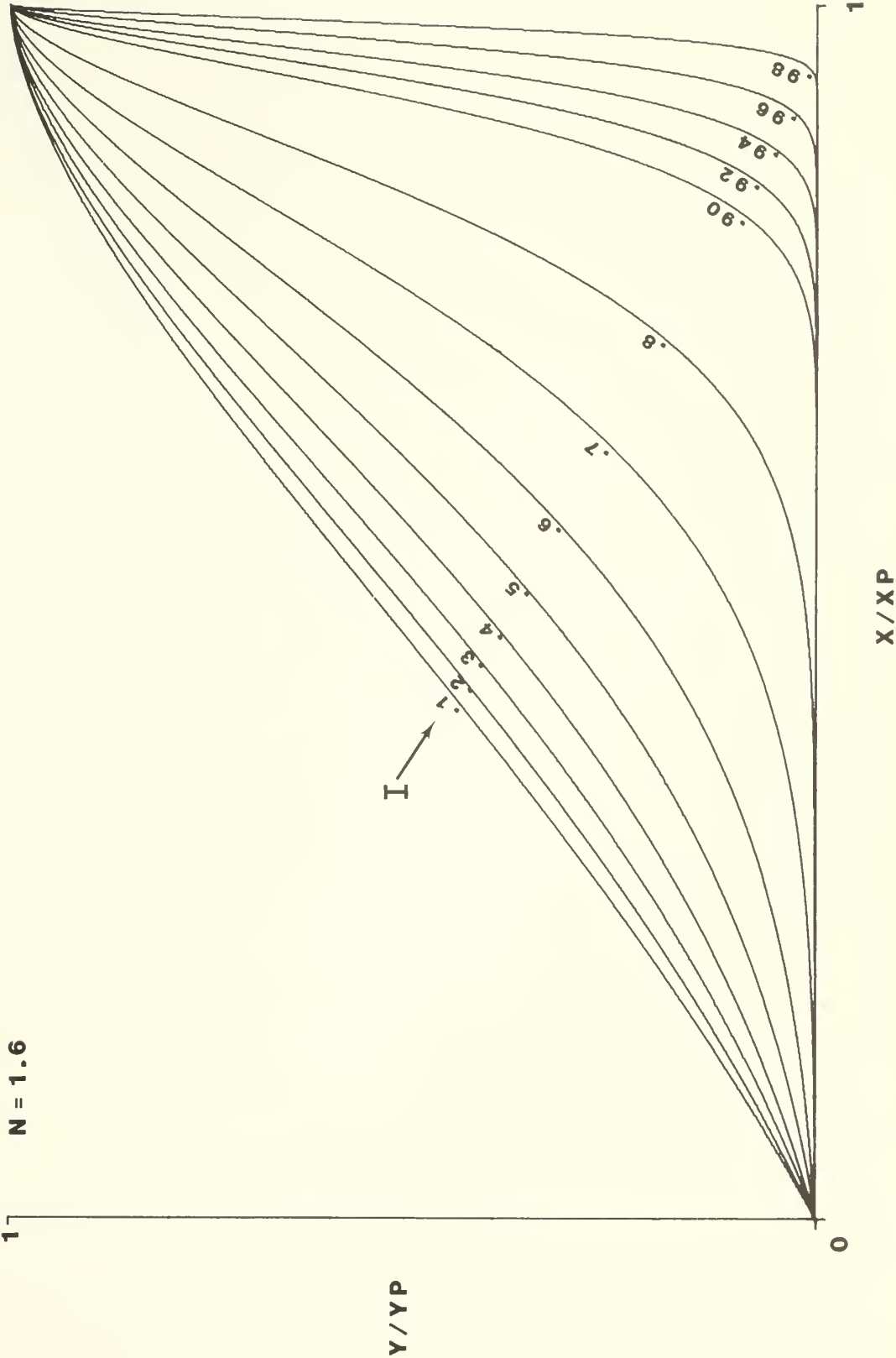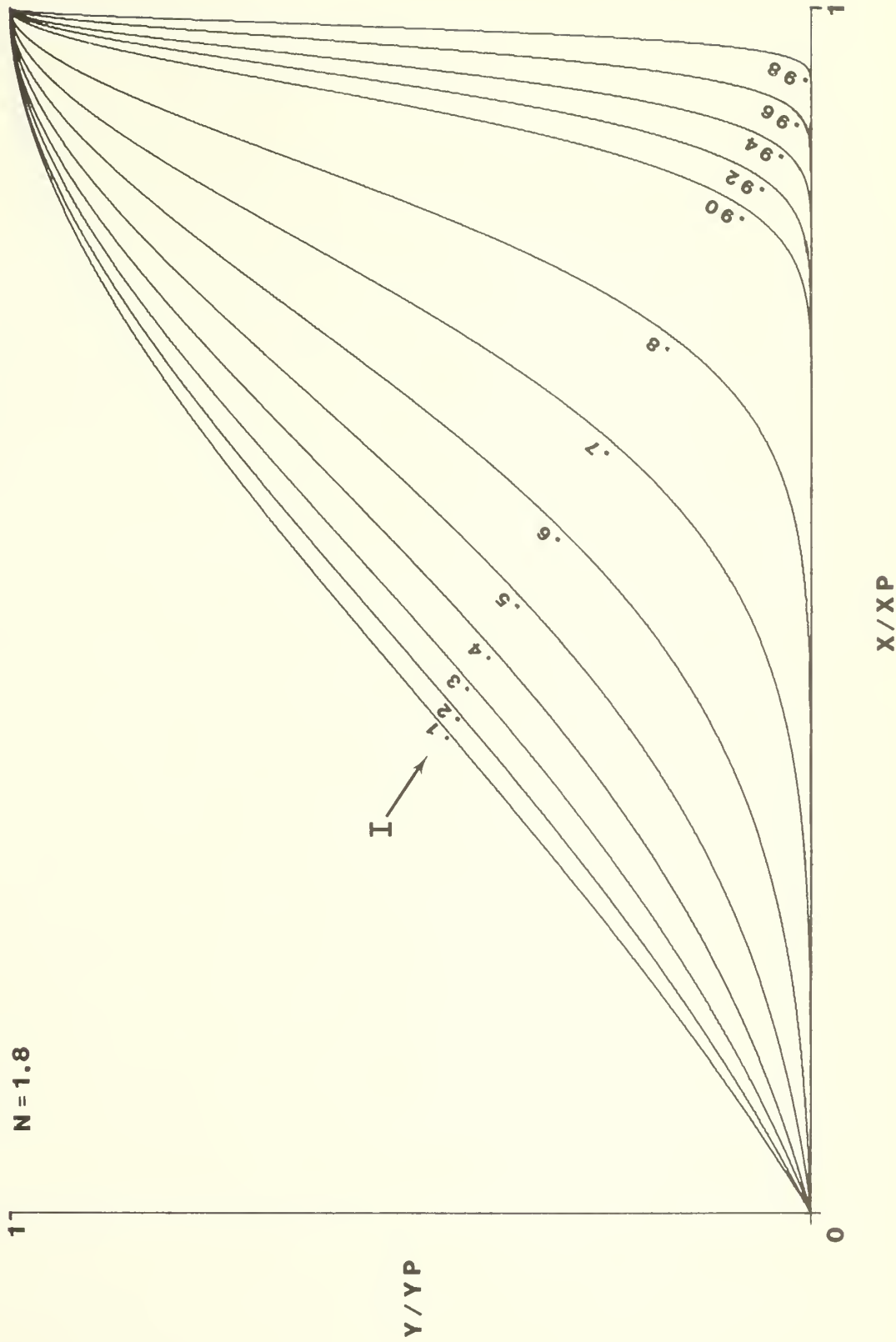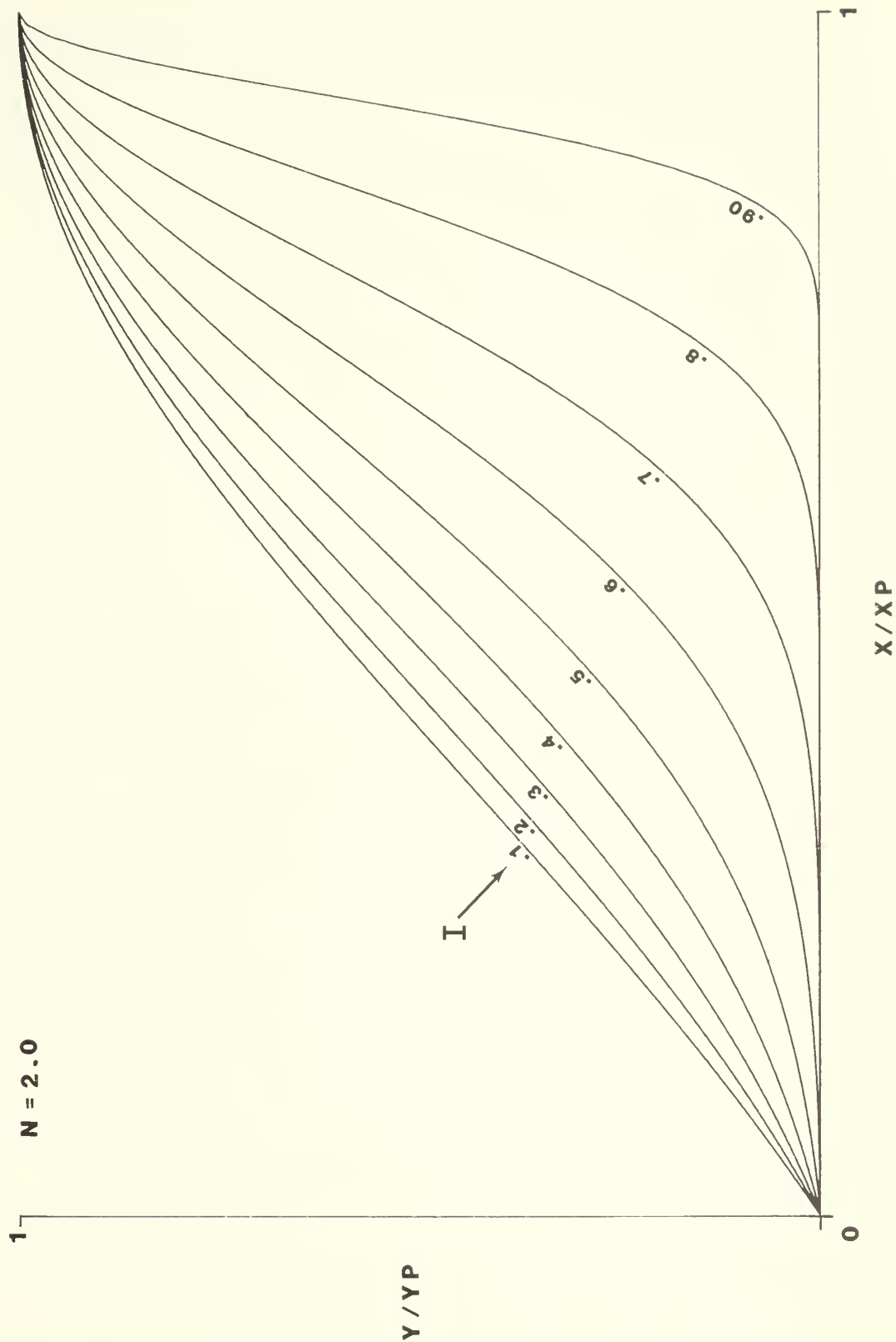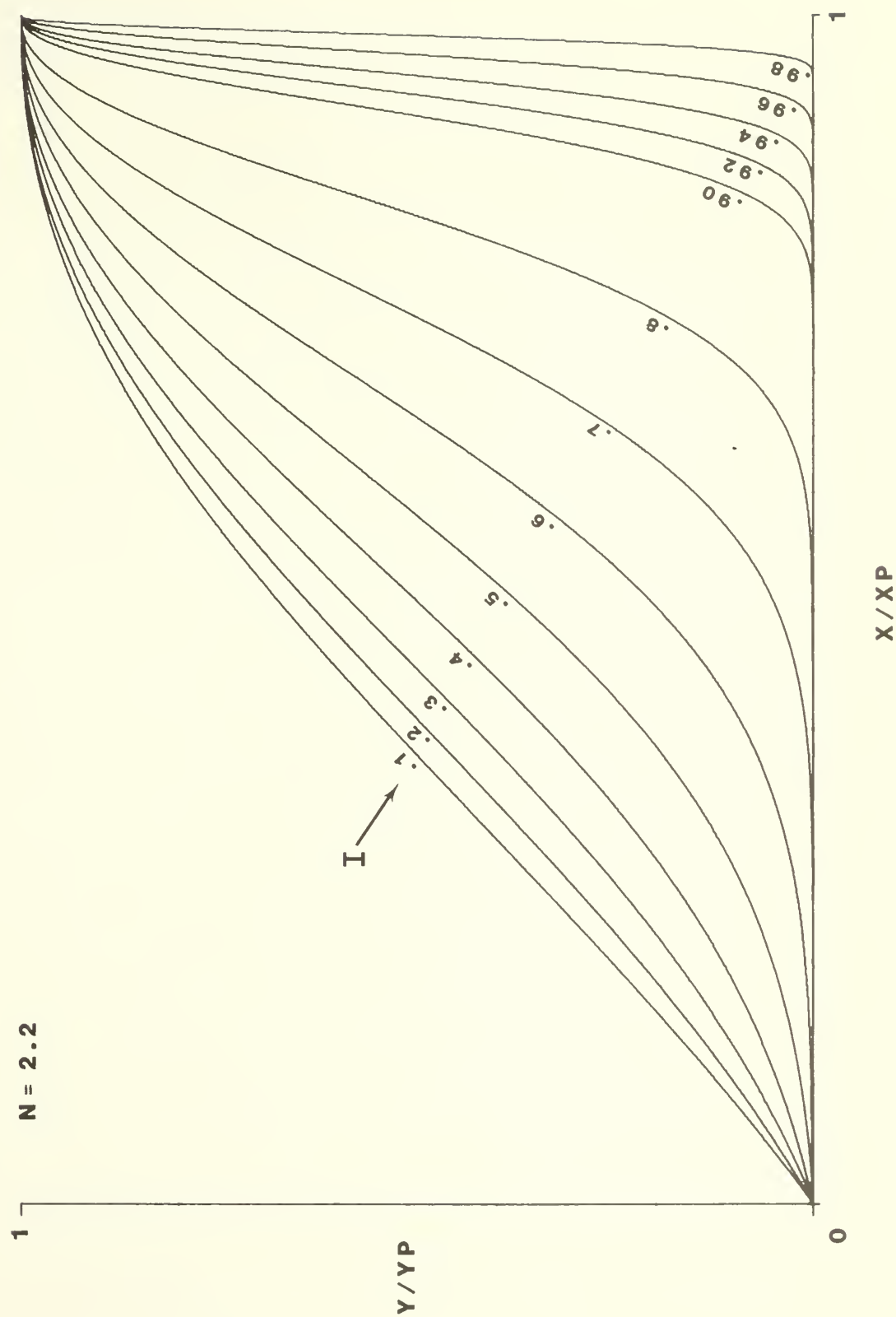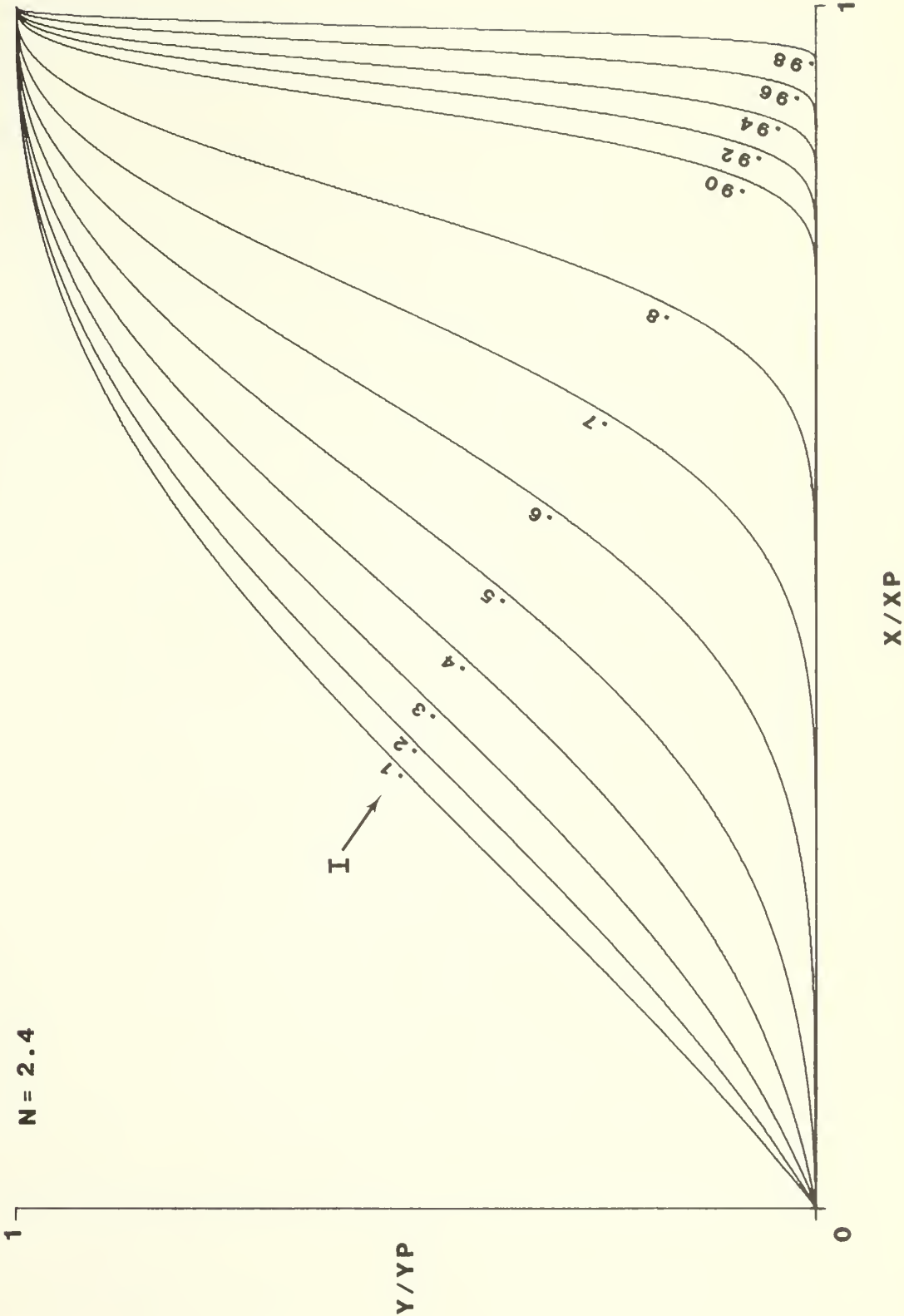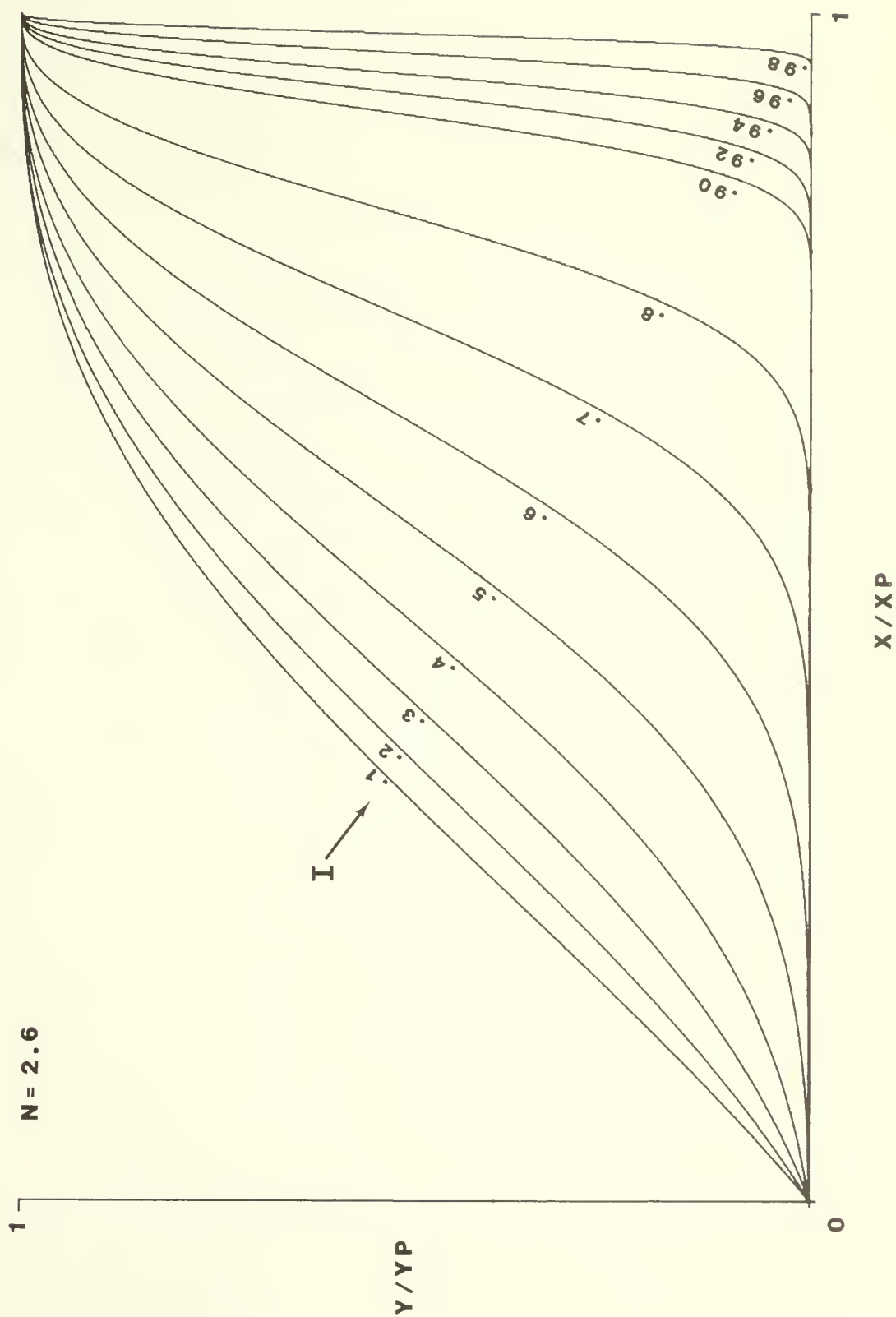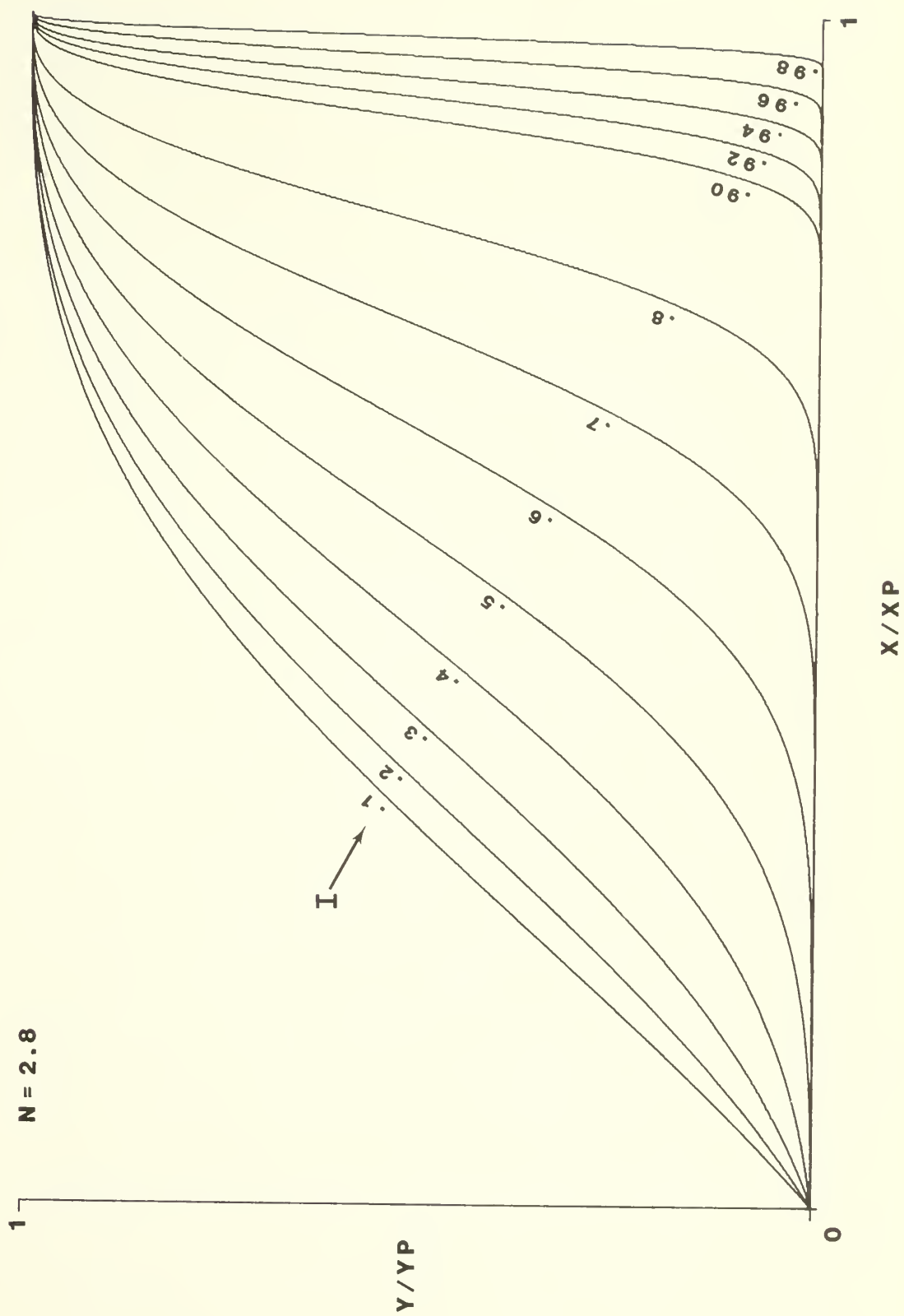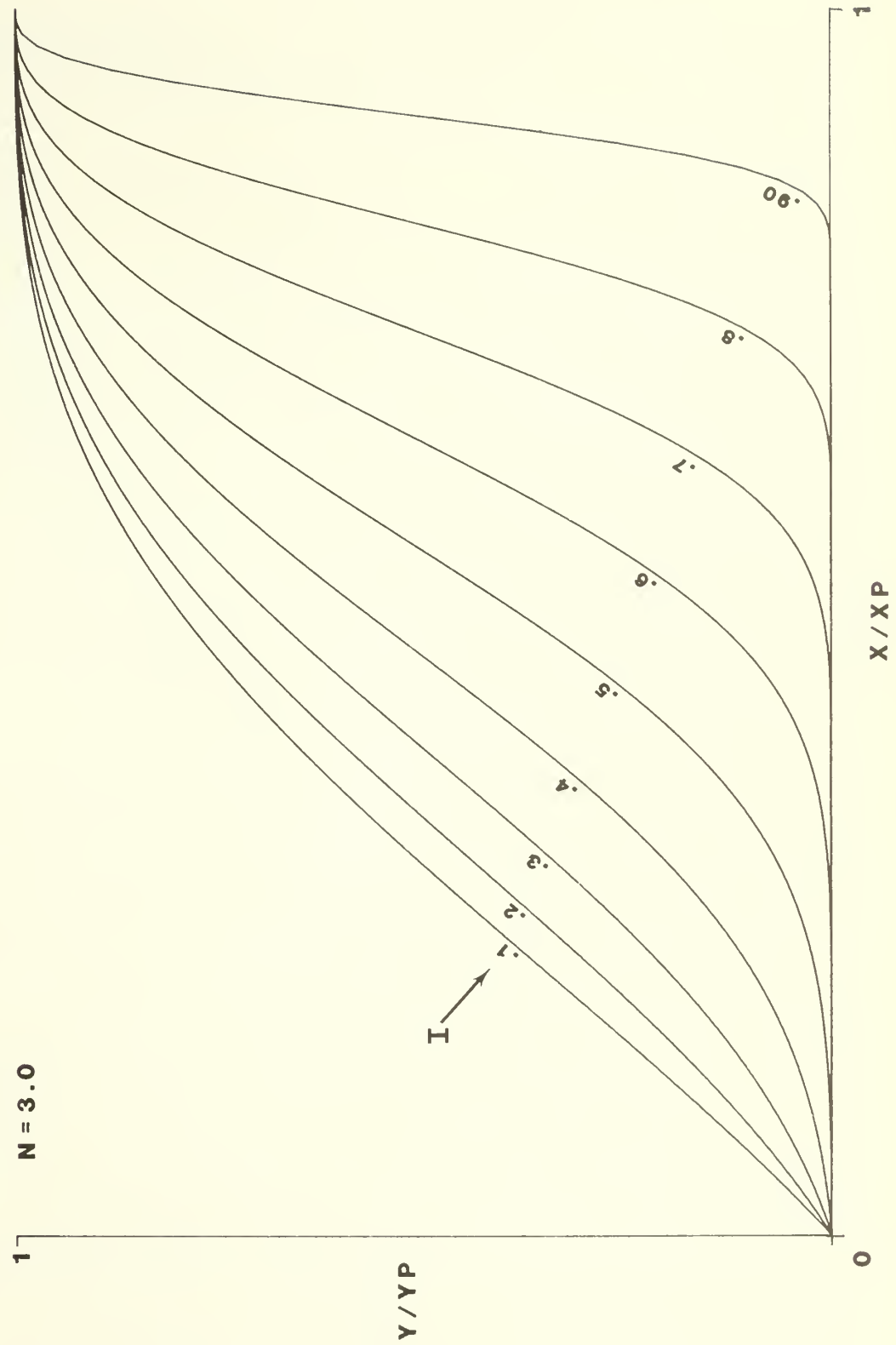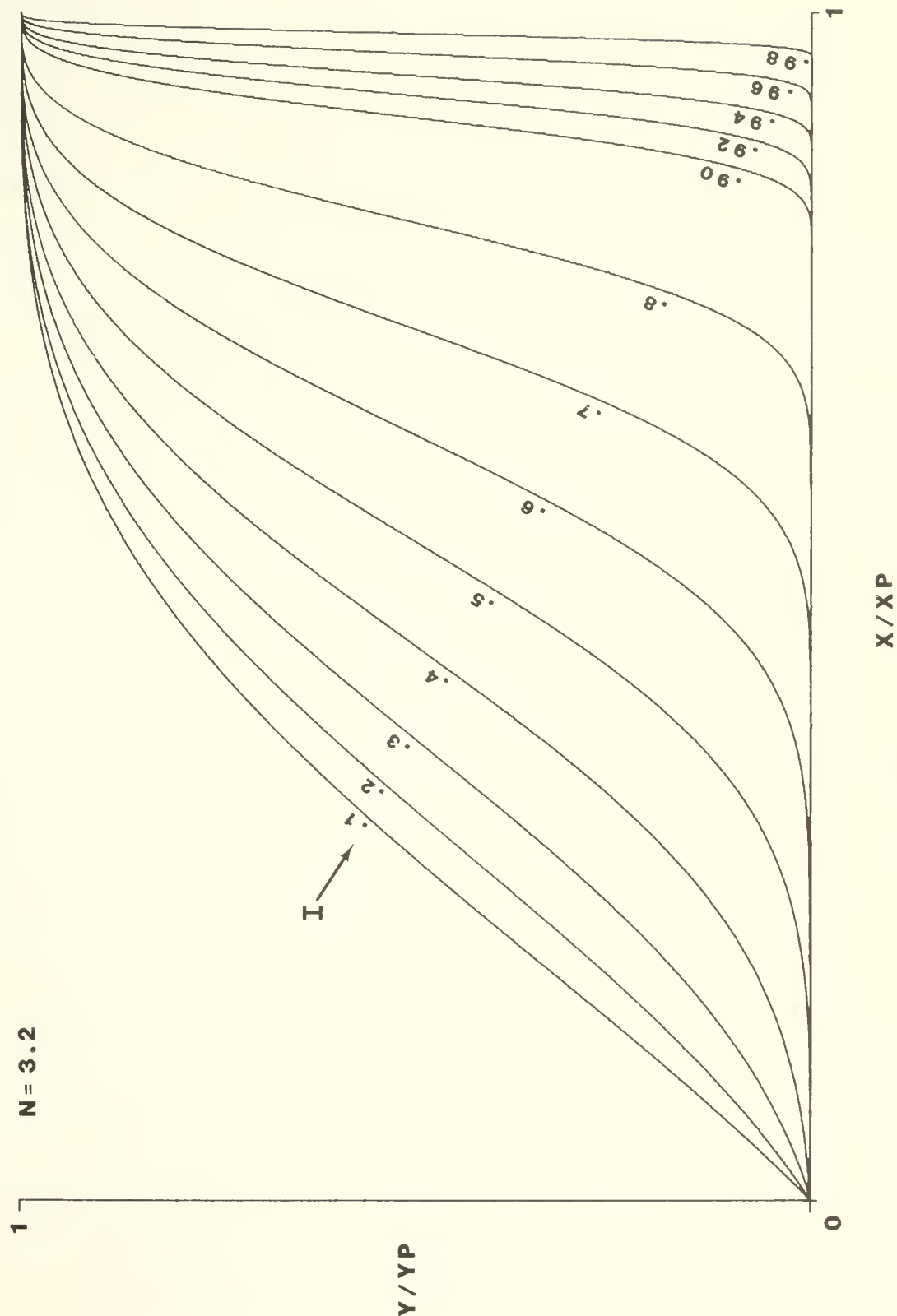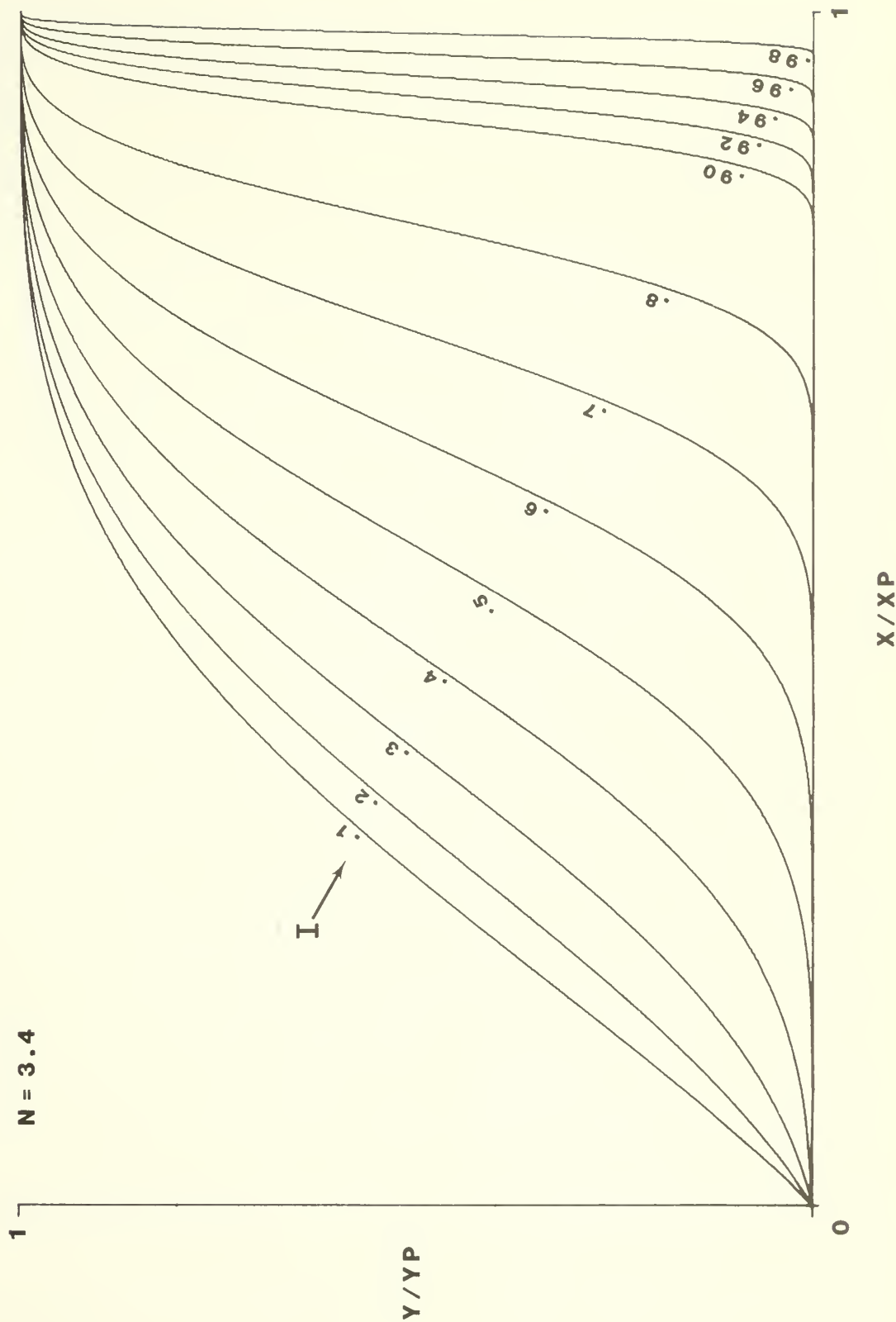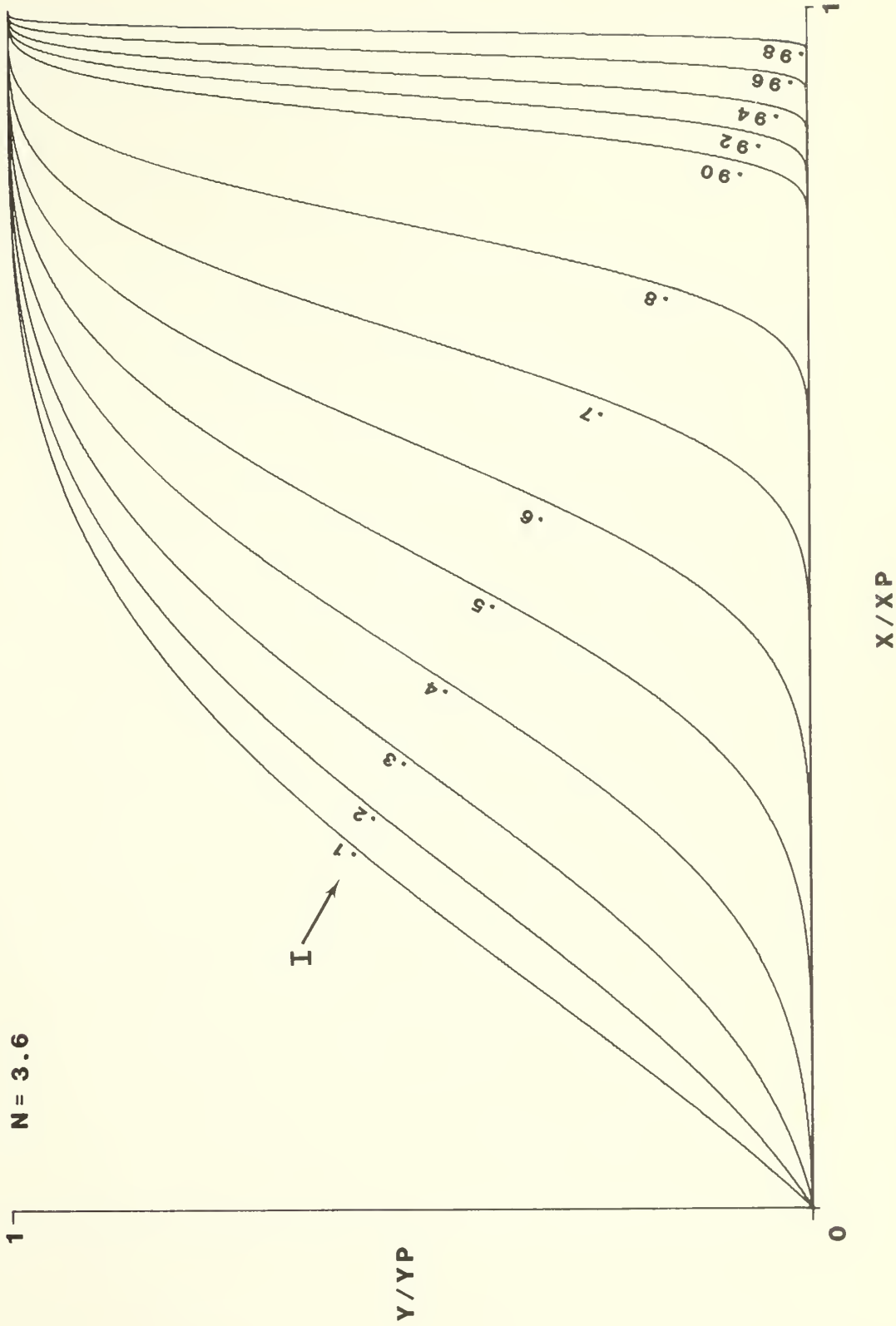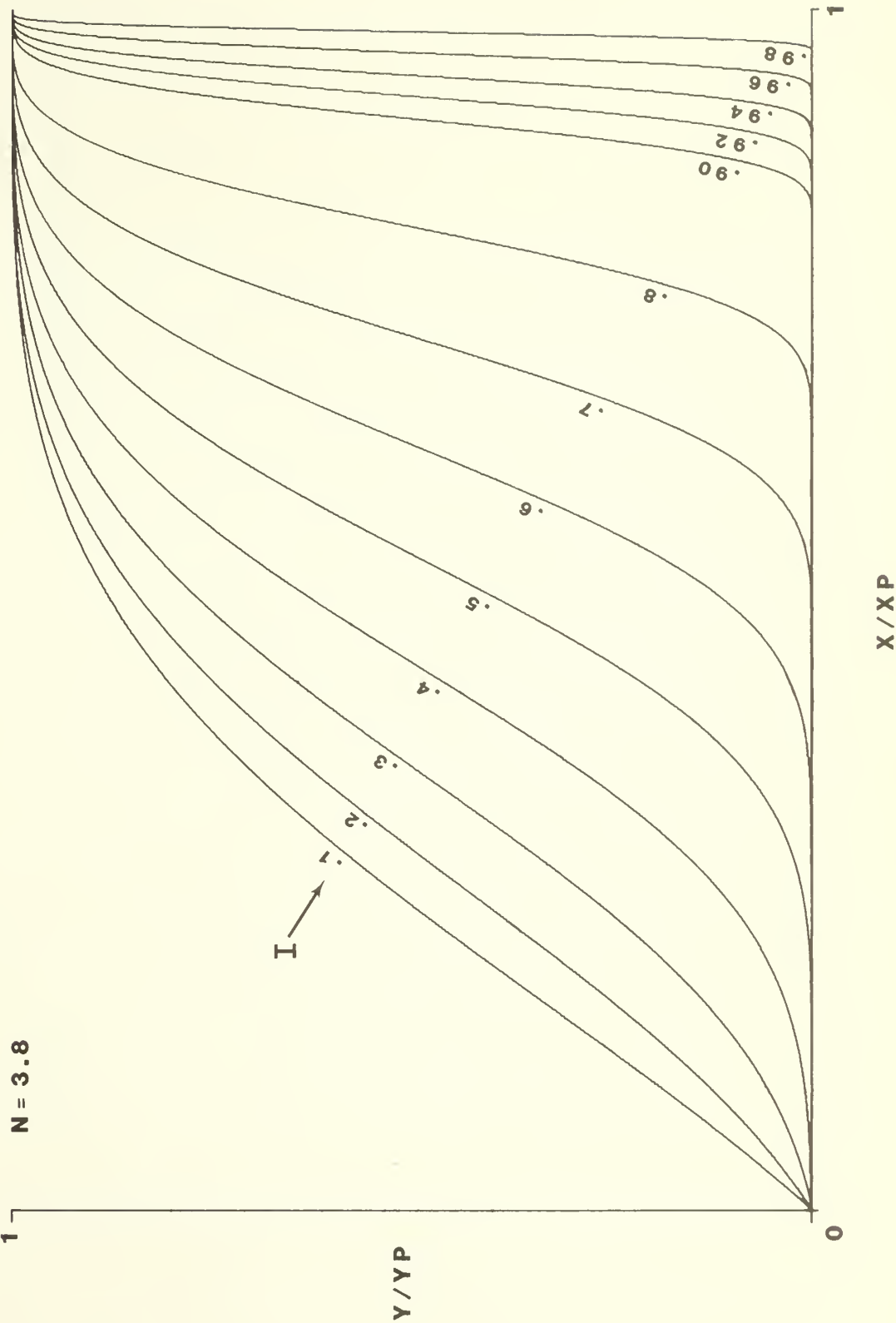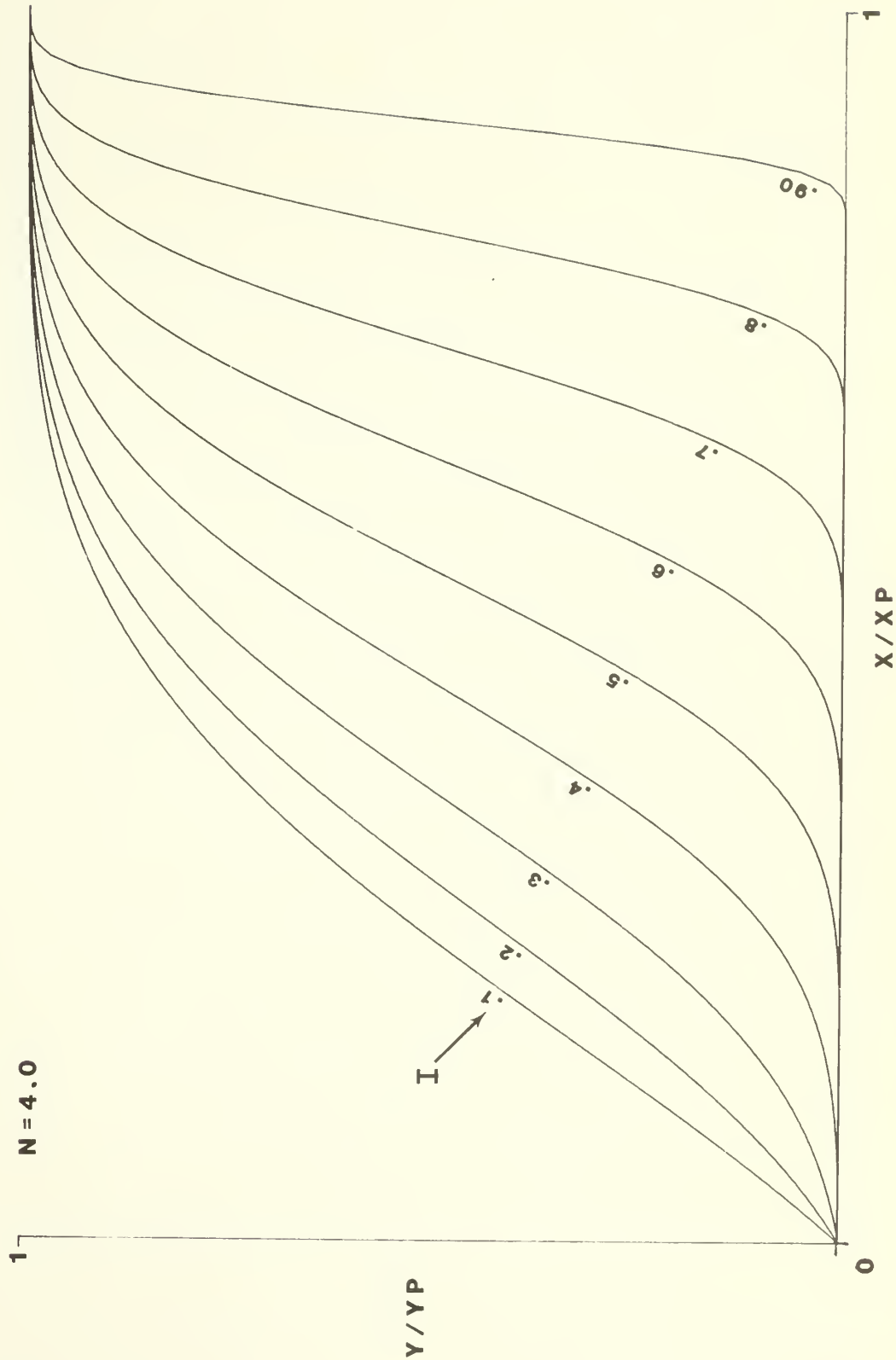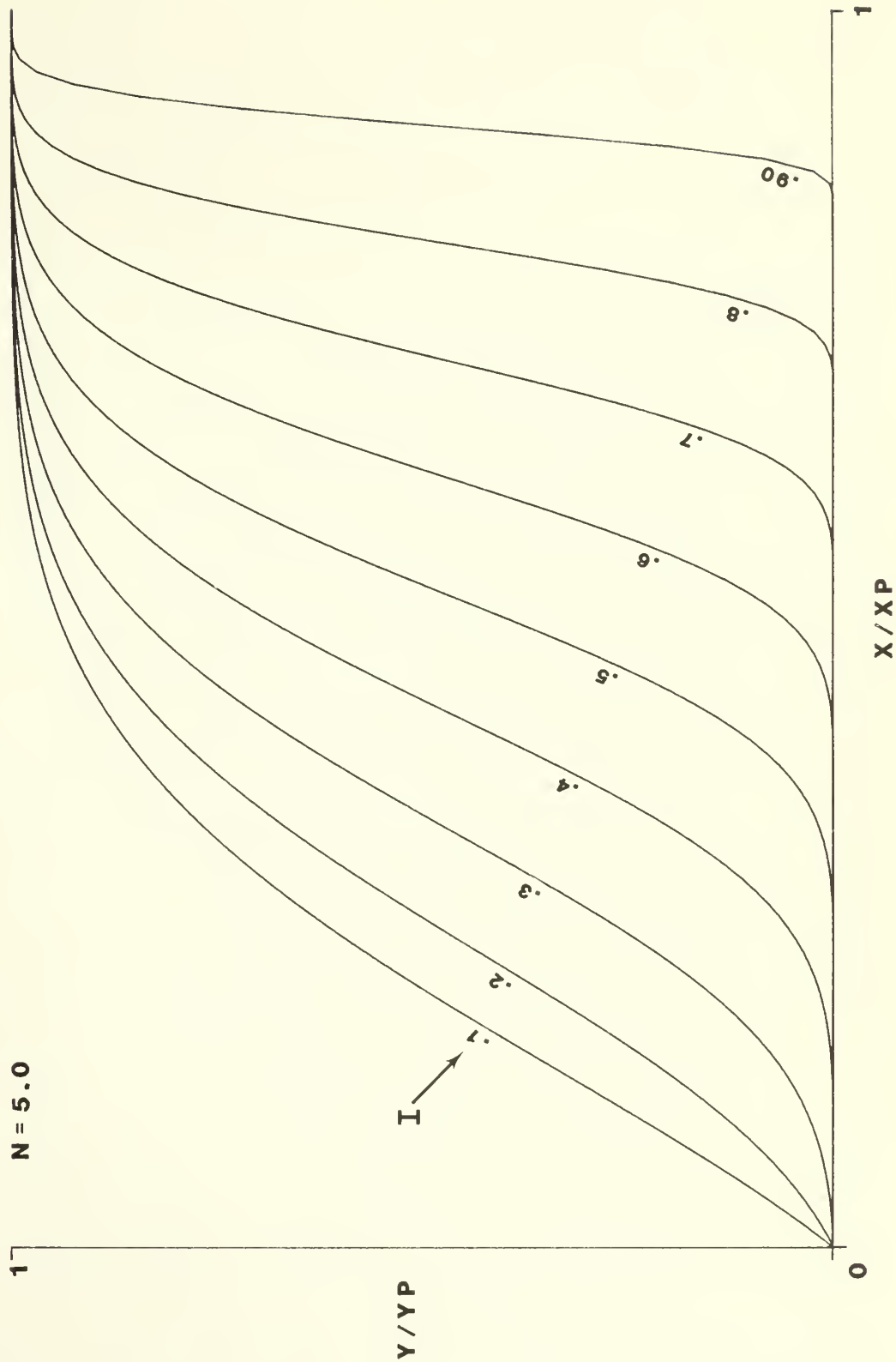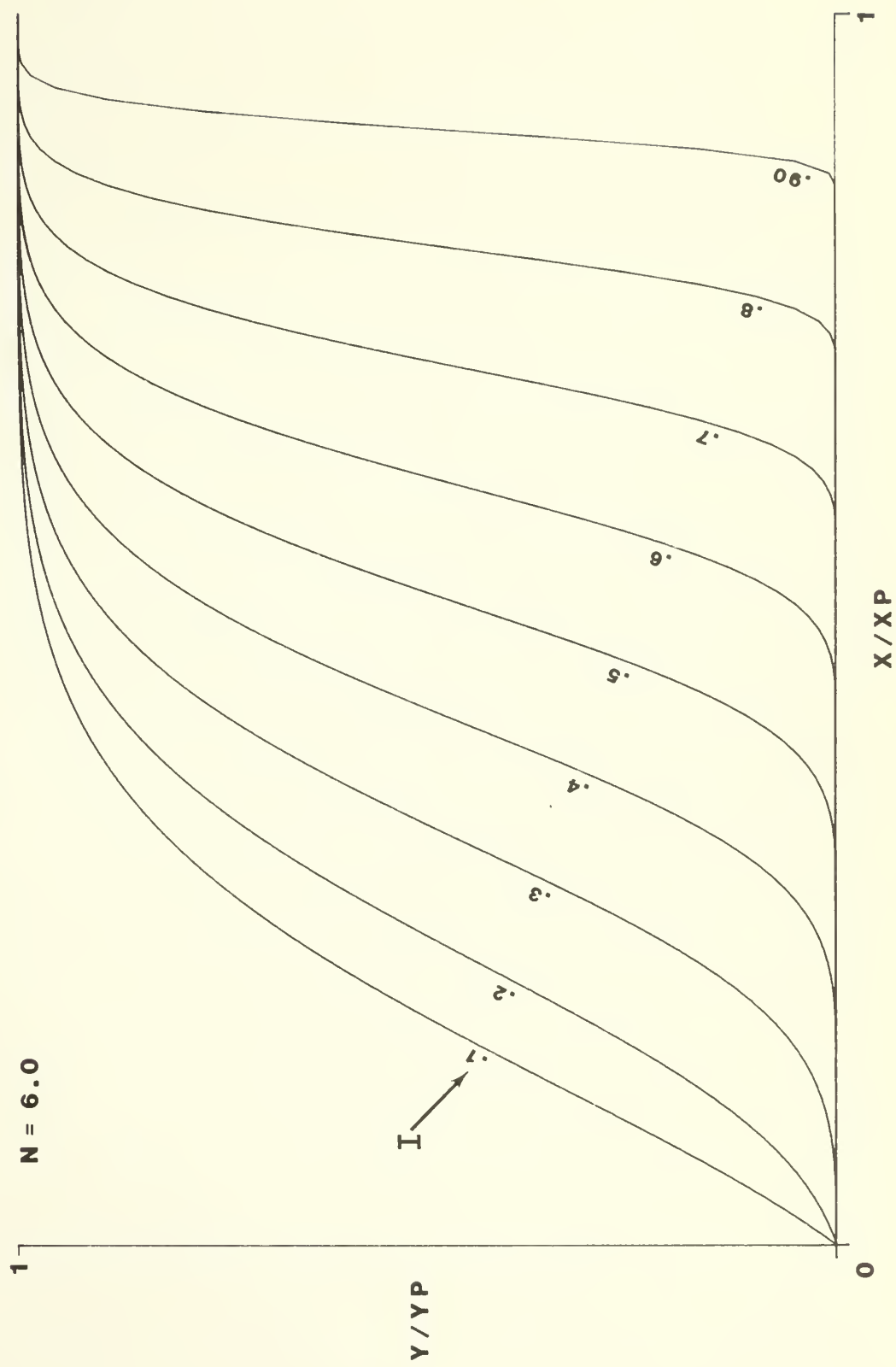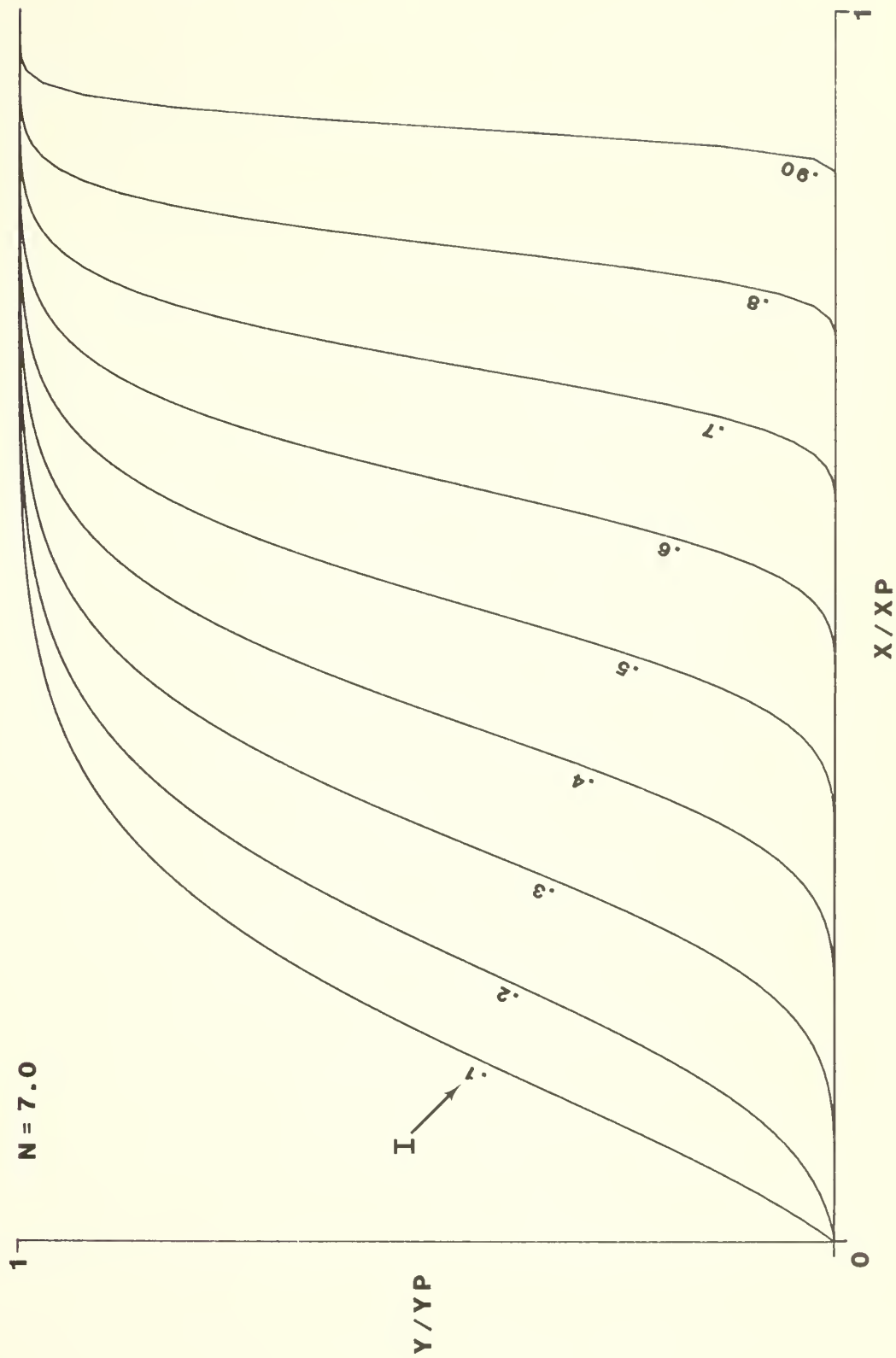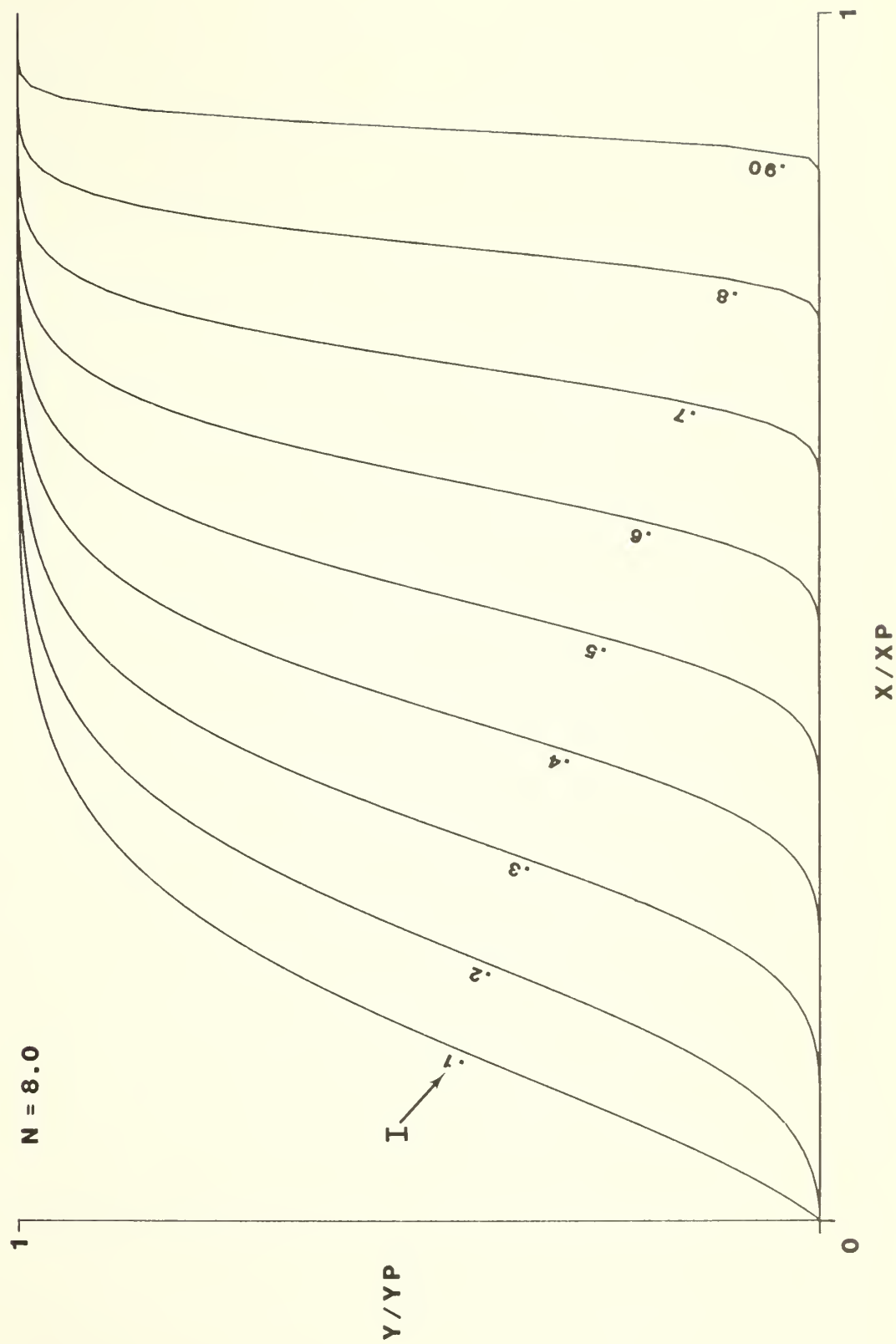
N = 1.2

X / XP

Y / YP

N = 1.4

----- cut here -----

X / XP

Y / YP

cut here

N = 3.6

Y / YP

X / XP

N = 4.0

Y / YP

X / XP

N = 10.0
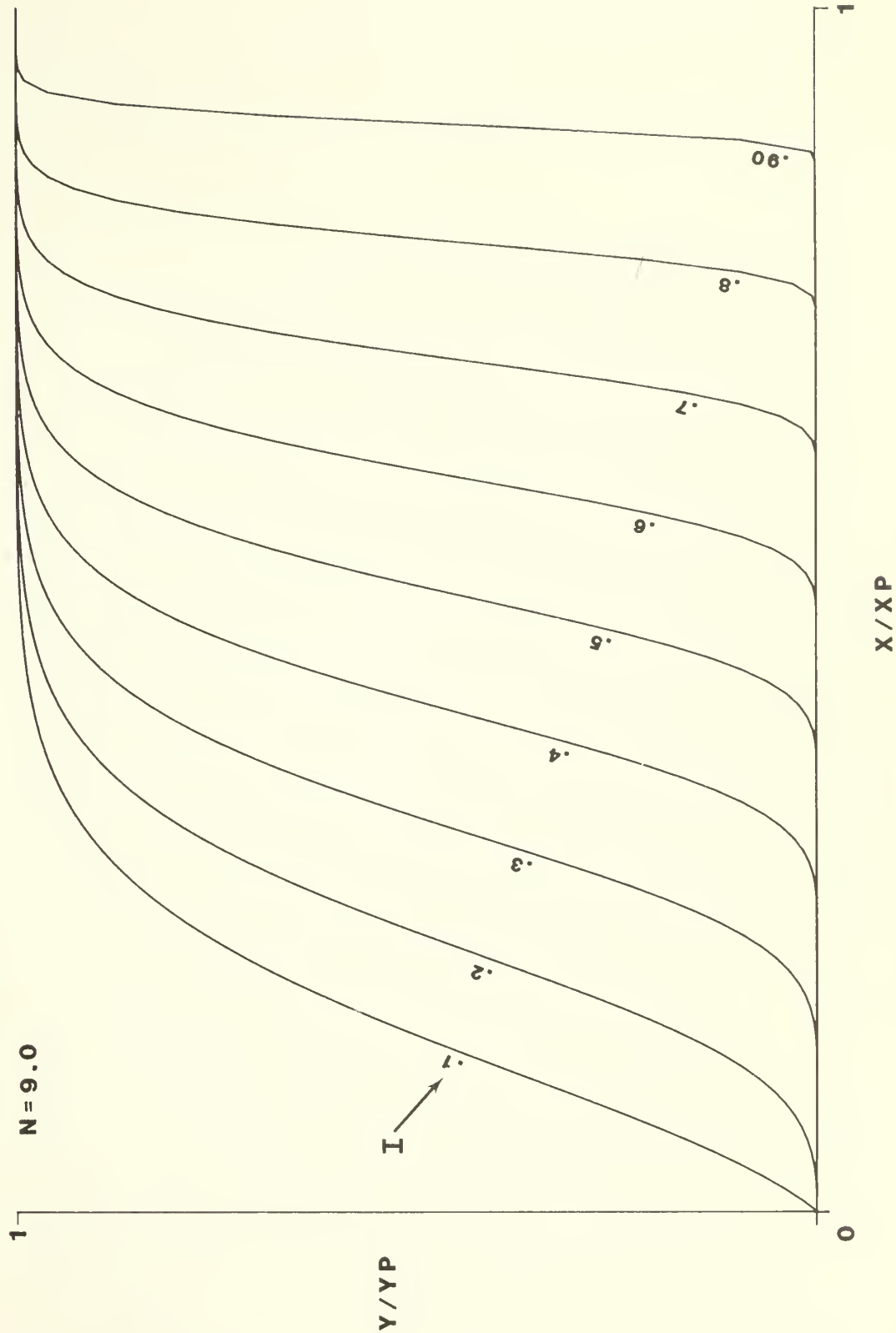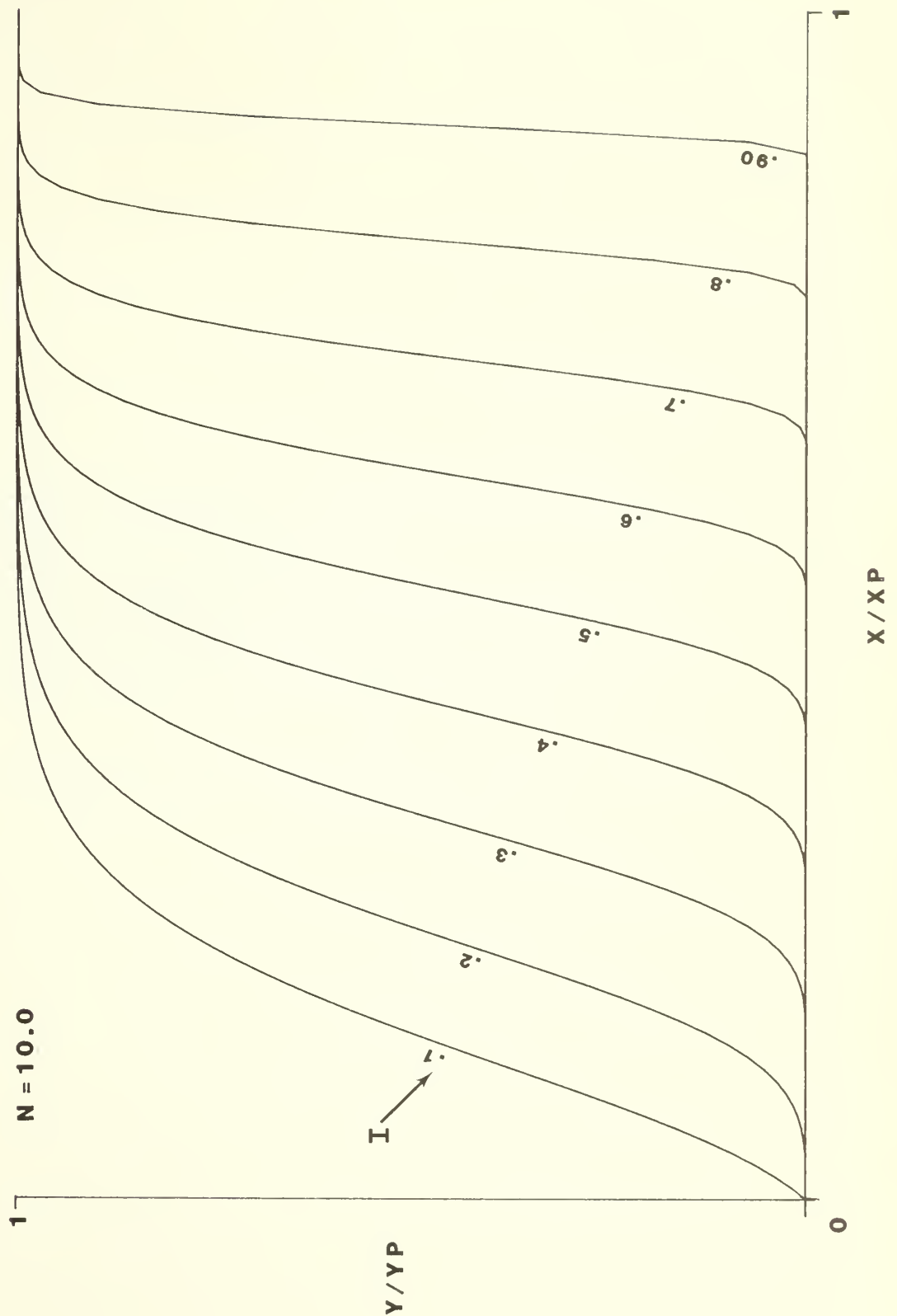
The problem of over-simplified regression hypotheses is identified and alter-
natives are discussed. Methods for developing structured hypotheses, first
graphically and then mathematically, are shown for two- through five-
dimensional cases. Mathematical formulation is accomplished through use of
two families of curves: X^n, $n \geq 1$, and e^{-K}, a highly manipulable function for bell-
shaped curves or portions thereof.

The Intermountain Station, headquartered in Ogden, Utah, is one of eight regional experiment stations charged with providing scientific knowledge to help resource managers meet human needs and protect forest and range ecosystems.

The Intermountain Station includes the States of Montana, Idaho, Utah, Nevada, and western Wyoming. About 231 million acres, or 85 percent, of the land area in the Station territory are classified as forest and rangeland. These lands include grasslands, deserts, shrublands, alpine areas, and well-stocked forests. They supply fiber for forest industries; minerals for energy and industrial development; and water for domestic and industrial consumption. They also provide recreation opportunities for millions of visitors each year.

Field programs and research work units of the Station are maintained in:

    Boise, Idaho

    Bozeman, Montana (in cooperation with Montana State University)

    Logan, Utah (in cooperation with Utah State University)

    Missoula, Montana (in cooperation with the University of Montana)

    Moscow, Idaho (in cooperation with the University of Idaho)

    Provo, Utah (in cooperation with Brigham Young University)

    Reno, Nevada (in cooperation with the University of Nevada)